

Statistics of aberrations in
polycrystalline materials

by José A. Hernández Servín

Thesis submitted to
the University of Nottingham
for the degree of Doctor of Philosophy

July, 2007



The University of
Nottingham

Abstract

This thesis is concerned with the propagation of elastic waves in polycrystalline materials. In particular, in establishing a relationship between the statistical properties of the wavefield and the statistical properties of the material via a correlation function. Here the study of elastic waves has been restricted to surface acoustic waves (SAWs), mainly because they are readily accessible using an optical scanning acoustic microscope (OSAM).

Polycrystal materials considered as stochastic media exhibit random properties at some scale. This generally includes most common engineering materials such as metals which are constituted by anisotropic regions known as grains. This thesis uses a stochastic model for both microstructure and wave propagation in polycrystals based on the stochastic Helmholtz equation. The main objective of the model proposed is to obtain a correlation theory that best characterises aberrations in acoustics due to microstructure in polycrystals. The model has been built upon the existent theoretical background around scalar theory for waves in inhomogeneous media in order to find an expression for the correlation function Γ_u of the field.

The interaction of SAW and microstructure is experimentally observed as deviations or aberrations of the wavefront by imaging the acoustic field as it propagates in polycrystals using the OSAM. The aberrations regarded as random process are statistically analysed from an ensemble of acoustic fields built upon performing multiple measurements on the surface of a sample, thus measuring a transverse correlation Γ_e .

The mean grain size and the correlation length are connected through the second moment Γ_k of the wave number. The theoretical model predicts that Γ_u depends exponentially on Γ_k . A comparison of Γ_u and Γ_e provides a relationship between Γ_e and Γ_k , therefore an indirect way of measuring mean grain size. The theoretical-experimental analysis has been supported with simulated acoustic propagation on simulations of grain growth for real microstructure.

Acknowledgement

I would like to thank my supervisors Dr. M. Clark and Professor M. Somekh for the opportunity that they gave me to join their research group and for all the useful discussions during my PhD. I would also like to thank the University of Nottingham for the scholarship awarded to fund my PhD.

Thanks to all my colleagues and friends, Ian Collison, Teti Stratoudaki, Efstathios Tapinos for the tertulia and enjoyable meals during my PhD. To Steve D. Sharples for his willingness to help during the experimental work. I am particularly grateful to Ian for the experimental work carried out when I was away.

I would like to thank Dr. Alberto Mendoza for recommending me to join the PhD program, and to Professor Richard E. Challis for the useful comments in order to improve my work.

I would also like to express my most sincere gratitude to the mathematician Sevin R. Pishmish for all the support during my BSc and Masters degree. He has always encouraged and helped me to continue my studies. Thank you Prof. Sevin.

Finally, I would like to thank my family, all my brothers and sisters, but especially my parents who have always encouraged me to pursue a university degree. To my sister Veronica for keeping me informed about the family affairs all this time I have been away.

Dedicated to

*To my wife Reyna N,
who has always been on my side supporting me.*

Contents

1	Introduction	10
1.1	Background and Motivation	11
1.2	Imaging acoustic aberrations	13
1.3	Effects of aberrations and adaptive acoustics	15
1.3.1	Correcting for acoustic aberration	16
1.4	Aberrations and scattering of waves	18
1.4.1	Modelling the medium	20
1.5	Aim and contributions of the work	21
1.6	Objectives and thesis layout	22
2	Literature Review	26
2.1	Elastic waves in inhomogeneous medium	26
2.1.1	The elasticity equations	29
2.1.2	Survey on some methods of solution	32
2.2	Mean grain size and attenuation	34
2.3	Scalar acoustic waves (SAW)	36
2.3.1	Methods of solution for scalar waves	36
2.3.2	Phase screen method	37
2.4	The mutual correlation function	39
2.4.1	Correlation for a scalar field	40
2.4.2	Survey on correlation function	41
2.5	Simulation of microstructure	43
2.6	Ultrasonics	43

<i>CONTENTS</i>	4
2.6.1 Point sources	44
2.6.2 Ultrasonics generation	46
3 Waves in polycrystalline materials	48
3.1 Theory of elastic waves in stochastic media	49
3.2 Elastic waves in polycrystals	51
3.2.1 Linear elastic polycrystal	52
3.2.2 The effective parameters	54
3.2.3 The anisotropy of the grains	56
3.2.4 The elastodynamics equations	57
3.3 SAWs in polycrystalline materials	59
3.3.1 The scalar approximation	60
3.3.2 The degree of inhomogeneity	61
3.3.3 The statistical characteristics of the medium	64
3.3.4 Simulating the microstructure of polycrystals	66
3.4 Concluding remarks	72
4 SAW waves in polycrystalline materials	74
4.1 Propagation in random media	75
4.1.1 Displacement from a line source in the half space	76
4.1.2 Propagation through a random thin layer	81
4.1.3 Propagation through many layers	84
4.1.4 Realisation of phase variations	86
4.1.5 Realisation of the acoustic field	89
4.1.6 Solids in general	91
4.2 Conclusions	91
5 Propagation of correlation function	93
5.1 Moments of the acoustic wave field	95
5.1.1 Initial correlation function	95
5.1.2 The structure function of the medium	96

5.1.3	Multiple screens	99
5.1.4	Correlation function by averaging over the ensemble	101
5.2	Using a derived differential equation	106
5.2.1	Equation for the second moment	106
5.3	Concluding remarks	108
6	Experimental methods and results	110
6.1	Sample selection	111
6.2	Sample preparation	111
6.2.1	Procedure for refining grains in Al	112
6.3	Metallographic characterisation	114
6.3.1	Digital characterisation	114
6.3.2	Error in characterisation	118
6.4	Experimental setup	119
6.4.1	SAW generation systems	119
6.4.2	Detection system	121
6.5	Measurements	122
6.5.1	Measurements in Ti	130
6.6	Analysis of experimental data	133
6.6.1	Procedure for spatial correlation	133
6.6.2	Results	134
6.7	Comparison	136
6.7.1	Comparison for Al	136
6.7.2	Comparison for Ti	139
6.8	Analysis of the best fitting procedure	141
6.8.1	Noise in measurements	142
6.9	Comparison of simulated microstructure	143
6.9.1	Simulated degree of inhomogeneity σ	144
6.9.2	The correlation length l	145
6.10	Conclusions	147

7	Discussions and further work	150
7.1	The scalar model	150
7.1.1	Modelling the medium	152
7.2	The phase screen model	153
7.3	Experimental work	154
7.4	Final comments	155
A	Appendix	157
A.1	Multivariate propagation function	157
A.1.1	Remarks	160
A.1.2	The mean for multiple phase screens	160
A.2	The angular representation in inhomogeneous medium	162
A.3	The Green's function for the correlation equation	164
A.3.1	Helmholtz's equation	164
A.4	Colouring Voronoi cells	166
A.5	Algorithm for wave propagation	167
A.6	Principle of laser-generation	167
A.6.1	Displacement from an array of lines	170
A.7	Useful integrals	171
	Bibliography	172

List of Figures

1.1	Amplitude and phase distribution	14
1.2	Schematic representation for correcting aberrations	17
1.3	Adaptive optical configuration	18
1.4	Chart of thesis layout	23
2.1	The correlation of the field	40
2.2	Experimental setup using transducers	46
3.1	Anisotropy of polycrystalline materials	54
3.2	Geometry of SAW in polycrystals	59
3.3	Mean calliper diameter	66
3.4	Voronoi tessellation for simulating microstructure	68
3.5	Modelling the phase and wave number	70
3.6	Correlation function of simulated microstructure	71
4.1	Geometry of SAW on the half-space generated by a line source S	77
4.2	The field in half space	80
4.3	Schematics of propagation in random media	82
4.4	Schematic representation of the n th layer	85
4.5	Generation of realisation of ϕ	88
4.6	The transverse light distribution of a laser	90
4.7	Realisation of the field in simulated media	90
5.1	Idealised correlation function of the field	96
5.2	The structure function of random process	99

5.3	Image of the energy correlation function in a random medium	105
6.1	Photomicrograph of elongated grains in aluminium	112
6.2	A histogram of the grain size distribution for M_A	115
6.3	A histogram of the grain size distribution for M_B	116
6.4	A histogram of the grain size distribution for M_C	117
6.5	Photomicrograph of titanium	118
6.6	The OSAM system	120
6.7	Experimental setup for SAW using transducers	121
6.8	Scanning area and source location for multiple measurements	122
6.9	Scanning area for multiple measurements	123
6.10	Aberrations in aluminium block A	125
6.11	Aberrations in aluminium block B	127
6.12	Aberrations in aluminium block C	129
6.13	Aberration in titanium	131
6.14	Acoustic field in an ideal sample	132
6.15	Experimental correlation function in an aluminium	135
6.16	Comparison of correlation Γ_u and Γ_e	137
6.17	Experimental correlation in titanium	140
6.18	Plot of r as a function of σ	142
6.19	Comparison of the best values in simulated media	144
6.20	Comparison of the best values for the correlation length	145
A.1	Array of N illuminated lines by a laser	171

List of Tables

6.1	Summary of some of the values used and obtained for mean caliper diameter \bar{b} , mean Rayleigh wavelength λ_R , and the number of images n in aluminium samples at 82MHz. p_x, p_z denotes pixel size in x and z , respectively.	128
6.2	Experimental values for σ, l obtained by minimising Eq. (6.4) for the aluminium samples A, B, C. The spread in both quantities σ, l indicates that they are to be found within a 20% accuracy.	138
6.3	Parameter values used for comparison of the predicted and measured correlation function.	139
6.4	Parameter estimated by minimising χ^2 without filtering the data . . .	143
A.1	Useful integrals	171

Chapter 1

Introduction

The research presented in this thesis is concerned with elastic waves in polycrystalline materials and the effect that the materials have on wave propagation. Specifically, the interaction of surface acoustic waves (SAWs) and materials composed of non-intersecting anisotropic regions or grains, such as aluminium. The overall geometric properties, such as shape and spatial arrangement of grains within a polycrystalline material shall be termed microstructure.

The interaction of SAW with microstructure results in deviations or aberrations of the wavefront causing the amplitude and phase of the wave to spread transversally along the direction of propagation. The aberrations or deviations of the wavefront can also be observed in other types of waves, such as electromagnetic waves. For instance, rays of light entering to the earth emanating from a distant object, such as a star, are deviated by the atmosphere [1]. Aberration of light by the atmosphere is at a very advanced stage of research compared to aberration in acoustics. The reference [1] just mentioned is a review on what is known as *Adaptive Optics*, which deals with the problem of aberrations of light affecting the performance on ground-based telescopes.

In this chapter acoustic aberrations are introduced and compared to methods used in Adaptive Optics. One thing they have in common, is that one wishes to correct or to minimise the effects caused by aberrations of waves. Many mathematical techniques in Adaptive Optics can also be applied to explain aberration in acoustics

as discussed later. The temporal and spatial correlation of light plays a fundamental role in adaptive optics [1]. This would also apply to acoustic aberrations as this work deals with the moments of the acoustic field. That is, the second moment of SAW is of great importance in studying acoustic aberrations since it is directly related to the spatial correlation of microstructure.

From the theoretical point of view, aberrations caused by material microstructure are studied within stochastic calculus because of the stochastic nature of microstructure in polycrystalline materials. This, in turn, implies the use of the theories of elasticity in polycrystalline materials, which is rather similar to linear elastic theory for non-polycrystalline materials.

Experimental evidence of aberration in acoustics is demonstrated using an imaging system developed at the University of Nottingham. The system is an optical scanning acoustic microscope (OSAM) that fundamentally generates and detects SAW using lasers for both generation and detection of SAWs. The OSAM system is capable of performing measurements at many positions of SAW in stochastic media, thus being able to produce an ensemble of SAW. This way, it is possible to statistically assess the effect that microstructure has on a SAW travelling in such medium. As a consequence of this procedure, it is possible to measure a correlation function from the experimental ensemble that quantifies aberrations.

1.1 Background and Motivation

The term ultrasound refers in general to sound at high frequencies or above 20kHz which is the normal frequency that the human ear can detect. The experimental work is carried out in the high frequency regime (82MHz) which is the fundamental frequency at which the OSAM generates ultrasound. In the theoretical framework, ultrasound can be described by the linear elastic theory for solids. This theory predicts many types of wavemodes that have a wide range of applications in industry and/or medical diagnostics. Common wavemodes could be longitudinal, shear and Rayleigh or SAW depending on particular applications or boundary conditions. Ul-

trasound and SAWs will be synonymous in this thesis since the experimental work has been carried out using SAWs.

For instance, in medical ultrasound [2, 3] advantage is taken of the scattering process occurring in tissue, muscles, etc. to image objects within the human body for medical diagnostics, an example of this, is fetal imaging [4, 5]. Lamb and Rayleigh waves, in particular can have a variety of applications. Lamb waves are useful in locating and sizing flaws in pipes [6, 7, 8] as well as in assessing train rails [9]. Other applications of Rayleigh waves is the characterisation of cracks on complex geometries [9]. In the area of sensors, acoustic-wave devices have gained importance in the design of transmitting and receiving inter-digital transducers using Rayleigh waves [10].

Ultrasound is one of the many techniques that can be used to image objects such as micro-cracks [11]. Other methods include X-ray tomography [12], electromagnetic waves and radio waves [13]. The main motivation of this work is to say that aberration of SAWs can be used to indirectly extract information from the medium in which the wave is travelling. In the next paragraph, a more precise meaning of acoustic aberrations is introduced.

Many engineered materials such as aluminium are composed of anisotropic grains with random spatial orientation. This type of solid is polycrystalline. They can have grains of different shapes and the degree of anisotropy will depend on the type of metal considered. The important point at this stage is what happens with SAWs propagating in polycrystalline materials.

Let us consider an experiment which measures the field of a plane wave propagating in a polycrystal. As the wave propagates away from the source, the phase and amplitude of the wave would experience changes due to the anisotropy of grains. The random orientation of grains and the fact that in anisotropic solids the wave velocity is highly dependent on angular direction, is the main cause of those changes. These changes can be observed as deviations in the amplitude and phase of the field as it propagates from one grain to another in a random fashion. Those effects were observed and postulated to be the cause of erratic performance in surface

wave velocity measurements in [14]. The effects, now known as acoustic aberrations, can be observed in polycrystalline materials or in media which have a random microstructure. As the research went further it was necessary to systematically study aberration phenomena since it became important for improving the performance of the OSAM system. The other reason why aberration became an interesting subject is the intrinsic relationship between the statistics of aberrations and microstructure of polycrystalline materials. Perhaps, one of the first works to appear on this subject was [15], where the authors took a two-dimensional image of SAW wavefront distortions as they travelled in stochastic media. By using an optical beam deflection[16] technique for detecting small displacements on the surface of the sample, they were capable of showing many interesting features inherent to the sample. The most significant is that aberrations are clearly seen on a piece of titanium using 10MHz Rayleigh waves.

The acoustic aberration can be quantified by a transverse correlation of the acoustic field. This in turn is related to the correlation of the stochastic medium by means of a scalar theory for SAWs. From this relationship, characteristics of the medium, such as mean grain size as well as the degree of anisotropy can be extracted.

1.2 Imaging acoustic aberrations

The OSAM system has been used to image and measure the acoustic deviations in polycrystalline materials. The preliminary results presented in this section were carried out in aluminium. Let us denote the acoustic field as $U(x, z) = A(x, z)e^{i\Phi(x, z)}$, where A denotes amplitude and Φ phase. U is the displacement normal to the plane where the wave propagates. The scan has been performed in the xz plane measuring the normal displacement point by point. It is a plane wave that propagates from left to right on the surface of an aluminium sample, Fig. (1.1). Both the amplitude and phase distributions are shown and it can be observed how the wavefront changes in both images as the wave propagates away from the source. Several processes

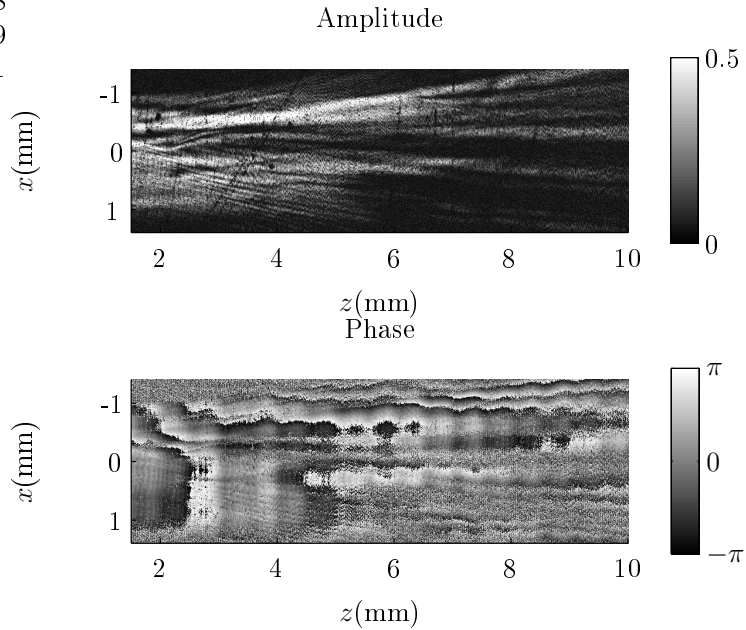


Figure 1.1: The image on top is the amplitude distribution A whereas the image on bottom is the phase distribution Φ of a plane wave at 82MHz, travelling from left to right on an aluminium sample. The two images were obtained with OSAM system.

may be involved to cause acoustic deviations, as observed in Fig. (1.1). Every point belonging to the wavefront interacts with grains causing the phase to deviate from what would be expected to be if there were no grains, i.e. non-polycrystalline material. The cause of those aberrations is due to the anisotropy and orientation of each grain. Whatever the process involved it is desirable to characterise overall aberrations from a statistical point of view. It is clear that aberrations depend somehow on microstructure of the sample under consideration. This dependency can carry considerable information and presents difficulties for a theoretical description of the system.

Statistical analysis of aberrations requires multiple measurements of the acoustic field over the microstructure, to obtain unbiased estimation of aberrations in polycrystalline materials. This is because grain characteristics vary randomly. That is to say, grain orientation, anisotropy and grain topology have to be described by stochastic processes. Fig. (1.1) is the acoustic field measured on a particular location on the surface of the sample. Consider the experiment of measuring the acoustic field with the source located at two different locations on the surface of the same

sample, such that the scanning areas do not overlap, then because of the stochastic nature of microstructure, it is expected to obtain a different deviation pattern for each measured field. That is, the acoustic deviations as shown in the amplitude distribution in Fig. (1.1) would follow different paths. The reason for this is as one changes source and scanning location the wave is propagated in a different realisation of the ensemble of processes describing microstructure. Continuing in this way one would be able to build an ensemble of the acoustic fields and be able to make a statistical characterisation of acoustic aberrations, which would depend on the ensemble of microstructure.

Acoustic aberrations are absent in non-polycrystalline materials, such as glass or any other solid with no microstructure, as stated before. The word *homogeneous medium* is sometimes used in this thesis as synonymous for non-polycrystalline materials. But a polycrystalline material can also be considered as a homogenous medium if the wavelength is relatively bigger than the scale of the inhomogeneities. At this scale elastic waves, such as SAWs do not interact with the microstructure, so aberrations are wavelength dependent.

The object of study will be images of the acoustic field in a form presented in Fig. (1.1) for the statistical study of acoustic aberrations.

1.3 Effects of aberrations and adaptive acoustics

Aberrations can be undesirable since they affect the accurate measurement of mean wave velocity [14]. The problem of compensating for aberrations requires knowledge of the stochastic Green's function of the system. One method in dealing with this problem is presented in [14], where the author realised that by improving the correlation of the acoustic field with an optimised Green's function measured directly from the specimen, the accuracy of wave velocity measurements in the region of interest could in theory be improved. This section explains fundamentally the problem for compensating aberrations in acoustics arising in the OSAM system. As this work advances, it will be seen that it is possible to exploit this phenomenon to gather

information about solid microstructure.

1.3.1 Correcting for acoustic aberration

This section explains the mechanism for correcting acoustic aberrations in polycrystalline materials, which is an integral part of the OSAM system. The OSAM system uses a spatial light modulator (SLM) to project a light pattern onto the surface of the sample. This acts as a thermoelastic ultrasonic source for SAW generation [17].

Consider the experiment of exciting a focused acoustic wave to a point by delivering a series of arcs onto the surface using the SLM. Two things will happen if one measures the point spread function (PSF) of the system at the focus point.

a) The PSF is the amplitude of a wave with undistorted spherical wavefronts. Acoustic aberrations are absent if the sample is an isotropic material Fig. (1.2)(a).

b) The PSF is the amplitude of a wave with distorted spherical wavefronts. Acoustic aberrations are present if the sample is a polycrystalline material Fig. (1.2)(b).

To compensate for aberration in this context would mean to backpropagate the distorted PSF, Fig. (1.2)(b) to the zone of ultrasound generation where the phase error is calculated by comparison with the non-distorted PSF as in Fig. (1.2)(a). This procedure is equivalent to feeding the SLM with an optimised source that depends on the characteristics of the medium. The distorted PSF is back propagated to the source in a homogeneous half space using an angular representation of the field to feed the SLM with the new pattern [18]. The resulting PSF at the focus point would be as if there were no microstructure to interact with as illustrated in Fig. (1.2)(c). The correlation of the acoustic field is an important part in correcting for aberrations and also the core of this thesis for other reasons which are explained later. There are some hardware issues to deal with in order to succeed in correcting for aberrations, specifically how to detect them, and these are carefully reviewed in [19].

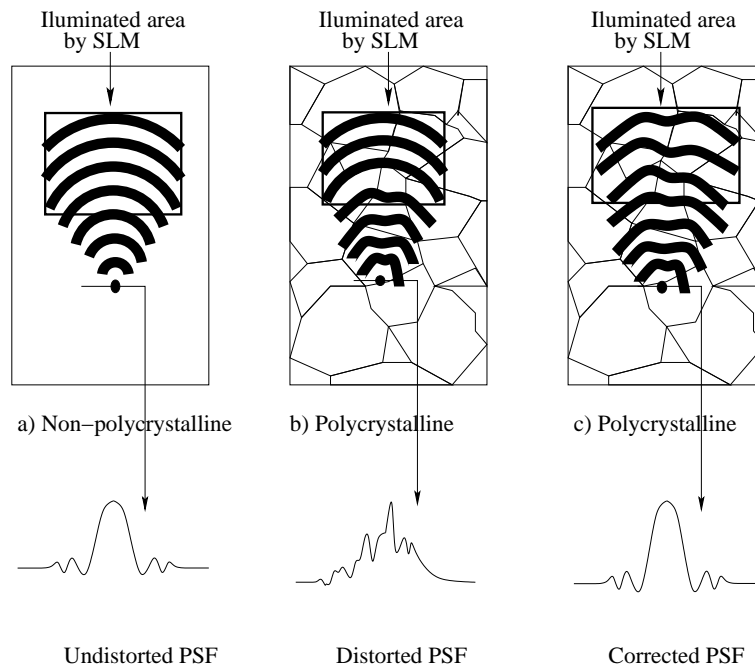


Figure 1.2: Schematic representation of the mechanism in correcting for aberrations. a) It shows a focused SAW in non-polycrystal material by projecting arcs of light onto the sample through SLM. Below it, is the graph of the PSF at the focus point. b) Similar situation as in (a), but the medium is a polycrystal, showing also the distorted PSF at the focus point. c) Similar experiment as in (b) but the arcs this time are distorted by feeding the SLM with the back-propagated waveform in a homogeneous half space from (b). The undistorted PSF is also shown in (c) illustrating the corrected aberrations.

The above procedure is similar to the one followed in optics for correcting aberrations of light for ground-based telescopes [1]. Light passing through a turbulent

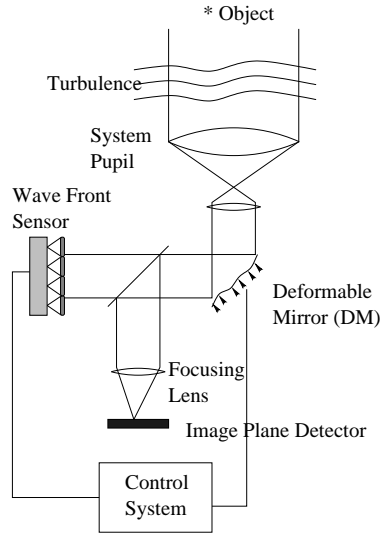


Figure 1.3: A simplified optical configuration of an adaptive optical imaging system, redrawn from [1].

medium such as the atmosphere with a variable index of refraction, is spatially aberrated in a random fashion causing images from distant objects, e.g. stars, to be distorted. The problem is how to correct these deviations or aberrations in order to get an accurate image of the object. The area dedicated to this type of problem is *Adaptive Optics* and is a very active subject since aberrations are an undesirable effect in gathering information. Many sophisticated instruments have been built in order to correct or minimise this effect. Fig. (1.3) shows a simplified version of a typical optical imaging system [1]. This type of instrument corrects for the aberrations using a hardware, deformable mirror(DM), shown in Fig. (1.3). The OSAM system works in a similar way in the sense that it is also capable of correcting aberrations arising in solids.

1.4 Aberrations and scattering of waves

Theoretically speaking aberration in polycrystalline materials could be described in a more general theory for waves in media with variable characteristics, specifically the

scattering of elastic waves by microstructure. The process of scattering is far more complex than aberrations, since acoustic aberrations could simply be described as distortion of the wavefront of forward scattering of elastic waves. A wave can travel in the forward and backward direction due to interactions with the scatterers or grains in polycrystals. For instance, let us imagine a vector normal to the wavefront travelling in the forward direction within a polycrystalline material. The vector will change direction, but still part of the forward field by interacting with grains (aberrations). It can, however, be reflected and reflected again by grain boundaries. This process is repeated for all points belonging to the wavefront, This is what we mean by *multiple scattering*, causing the field to be extremely complex and usually randomised. In the very specific case of a SAW in a polycrystal, waves can be reflected by grain boundaries and forward reflected again causing a complicated wave interaction, even mode conversion.

All energy carried by elementary waves travelling in the direction of propagation constitute the so called forward scattering whereas backward scattering is the opposite. In many practical applications forward scattering is stronger than its counterpart and therefore backscatter very often is neglected. As shown in Fig. (1.1), aberrations are the wavefront distortions of the field in the forward direction.

The scattering theory of waves in polycrystalline materials is described by the theory of elastic waves in random media. This theory is an extension of linear elastic theory for homogeneous solids, in the sense that elastic characteristics via elastic moduli is a spatial random tensor that depends on position [20]. The elastic characteristics of each grain is a major problem in this theory since each grain is an anisotropic solid in its own right. Therefore, the theory can get very complicated if considering all the right elastic properties of each of the grains. It is well known that anisotropic single grains are difficult to study not because of the number of elastic constants involved but also of the complication in obtaining the displacements. The authors in [21, 22] have studied solids of general anisotropy, for instance. On top of that, one still has to consider the orientation of the grains with respect to each other. It would be seen that some approximations in grain anisotropy have to be

introduced in order to get useful results about the elastic response of a polycrystal.

In this thesis the elastic model for SAWs is replaced by the stochastic scalar model, where the medium is described by a single scalar random process simplifying the mathematical development. This avoids the use of a tensor random process necessary in the full theory.

1.4.1 Modelling the medium

Modelling or specifying the medium is part of the problem of wave propagation in polycrystals. It is a complicated problem in the theory of wave propagation in polycrystals since microstructure of the polycrystal can have complicated geometrical forms. In the theory all the geometric and elastic properties are embedded in the elastic moduli c . Thus, the specification of tensor c is important in wave propagation, where c is a tensor that depends on position.

The theoretical description is greatly simplified by modelling the elastic moduli as $c(\mathbf{r}) = c_0 + c'(\mathbf{r})$ [23, 24, 25, 26], where c' is a stochastic process representing the fluctuation with respect to c_0 . The process c' accounts for wave velocity variations within grains due to the anisotropy and random orientation of grains. The simplification is introduced by imposing simplified constraints as a random process, for instance, using known correlation functions, $\langle c' \rangle, \langle c'(\mathbf{r})c'(\mathbf{r}') \rangle, \dots$ where the broken brackets represent an ensemble average. The c_0 elastic moduli is the average over orientation and number of grains within a volume. The constants c_0 correspond to the elastic moduli for homogenous solids. This model can equally be applied to the scalar approach, in the sense that the wavenumber is modelled as $k = k_0(1 + \mu)$ where μ is the fluctuating part. It will be seen that by specifying the second order moments for μ as being exponential form, many polycrystals with mainly convex grains can be modelled. This model will allow a formulation of a theoretical description for the correlation of the field to be obtained. Experimental results will show how this is related to the actual material.

1.5 Aim and contributions of the work

One of the purposes of this work is to provide a tool for a statistical study of aberrations based on correlation of the acoustic field. The work is aimed not only for the likely use in material characterisation but also to aid in the problem of compensating for aberrations in acoustic propagation.

The correlation of the field is measured using a transverse correlation. This function is to be related to the second order moments of the process characterising the medium via a scalar theory. From this relationship, some characteristics of the investigated polycrystals are obtained such as the mean grain size. The knowledge of mean grain size is an important parameter in material characterisation. The NDE methods applied in this thesis for testing materials indirectly measure material characteristics. There is still a lot of work to do, but it is believed that this work will be valuable in reaching that point.

The aberrations of the field, regarded as a random process, are statistically analysed from an ensemble of acoustic fields built up by performing multiple measurements on the surface of a sample. This analysis permits the measure of the transverse or two-point correlation Γ_e directly from measurements with the purpose of comparing it to a theoretical model which is able to extract the mean grain size. The theoretical work is based on stochastic waves in inhomogeneous media. The purpose is not to give a general treatise on the subject but a useful theoretical treatment applicable to aberrations. This is done by approximating second moments within the framework of a stochastic process, despite the apparent restrictive assumption on microstructure.

In summary, the contribution of this work is the establishment of a wave correlation function that quantitatively describes the local anisotropy and mean grain size of a certain polycrystalline materials. This provides a relatively simple way of understanding wave propagation in inhomogeneous media and its direct relationship to actual microstructure.

The statistical properties of SAWs in polycrystalline materials are defined by

second order moments of the acoustic fields and these relate to material grain size and anisotropy via the wave correlation function.

1.6 Objectives and thesis layout

This thesis has been organised into three main parts comprising seven chapters that contain theoretical aspects of waves in inhomogeneous media, experimental work in solids with microstructure and simulations.

The literature review, is carried out in chapter (2) focusing on waves and aberrations from 1900 up to the present in inhomogeneous media. This review emphasises the importance of the first and second moments of random fields applied to ultrasonic propagation. It covers both elastic and scalar waves which are later used for the theory of SAWs in polycrystals.

A number of the articles come from a different area such as the stochastic wave equation that has extensively been applied there. A few articles on the importance of numerical techniques used in metallographic studies are mentioned. These are later used to study the anisotropy of polycrystals in simulated media.

The theoretical aspects of wave propagation are covered in chapter (3) based on elastic waves and scalar waves. The methodology is to reduce the full wave theory to the scalar approach for SAWs in polycrystals. The elastic properties of polycrystals are discussed connecting the anisotropy of the grains to local geometric features of the microstructure.

The following diagram, Eq. (1.4) shows schematically the main parts of the thesis. The starting point is a polycrystal as the object of study. As the diagram (1.4) shows, the important aspect in this part will be the second order moments Γ_{μ} from which the geometric characteristics of the microstructure can be modelled. A prescribed exponential form of Γ_{μ} is discussed as a possibility to approximate microstructure for the type of polycrystals investigated in this thesis. Towards the end of chapter (3) numerical techniques are introduced for microstructure simulation. Also a simple model to simulate wave velocity variations in polycrystals is discussed. Realisation

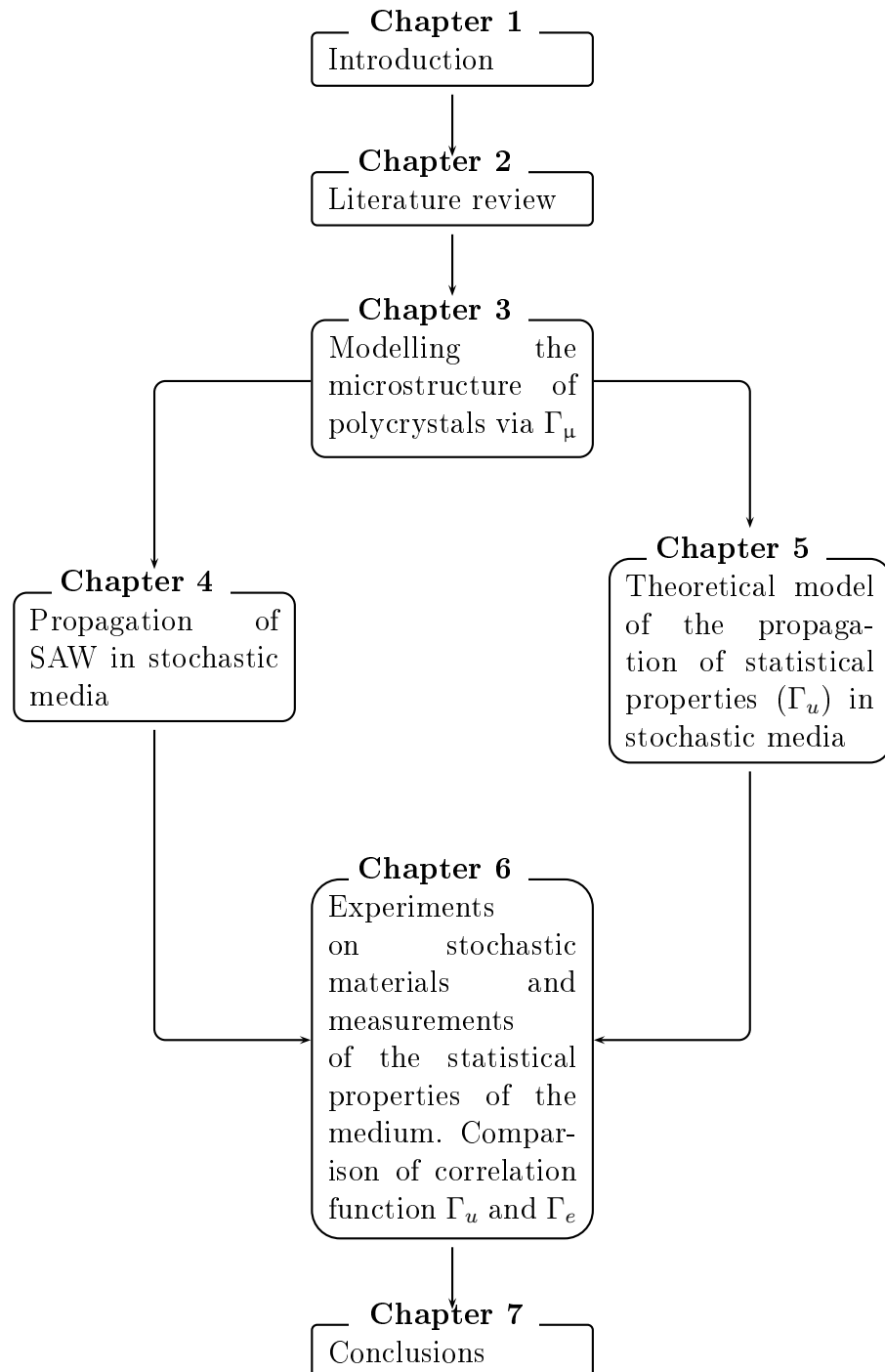


Figure 1.4: Chart showing schematically the thesis layout, highlighting the most important aspects of thesis and chapters where they are discussed.

of phase variation of the phase screen model were modelled using this technique to give realisations of the field.

Chapter (3) was intended to deal not only with microstructure but also with acoustic simulation. The Voronoi tessellation is briefly discussed and is used to simulate real microstructure. The wave number in a discrete medium is modelled based on this. This simple algorithm used to evaluate the multiple integral representation of the field based on the discrete Fourier transform is given in appendix (A.5). The correlation length of the random process representing the inhomogeneities and its relationship to the mean caliper diameter of grains is also discussed.

Chapter (4) introduces the SAWs in the half space and its relation to the well known angular spectral representation of a field discussing briefly SAW generation from a line source. This chapter also introduces and develops the phase screen model for wave propagation in random media which will be a fundamental part in the study of correlation of the field. The overall aim of the chapter (4) is to give an expression for the acoustic field which allows us to calculate the correlation function of the field in chapter (5).

The quantification of aberrations is based on the correlation of the field. It is the most important part of the thesis, thus correlation of the field is discussed in chapter (5). This quantification is made by means of a transverse correlation function and is the main contribution of this work. Therefore, chapter (5) is dedicated to the calculation of this function from two methods. The first approximation is given based on the expression calculated in chapter (4). This is presented on the first half of the chapter leaving the mathematical details for the appendix (A.1). The other half is dedicated to give an alternative approximation to the correlation function based entirely on the Helmholtz equation.

The experimental work is presented in chapter (6) along with the instrumentation. In the first part of this chapter the main components of the OSAM system are presented, which is followed by a section explaining in great detail the preparation and characterisation of samples. The aberrations investigated on these samples are given in a separate section along with the methodology to carry out the ex-

perimental work. The statistical procedure is given by introducing the correlation and arithmetic average for finite sequences. Finally, the main result of this thesis is presented in a graph comparing the theoretical and observed correlation function. The aberrations are statistically analysed from an ensemble of acoustic fields built upon performing multiple measurements on the surface of a sample. The analysis permits an estimation of Γ_e , a transverse 2-point correlation from the acoustical ensemble. This experimental correlation function is compared to a theoretical correlation Γ_u , given in chapter (5) from which, by solving a non-linear fitting, the degree of anisotropy as well as mean grain size are obtained, see diagram (1.4).

The final part of chapter (6) is intended to corroborate the theoretical and experimental aspects of this work. The analysis of chapter (6) is repeated here using purely the acoustic field in a simulated microstructure. The simulation of microstructure is from an independent source and unrelated to the point of view presented in (4). The very last part of chapter (6) is to do with the noise present in measurements and the filter for de-noising the signal is discussed.

The final part of the thesis comprises chapter (7) and the appendices (A). The former is dedicated to conclusions and future work whereas the latter are appendices complementing the theoretical work developed in earlier in chapters (4) and (5).

Chapter 2

Literature Review

Introduction

This is a brief review of the existing theoretical and experimental methods of elasticity in materials that are an aggregate of grains randomly orientated in space. This includes any engineering material, with special attention to aluminium and titanium. It also reviews some aspects of material characterisation as it is partially the subject of this thesis. The mechanical properties and material characterisation with methods not related to ones treated here can be seen as further reading into the theory of waves in media with random characteristics, especially scalar theories. Much of the methods mentioned below were developed in areas other than acoustics in solids, especially correlation theory which fundamentally belongs to the theory of light propagation.

2.1 Elastic waves in inhomogeneous medium

Polycrystals

A polycrystalline material, roughly speaking, is an aggregate of grains with different geometric features and highly correlated elastic properties. The geometry of grains, or whole microstructure, is characterised in terms of grain orientation, grain boundaries, subdivision of grains, shape and texture [27], to mention just a few. Grains

as entities can be a single or a subdivision of crystals. These clusters of crystals are sometimes part of a subgrain and can be transformed to form entirely a new grain [28]. Thus, the crystalline structure determines the anisotropy or isotropy of individual grains.

The orientation of grains is measured with respect to the orientation of crystals forming the actual grain. One would have multiple orientation in those cases where the grains contain more than one crystal. The crystallinity and orientation have to be taken into account in establishing the anisotropy of grains [29] because of the effect on wave attenuation. Different grains have different degrees of anisotropy and from a theoretical point, those differences are considered to be a random process [30]. In some cases grain boundaries can take any geometric form depending on the material. For instance, at some scale pure aluminium contains elongated grains with well defined grain boundaries but can have complicated geometric characteristics during recrystallisation [27]. The recrystallisation and boundary formation occurs when, for instance a refiner [31, 32] is added to the melted material (aluminium), during heat treatment. Pressure is another well known process to modify the mechanical properties of metals because recrystallisation may occur. Polycrystals can have multiple phases, that is a grain need not be of the same material or they could have a mixture of two or more elements [27]. Because of the simplicity in microstructure, single-phased polycrystals are the subject of this work, in particular aluminium.

The grains in a polycrystal are in reality three dimensional [33]; characterisation, however, is performed in a plane that shows a cross section of each grain along the plane. *Characterisation* in this thesis means estimation of the grain size of the polycrystal. The statistical estimation of the diameter of the crystals have been developed [34] to obtain a realistic estimation of diameter of the grains. From a two dimensional cross section (photomicrograph) of polycrystals. Geometric features of grains in polycrystals can vary in complexity, it can take any shape such as polygonal as well as elongation in preferred or multiple directions [34] (textured polycrystals). The characterisation of textured polycrystals is slightly more complicated than polycrystals with polygonal grain shape. Equiaxed grains are those

in which the diameter of individual grains is independent of direction so they can be characterised by a single parameter unlike elongated grains where more than one parameter is needed. Polycrystals with equiaxed grains were preferred in this research because of the simplicity in their characterisation.

Elastic properties of grains

Homogeneous media is used here to define any single-phase elastic material with well-ordered atomic structure, e.g. silica; that is, materials with no polycrystalline structure. Polycrystals can be considered as homogeneous media at certain scales. This homogeneous property of the polycrystals is wavelength dependent, in the sense that if the wavelength of an elastic wave propagating in a polycrystal is much bigger than the mean grain size then the polycrystal is considered as homogeneous media since the wave does not interact with microstructure. On the other hand, if the wavelength is smaller than the scale of the inhomogeneity then the polycrystal is considered to be inhomogeneous media. The grains, in particular at certain scales are considered to be a homogeneous medium showing the same sorts of elastic properties as any other solid, such as glass. In fact, most of the elastic properties of the polycrystals are described in terms of the elasticity of grains. The orientation of the crystals is important for describing many of the elastic properties as a homogeneous medium. The orientation is determined by the orientation of the crystal or crystals of which the grain is conformed. A principal axis can be assigned to each grain from which all symmetries and orientation of the grain are defined [35]. Crystals can show cubic, triclinic, orthorhombic, etc. symmetries as defined in [36]. In a polycrystal grain orientation may be clustered round a specific direction (*preferred orientation*), or they can have *no-preferred orientation*. In the latter, one speaks of polycrystal with grains randomly orientated with respect to the crystallographic axis [27, 35].

On this basis, each grain is seen as a linear elastic solid and can be isotropic or anisotropic [37]. Their anisotropy here would be measured in terms of the elastic moduli [35]. Thus, the elastic properties in a polycrystal are characterised by a tensor of rank four being denoted by c_{ijkl} , which in general will be a function of

position or a function of the angle of orientation [29, 35]. To avoid writing the sub-indices every time one refer to it, the elastic moduli are denoted by the single character c .

2.1.1 The elasticity equations

The elastic response from a theoretical point view considers the polycrystal as a medium with stochastic characteristics. That is, its inner spatial structure follows a stochastic or random pattern. Therefore propagation of elastic waves in materials with such properties is studied from probability theories for elastic waves in the sense that c not only depends on position but it is also a tensor process [24, 25, 30]. That is, $c_{ijkl}(\mathbf{r})$ are random processes for each $i, j, k, l=1,2,3$, $c_{1111}(\mathbf{r})$ would be a random field, for instance.

A comprehensive list of references from 1800 on elasticity of polycrystals can be found in [20], this includes W. Voigt [38] and A. Reuss, pioneers in elasticity theory in polycrystalline materials. The review is on the foundations of elastic propagation in polycrystals and a precise stochastic definition of the meaning of mean fluctuations, and mean stresses of crystallites based on these theories. The authors also emphasises the importance of quantities such as mean and n -point correlation function.

In most applied works in acoustics the above mentioned theories focused mainly on the solution of stochastic differential equations describing the system. There is a very well founded mathematical background on stochastic systems and its formal solution [39]. Here, however, the meaning of obtaining a solution will be simply the calculation of the n -point correlation function if possible, and in particular for $n = 2$, which is the subject of this work.

The elasticity equations are presented without any discussion with the sole purpose of presenting theoretical methods for studying elasticity in polycrystals.

The elastic response of a polycrystals under stress in terms of displacements u_k

in all directions of a three dimensional body is governed by

$$\frac{\partial}{\partial x_j} (c_{ijkl}(\mathbf{r}, \xi) u_{k,l}(\mathbf{r}, \xi)) + \rho \omega^2 u_i(\mathbf{r}, \xi) = 0 \quad (2.1)$$

For simplicity the displacements are assumed monochromatic of frequency ω . The density ρ is considered constant, thus considering only polycrystals with no voids or inclusions. Many authors consider the density to be a random process [40] as well.

Note that ξ indicates that u should be regarded as a stochastic field since c_{ijkl} is a spatial random process, that is, each grain has its own elastic properties. Equation Eq. (2.1), is extremely difficult to solve and to the authors knowledge there is no general solution for it; therefore the theory of wave propagation breaks into many approximations depending on the application or boundary conditions.

Before giving the methods for solving Eq. (2.1) we briefly explain the meaning of giving a solution.

The question is, given Eq. (2.1), how does one obtain an expression for $\langle u(\mathbf{r}) \rangle$, $\langle u(\mathbf{r})u(\mathbf{r}') \rangle$, etc. or 1-point, 2-point correlation in terms of the statistical properties $c(\mathbf{r})$? To begin with one has first specify the statistical properties of c . This is a major problem and is the subject of intense research as described below. The other alternative would be purely in terms of probability distribution from the probability laws for c but this point of view is beyond the scope of this work. Now, in practice it would be virtually impossible to give an expression for the moments of all orders for the field u since there is an infinite number of them, although their importance diminishes as the order increases.

The effective parameters

To begin with, in order to even start dealing with a solution to Eq. (2.1) one has to know the stochastic properties of the elastic moduli $c(\mathbf{r})$. The direct answer would be to measure it from the specimen. This, as it is obvious would be a difficult task not only because one would have to measure random processes defining c but also because of the number of them involved. Nevertheless, in some special cases it is

possible to do the inverse problem by assuming that c is a function of the orientation angle [41] measured with respect to a fixed axis of symmetry. The authors assume that Hooke's law or the strain-stress relationship is $\sigma_{ij} = c_{ijkl}(\theta)\epsilon_{kl}$ and develop a formalism to extract the angle defining c . A more general statement is given in [42] where the Taylor series expansion for the elastic moduli is obtained from values of the displacement vectors. This formalism is applied to inhomogeneous isotropic media but the two-dimensional anisotropic case is also considered. Others have also studied the effective elastic moduli in composite materials [43].

The other alternative is to homogenise the elastic response of the polycrystals by finding effective elastic moduli so the polycrystals could be studied as if they were homogeneous. These theories were first proposed by Voigt and later on by Reuss [20].

Here we reproduce the definition of Reuss's average as it will be instructive and useful in other parts of the thesis as it appears in [44], thus

$$c^0 = \frac{1}{2\pi} \int_0^{2\pi} T^t c T d\theta \quad (2.2)$$

where T is the matrix that rotates the elastic moduli an angle θ with respect to the principal axis attached to each grain and T^t denotes the transpose of the matrix T . Later research showed that average Eq. (2.2) is only bound for the true elastic moduli as reviewed in [20]. Thus, homogenisation would lead to erroneous descriptions of the elastic response of a polycrystal. The average is a very general expression for the average moduli over orientation since c could in principle have any symmetry.

A more quantitative expression for the average moduli over the orientation of the grain [37] with hexagonal symmetry aligned with the degree of preferred orientation is given by

$$c^0 = 1 + \frac{ab}{2} \cos 2\Phi \quad (2.3)$$

where a is the anisotropy degree and b the degree of preferred orientation. The angle Φ is the angle between the crystallographic axis and a fixed coordinate system. With

average Eq. (2.3) the authors in [29] studied how the scattered energy is affected by parameters a and b causing attenuation of the wave.

The first step in giving a solution to Eq. (2.1) is to model c as a constant part c^0 plus a fluctuating part c' . That is $c = c^0 + c'$, where c' is random tensor of zero mean and c^0 is some sort of average that could be well defined by Eq. (2.2) as a good approximation. Or Eq. (2.3) could be used if the crystals have hexagonal symmetry within the polycrystals. Polycrystals based on the above model are also called random media in the sense that their properties differ randomly from the homogeneous medium. The elastic moduli will have from now on, after averaging, the meaning that they have for linear elastic theory in homogeneous media. Then the form c^0 would be completely determined from the specimen in question. This model is the starting point for many authors in giving approximated solutions for the displacements in Eq. (2.1) which are reviewed below.

2.1.2 Survey on some methods of solution

In most applications the important quantity is the mean response $\langle u_k(\mathbf{r}) \rangle$ for the displacement and many articles have been written on the subject. The purpose of many of the articles mentioned below is to solve the scattering problem posed by Eq. (2.1) by obtaining the average $\langle u_k(\mathbf{r}) \rangle$ as a function of the statistical properties of the elastic tensor c . The aim is to obtain a quantitative measure of the attenuation coefficient as a function of the mean grain size. This is an important point of interest for this work so is reviewed separately.

Perturbation theory

Perturbation theory roughly speaking assumes that fluctuating part c' in Eq. (2.1) differ slightly from c^0 so c can be expressed as $c = c^0 + \epsilon c'$ where ϵ is a small parameter characterising the degree of inhomogeneity. Under these circumstances the displacement can be expanded as a series

$$\mathbf{u} = \mathbf{u}_0 + \epsilon \mathbf{u}_1 + \dots$$

in terms of the parameter ϵ to be able obtain an approximated expression for $\langle \mathbf{u} \rangle$ up to second order [30]. These authors additionally assume that c can be described by two scalar process $\lambda(\mathbf{r})$, $\mu(\mathbf{r})$ and the density is also a scalar random field, this assumption sometimes is termed *local isotropy*. The local anisotropy of the grain complicates greatly the theoretical development of elastic response of a polycrystalline material so additionally one has to assume local isotropy but this is only an approximation to real polycrystals.

Local anisotropy can also be accurately described by geometric optics [45] in the sense that the theory describes the evolution of rays locally. The theory reduces to the eikonal equation but other methods have been shown to have a wider range of practical applicability [46, 47]. The authors in [30] have also applied perturbation theory to scalar and electromagnetic waves and have given a quantitative measure of energy lost in the propagation by obtaining an attenuation coefficient. Others have applied perturbation techniques [25] to obtain the mean displacement in textured polycrystals. A slightly more general account of elastic propagation in heterogeneous media within the framework of perturbation theories is given in [24]. The authors take into account the anisotropy of the individual grains with cubic symmetry, that is the, elastic moduli are expressed by three scalar random processes, $c_{11}(\mathbf{r})$, $c_{12}(\mathbf{r})$ and $c_{44}(\mathbf{r})$ approximating $\langle \mathbf{u} \rangle$ satisfying Eq. (2.1). In the case of anisotropic (random processes context) moduli the attenuation depends on the propagation distance [48]; grains are no longer equiaxed so texture has to be taken into account. This author has solved the scattering problems under more general circumstances than the authors already mentioned. His approach is to use a Green's function, allowing him to give general expressions for attenuation coefficients for different wave modes.

Parabolic approximation and perturbation theory

Perturbation theory and parabolic approximation can be combined to obtain approximated solutions to Eq. (2.1)) for locally isotropic polycrystals [49]. The authors assume that the field is a slowly varying function along the propagation path and make the following substitution $\mathbf{u} = \mathbf{U}e^{ikx_1}$. That is the field \mathbf{U} varies more slowly

in the direction x_1 than that in the x_2, x_3 planes. This approximation is well known in scalar theory [47, 50] and it will be used in the forthcoming chapter (4) to approximate the acoustic field. They give a series of equations for u_k without explicitly solving them. These approximated equations for displacements are given in the first order approximation that allows them to propagate in the forward direction.

A theory developed for linearly elastic solids in which the scales of inhomogeneities are very large relative to wavelength is given in [40] and could be well applied to the case of SAWs in polycrystalline materials solids considered here. The range of applicability is when $\bar{\lambda} \ll l$, where $\bar{\lambda}$ is the mean wavelength and l is the scale of the inhomogeneity. There are some constraints imposed in this development such as only forward propagation can be handled by this theory. The author derives a vectorial differential equation based on a range-increment procedure that solves the full vectorial equation within a slab. By dividing the region of interest into slabs this procedure allows the author to obtain local solutions to finally assemble the results into a vectorial equation. From this reference, it is interesting to note that the author concludes that for two dimensional problems, the aforementioned equations are reduced to the well known stochastic Helmholtz equation in its parabolic form. More work was published on the subject [49] on the potential of the parabolic approximation for a system described by Eq. (2.1)). Another interesting reference in the same direction for surface waves in heterogenous media is [51]. More methods have been successfully applied to the scattering problem and these are reviewed below where the relationship between mean grain size and attenuation has been established.

2.2 Mean grain size and attenuation

The mean grain size is a useful parameter for material characterisation in many applications of scattering theory governed by equation Eq. (2.1) and scalar theories. The aim of many authors was to solve the scattering problem posed by Eq. (2.1), approximating the mean field $\langle \mathbf{u} \rangle$ and extracting an attenuation coefficient from

there. This in turn is related to mean grain size, and thus, microstructure has direct consequences on wave propagation [23, 25, 24].

The correlation length is the distance at which two points \mathbf{r} , \mathbf{r}' are no longer statistically correlated. This property is defined in terms of the moments of c or the wave number in the scalar theories. The $\langle \mathbf{u} \rangle$ is expressed in terms of the correlation $\Gamma_c = \langle c(\mathbf{r})c(\mathbf{r}') \rangle$ or possible higher orders. This function assesses whether or not two points are in the same grain, thus it relates to the mean grain size. The problem here is that the grain shape may have complicated geometric features. The overall geometrical features of the microstructure, in order to fit the theory is approximated by assuming that the diameter of the grain is independent of the direction. Some authors referred to it as grains with spherical properties [25]. In this case, Γ_c will depend on a single parameter or one correlation length. A extension when it is so evident that the grains do not have spherical symmetries is to allow Γ_2 to depend on one or more parameters, perhaps direction. This extended model generally applies to polycrystalline metals with elongated grains or texture. In general terms, the correlation function Γ_c cannot describe all the relevant properties of microstructure so the elastic response in terms of the statistics of the field displacements is affected by this.

Under the above circumstances, it is expected to obtain a quantitative measure of mean grain size by solving the scattering problem posed by Eq. (2.1)). The scattering coefficient quantitatively measures the amount of energy removed by individual grains [24] from the forward scattering field of a travelling wave within the medium. It depends on frequency and it is proportional to mean grain size [24, 25, 23]. In the above paper the authors considered polycrystals with cubic symmetry but others have considered triclinic symmetry [52]. More, recently [48] has considered textured polycrystals and was able to express attenuation coefficients for different wave modes. A review of how attenuation is related to mean grain size for polycrystals of different symmetries is given in [29].

2.3 Scalar acoustic waves (SAW)

The discussions below are based on the stochastic Helmholtz equation and its parabolic form. To avoid repeatedly referring to it in words the equation and the parabolic approximation are written without any derivation. Let us denote the wave number by k which is a stochastic process with certain statistical properties. It is customary to denote the three dimensional Laplacian by $\Delta = \frac{\partial^2}{\partial x^2} + \frac{\partial^2}{\partial y^2} + \frac{\partial^2}{\partial z^2}$. The transverse Laplacian shall be denoted by $\Delta' = \frac{\partial^2}{\partial x^2} + \frac{\partial^2}{\partial y^2}$. Thus the Helmholtz equation is

$$\Delta u + k^2 u = 0 \quad (2.4)$$

and in the parabolic form

$$2i\bar{k}\frac{\partial u}{\partial z} + \Delta' u + k^2 u = 0 \quad (2.5)$$

where $\bar{k} = 2\pi/\bar{\lambda}$ is the mean wave-number over all possible realisations of the process $k(\mathbf{r})$ and $\mathbf{r} = (x, y, z)$. The first thought to theoretically describe SAWs in polycrystals would be to consider Eq. (2.1). Equation (2.4) looks simpler than Eq. (2.1) but unfortunately it is not so simple to obtain a solution. Since the primary interest is to use SAWs one would like to have a way of explaining SAWs setting the appropriate boundary conditions for Eq. (2.1) by reducing the problem to Eq. (2.4). The author [40] already mentioned, concluded that it is possible under certain conditions.

2.3.1 Methods of solution for scalar waves

The first step in obtaining a solution to the stochastic equation (2.4) is to reduce it to Eq. (2.5) by neglecting $\partial_{zz}u$ along the propagation distance. The parabolic equation Eq. (2.5) considers only the forward scattering because of the neglected terms leading to one way propagation only. In order to include the back-propagated field the equation is solved for the incident and reflected field [53], separately. Using ray tracing theory it is possible [54] to consider the reflected field in Eq. (2.5).

The difference between equation (2.5) and the one presented in [54] is that the factor $2ik$ is replaced by $2i\bar{k} \exp[i(\beta/\alpha) \exp(2i\bar{k}z)]$ where α is the amplitude of the incident wave and β the amplitude of the reflected wave with $|\beta| < |\alpha|$. The parabolic version of the Helmholtz equation is well known in underwater acoustics [50] where it was first proposed. An overview of the approximation and the range of applicability can be found in [55]. For an update review up to the year 2000 on the importance of the parabolic equation (2.5) and its applications to other areas [56] is a good reference. The authors reviewed most of existing methods of solution to equation (2.5), including numerical methods and extensions made to the theory to include wide angles in wave propagation using paraxial approximations.

The equation (2.5) is confined to narrow angle propagations but authors have improved these limitations by proposing wide angle approximations [57, 56]. More recent methods to study approximated solutions to Eq. (2.4) are efficiently implemented in [58] using the boundary element method. Perturbation theories have also been applied to equation (2.4) for obtaining the mean field [30].

2.3.2 Phase screen method

The phase screen method is widely used in optics for a wide range of applications including propagation of light through aberrating media such as the atmosphere, see [59] and references therein. Strong fluctuations arising from propagation of light through the turbulent atmosphere are studied within the framework of equation (2.5) and the phase screen method in [60]. The formal solution to Eq. (2.5) and the phase screen method is that the integrals representing the field in the former are written in ordinary integrals [60] rather than continual integrals. The analysis in the article is probably the formal justification of the suitability of the phase screen method to wave propagation.

Application of the phase screen method in imaging objects through the atmosphere is given in [61], where the author calculates the statistics of intensity from an object behind a random screen. This article is instructive to look at because of the statistical analysis of propagation involving a phase screen from sources of arbitrary

correlation.

Among the important approximations of practical interest to equation Eq. (2.4) related to phase screen, one could mention the Rytov and Born method among others which are well known in optics and reviewed in [47, 46, 26], for both elastic and scalar waves.

The approximated solution by phase screen

Roughly speaking if one would want to solve Eq. (2.4) within a slab and under the assumption that forward propagation is larger than the backward field, the phase screen is a good approximation. Under these circumstances, the phase of the field is the only modified aspect, having the amplitude field unchanged. This modification simulates the effect of the medium. Usually the amplitude is not modified since the medium is usually considered as a pure phase object but the screen can be an arbitrary transmission object. The field, within the slab is approximated by

$$u(\mathbf{r}) = \int v(\rho)G_0(\mathbf{r}, \rho)e^{i\phi(\rho)}d\rho \quad (2.6)$$

This expansion is analogous to Huygens's expansion [62] for extended sources but with an extra term ϕ which represents the medium. The function v is the incident field to the slab, G_0 is the Green's function of Eq. (2.4) with $k = \bar{k}$, and ϕ is a zero mean Gaussian process with known structure function D_ϕ which is defined as $D_\phi(\rho - \rho') = \langle [\phi(\rho) - \phi(\rho')]^2 \rangle$, where ρ denotes the transverse coordinate. That is, D_ϕ is the variance of the difference of ϕ at two arbitrary points ρ and ρ' in the transverse direction. The Limit of integration in Eq. (2.6) is over the spatial domain of definition of the incident field v passing through the screen.

Taking Eq. (2.6) as the starting point of propagation in a random medium many statistical properties can be obtained such as the spatial correlation function, as one will see in the forthcoming chapters, where Eq. (2.6) is taken as the basic model for propagation.

The statistics of the field u given by Eq. (2.6) depend on the statistical properties

of the processes v and ϕ . In the case when both processes are Gaussian the field u is Gaussian under certain conditions. The authors in [62] have studied the evolution of a Gaussian field under this operation by arbitrary random operators, in particular for operator Eq. (2.6). The authors quantify the strength of operator Eq. (2.6) by means of the variance $\sigma^2 = \langle \phi^2 \rangle$, being a weakly fluctuating operator when $\sigma^2 \ll 1$. Denoting the correlation length of the incident field by l , if $l \ll \sqrt{z/k}$ where z is direction of propagation and k is the mean wave-number, then the field u can be considered a Gaussian process behind the screen, but with a modified correlation function. Other analyses of the evolution of Gaussian fields in random media are revisited in [63]. The authors studied under which conditions a field u , satisfying Eq. (2.4) follows Gaussian statistics for large propagation distances.

2.4 The mutual correlation function

The concept of *correlation* in acoustics is analogous to *coherence* in light propagation. The physical meaning is similar to the coherence of light, and its definition is established mathematically as the second order moment of the field. The second order moment of the field is also called the mutual correlation function. There is *spatial correlation* or *temporal correlation* whether the field is spatially correlated or temporally correlated according to certain mathematical definitions taken from [64, 47].

The mathematical formalism to derive an equation for the moments Γ_n for Eq. (2.4), Eq. (2.5) is difficult and more challenging for Eq. (2.1) where one has to take into account not just the moments of one scalar process but several, depending on the complexity of the moduli $c(\mathbf{r})$. A mathematical formalism was developed in [65] to express the second moments of the process involved in Eq. (2.1)). That is, an expression for quantities characterising the elastic response of a polycrystalline materials such as $\langle \sigma_{ij}(\mathbf{r}) \sigma_{kl}(\mathbf{r}') \rangle$, $\langle \epsilon_{ij}(\mathbf{r}) \epsilon_{kl}(\mathbf{r}') \rangle$, $\langle u_{ij}(\mathbf{r}) u_{kl}(\mathbf{r}') \rangle$, $\langle \sigma_{ij}(\mathbf{r}) u_{kl}(\mathbf{r}') \rangle, \dots, \text{etc.}$, where σ_{ij} , ϵ_{il} and u_{ij} denotes stress, strain and displacement respectively. But, the formulation leads to a complicated expression which is an infinite series, which is at

best difficult and of worst impossible to develop further.

2.4.1 Correlation for a scalar field

The mutual correlation function is nothing else but the second order moment of the field seen as a stochastic process in time and space. Denoting the mutual correlation function or correlation function of the acoustic or electromagnetic field u by $\Gamma_u(\mathbf{r}_1, \mathbf{r}_2, t_1, t_2) = \langle u(\mathbf{r}_1, t_1)u^*(\mathbf{r}_2, t_2) \rangle$, one can define that the field u as *spatially correlated* at $\mathbf{r}_1, \mathbf{r}_2$ if $|\Gamma_u| = 1$ and *spatially uncorrelated* or *not correlated* if $|\Gamma_u| = 0$. If it happens that $0 < |\Gamma_u| < 1$ then the field said to be *partially-correlated*. Analogous definitions follow for the temporal variable or *temporal correlation*.

The above definition describes the correlation of electromagnetic or acoustic fields by means of an ensemble average for the random process u . Thus, the definition could in principle be applied to any random process representing something completely different. Let us denote by Γ_μ the correlation function representing geometric characteristics in a polycrystal. Consider two different points \mathbf{r}, \mathbf{r}' in a hypothetic polycrystal, Fig. (2.1). The function Γ_μ will tell whether or not \mathbf{r}, \mathbf{r}' belong to the same region. In the situation shown in Fig. (2.1), \mathbf{r} belongs to D whereas \mathbf{r}' to D' so in this particular situation the field is expected to be uncorrelated because Γ_μ will be zero. For the rest of this thesis the 2-point correlation function or simply the correlation function is equivalent to 2-point or second order correlation function. A

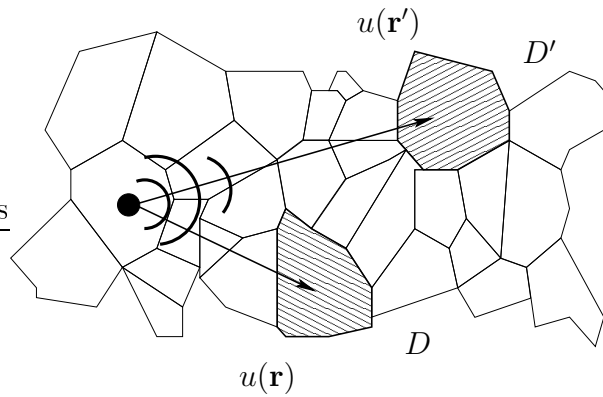


Figure 2.1: The correlation of the field at two different grains in polycrystalline materials.

mathematical theory of the coherence of light has been developed over the years by several authors. In [64] and references therein, the theoretical description is based on the propagation of light using the angular spectral representation or Sommerfeld expansion. Many concepts and developments from this reference have been suitably adapted to suit our needs in SAW propagation. The theory of coherence is not restricted to the second order moments. Other moments such as the fourth moment are also important in atmospheric propagation because it gives a measure of scintillation for stars, [66, 67]. The authors provide an analytical solution for the fourth moment based on Eq. (2.5).

2.4.2 Survey on correlation function

Let us start by introducing the equation for the second order moments in the parabolic approximation. Hence,

$$2i\bar{k}\frac{\partial\Gamma_2}{\partial z} + \Delta'\Gamma_2 + \bar{k}[\mu(\rho) - \mu(\rho')]\Gamma_2 = 0 \quad (2.7)$$

The above equation is derived in [47] from Eq. (2.5). The contribution to the theory of correlation in a random medium is vast and just a few of them will be reviewed here. In what follows, the m -point correlation function is the m -point moment of the acoustic or electromagnetic field that satisfies the stochastic wave equation.

One of the difficult parts in obtaining the m -point correlation function, which temporally will be denoted by Γ_m , is to find a suitable differential equation that is solvable under general terms. Many authors have used some approximations to the wave number characterising the inhomogeneities, in order to obtain useful solutions. The Markov approximation, as it is called, has shown to be the best approximation in many practical applications [47, 68, 63]. To be more specific, the 2-point moment of k bears the following form $\langle k(\mathbf{r}, \xi)k(\mathbf{r}', \xi) \rangle = \delta(z - z')f$, where f is an arbitrary function on the remaining coordinates and very often considered to be isotropic, that is, it depends on a single parameter. The other condition is on the probability law for k where many authors assumed, very often, a Gaussian distribution.

In reference [47], an equation for Γ_m is derived under the Markov approximation. The technique, used in this reference, makes use of the Furutsu-Novikov formula for functionals that depend on processes with Gaussian statistics. The differential Eq. (2.7) is a particular case of this general development. Another derivation of an equation for the moments of arbitrary order is given in [63]. The authors in [47] give a solution for $m = 2$ and discusses possible approximate solutions for $m = 4$. A few years later a solution of the fourth moment equation was presented in [66] for an incident plane wave.

The conditions under which the equation for the moments, in particular equation Eq. (2.7), is obtained are entirely based on the parabolic approximation that begun with the work of [50], where paraxial approximation was first proposed. This approximation has evolved and been used ever since, as reviewed in [56]. A more general development is presented in [69] where the author obtains a differential equation for Γ_m for different wave numbers under the Markov approximation but the Gaussian statistics condition for the wave number has been removed. As the author pointed out, the equation for $m = 2$ is the same as in [47], Eq. (2.7).

Moment equations will be useful in understanding correlation in forthcoming chapters, where the aim will be to give an approximate solution to the second moment with the aid of phase screens. It is worth mentioning that an approximate solution to Γ_4 is given in [67] for an incident plane wave as its solution is related to the phase screen concept used in this work. In the article [70], an approximate solution of the second moment is given by formally approximating a differential operator. The two-frequency mutual correlation function is given in [71] establishing a general power law for the correlation function. The general solution to Eq. (2.7) is given using the method of separation of variables and a modal approach for the differential Eq. (2.7). Other expressions equally important for the correlation function is given in [72], in the case of k a complex process. The important point here is that an explicit form for the correlation is given.

2.5 Simulation of microstructure

The stress-strain behaviour of polycrystalline metals is complicated and difficult to model due to the plastic deformation of grains which can be superimposed on linear Hookean behaviour. The elastic response of polycrystalline materials, expressed either as a solution of Eq. (2.4) or integral representation Eq. (2.6) depends strongly on the statistical properties of the medium. This, on one hand is difficult to predict because of the complexity of real microstructure, whereas on the other, the direct methods for investigating the morphology and statistics of the actual microstructure can be lengthy. Numerical simulation could well provide quicker answers in investigating the elastic response of polycrystalline materials. The authors [44] have simulated microstructure using Voronoi tessellation and comparatively investigated the Reuss and Voigt averages for the effective elastic moduli against the number of simulated grains. The authors concluded that the Reuss and Voigt averages are unaffected by the number of grains considered for the estimation as they closely coincide. The Voronoi tessellation is explained in great detail in the main body of the thesis and how it has been used to obtain realisations of the stochastic phase variation according to formulation Eq. (2.7).

An application of Voronoi tessellation to modelling of grain growth in minerals can be found in [73], and references therein. The analysis of grain growth under mechanical or chemical processes is beyond the scope of this work since one is investigating time-independent configuration of microstructure.

Ultimately, the study of elasticity in polycrystalline materials aims to replace local by global elastic properties and to be able to study the solid macroscopically. The authors in [74] make extensive use of a micro-mechanical model based on Voronoi cells to model elastic properties to obtain the *effective parameters*.

2.6 Ultrasonics

Ultrasound generally has a broad range of applications. It can be bulk, Rayleigh or Lamb waves. It all depends on the specific application. Guided waves can be

used to inspect for metal damage such as corrosion and erosion in pipes in places of difficult access, for instance. A very interesting application of Rayleigh waves is where one can make a map of the actual crystallite structure [75] by measuring the velocity variations within a region on the surface of a polycrystalline materials . This application is in fact directly related to this work and it will be discussed. Accurate description is therefore important for most applications.

Ultrasound, both theoretical and experimental has occupied the scientific community for a long time. A short, but very useful introduction to Rayleigh waves can be found in [76] whereas a more general treatment of elastic waves can be found in [77, 78].

2.6.1 Point sources

The study of point sources over a free surface or half space has been studied extensively. Most of the theoretical descriptions are based on the mathematical theory of Green's function for boundary problems for either partial or ordinary differential equations. This problem goes back to more fundamental problems addressed by many authors such as Lamb at the beginning of the 20th century [79].

One fundamental problem related to ultrasound and surface acoustic waves regardless of source is the calculation of the Green's function for a point source on the surface of a half space. This problem has an answer which is reviewed in [78] among other interesting problems related to different sources.

From the mathematical stand point, the problem of point sources either in three dimensional or half space anisotropic solids has caught the attention of many researchers. The importance of the Green's function has been long recognised to be the answer to many elastic problems such as SAW propagation. There are several methods for obtaining the Green's function of the system. The author in [80] has used Fourier integral representation for an anisotropic elastic half-space. Others have given explicit expressions for the Green's function [81, 22, 21].

Thermoelastic source as point source

A thermoelastic source, such as the one produced by an incident laser beam on a metallic surface can produce elastic waves. SAW waves due to a thermoelastic source have been studied extensively. The author [82] considered transient heating on the surface and studied sources with harmonic variations. Years later, [17] considered the light distribution of an incident pulse laser onto metallic surfaces, as a point source and developed an explicit expression of the Green's function for SAWs.

This theoretical aspect is taken to propagate ultrasonic plane waves in a homogeneous medium. Green's functions give the theoretical advantage of being independent of ultrasound generation. One of the problems is that Green's functions are in general rather difficult to find and when known difficult to implement. In the case of the SAW, the Green's function is known and it can be expanded into plane waves, and is extensively used in this thesis.

The author in [83, 84], however realises that a more accurate description of elastic waves from laser pulse would follow if the spot size is considered as an extended source. The author's motivation was that there is an extra spike in the waveform that the theory in [17] could not satisfactorily explain.

SAW waves from extended sources

The theory of extended sources would follow from that for a point source because it is just an integral over the region occupied by the source. In practice this can represent difficulties. For instance, in the OSAM system one would use arcs for ultrasonic generation of acoustic waves and the integration over such sources can be difficult. There has been a lot of attention to the problem of ultrasound from extended sources, [83, 85].

Analysis of extended sources closer to one used by the OSAM have appeared in [86]. The authors have carried out the calculations of Rayleigh waveforms from a thermoelastic line source. They gave an exact expression for the normal displacement. In order to find mechanical displacement, the authors assumed that the main contribution comes from the centre of the line by assuming the width of line in the

direction of propagation infinitely small and thus integration is reduced to one variable across the line source. The authors in [87] studied similar sources delivered by the SLM in the OSAM system. They used a four-element laser line array cut from a cylindrical lens.

2.6.2 Ultrasonics generation

Ultrasound or SAW waves can be generated from a wide variety of devices. The piezoelectric transducer is commonly use as a device for detection of sound as well as source generation. Fig. (2.2) shows a simplified version of typical experimental setup for SAWs using a transducer to generate ultrasound. The transducer is attached to a wedge, normally made of perspex, using a water based couplant. The author in [76] discusses some of the common transducer and boundary conditions to generate SAWs in this geometry.

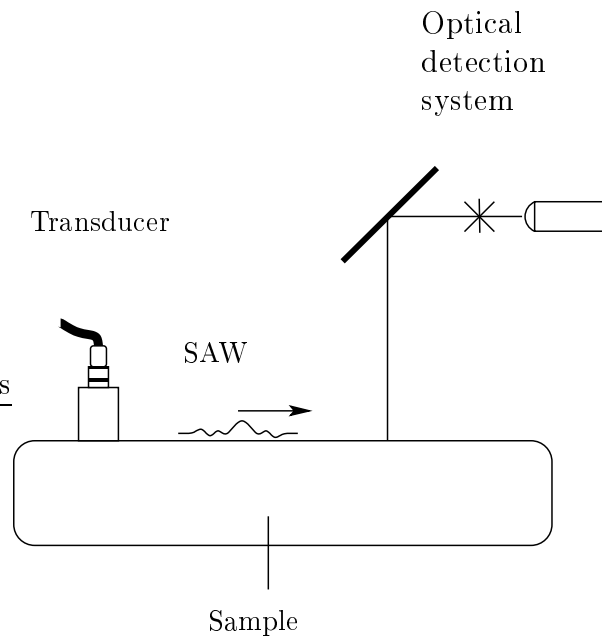


Figure 2.2: Simplified representation of a typical experimental setup SAW generation using a transducer as source of ultrasound. The detection system can vary but it could be used the knife-edge detection system.

The detection system can vary from system to system, so it could well be another transducer. The optical detection of system used in this thesis for the experimental work is based on the knife-edge technique [16] for detecting small displacements by

using a laser as probe.

Laser ultrasonics

Lasers are preferred in many applications for both ultrasonic detection and generation due to their non-contact nature. Sometimes this can be disadvantageous because ultrasound-laser generation prototype systems can be expensive and difficult to operate because they require highly accurate optical arrangements. This technique requires the surface of the sample to be polished to a mirror finish in order for the detection system to efficiently work. A good reference for laser ultrasonics would be [88].

An Optical Scanning Acoustical Microscope (OSAM) was used in this thesis for imaging SAW waves in metals. This system uses a Spatial Light Modulator (SLM) to image a pattern of light onto the surface of the sample for ultrasound generation. The pattern is modified to either focused SAW or to simply propagate a plane surface wave. The development of the OSAM has been published in a series of articles by the Applied Optics Group, at the University of Nottingham [89, 19, 14]. The main optical parts of the system are shown in chapter (6).

Chapter 3

Waves in polycrystalline materials

Introduction

The aim of this chapter is to introduce SAWs in polycrystalline materials by means of a general formulation for elastic waves in inhomogeneous media. The theory is first introduced trying to keep generality to include linear elastic theory for homogeneous medium. The theory is applied to materials with observable microstructure, that is, those one-phased materials composed of grains that can have an effect on elastic propagation at a certain scale. The theoretical model is based on stochastic process representing physical microscopical variations as well as elastic properties of the material.

In order to describe microscopic and macroscopic characteristics a brief introduction to stochastic processes is given. This is the first part of the chapter which briefly introduces many of the tools needed for elastic propagation.

The elasticity theory for polycrystals is then introduced for elastic wave modes that may arise in this type of medium, in particular to problems in a half space. The use of the full wave theory is rather complicated even for solids with no microstructure, so a connection is made to the scalar theory to describe SAWs in random media. The scalar theory uses the stochastic wave equation for waves in random media which is normally presented as the Helmholtz equation.

In most stochastic models describing physical quantities, such as geometric char-

acteristics of polycrystals, first and second order moments are the most important quantities. In particular the second moment, since it is related to the correlation of the acoustic field, is emphasised in this thesis.

The stochastic wave equation is a widely and well accepted model for sound propagation in other areas, such as underwater acoustics. There are certain limitations on its use as a general solution which has not yet been established. One important approximation, called the *parabolic or paraxial approximation* has been widely used in underwater acoustics. Its range of applicability is given in [50, 56]. This approximation has been used here to obtain an approximated description of SAW propagation in random media combined with a phase screen model used in optics, which is developed in [59].

3.1 Theory of elastic waves in stochastic media

The notion of mean, second and higher order moments is defined in terms of probability theory. This introduction is rather brief but an extended introduction can be found in any book on stochastic processes [90, 39]. For a more physical exposition and application of stochastic processes, [64, 46] are good references.

Preliminary on random processes

The probability space is a class $\{P, p\}$ where P is the space of events and p is a set function taking values in the interval $[0, 1]$. A random variable in $\{P, p\}$ is a set of real or complex numbers $\{x(\xi)\}_{\xi \in P}$ with probability distribution p . The set P can be either a countable or uncountable set, and so $x(\xi)$ is a discrete or continuous random variable, respectively.

A random process or random field is a family of spatial functions $\mu(\mathbf{r}, \xi)$, where μ is a random variable for each $\mathbf{r} \in \mathbb{R}^3$. This means that μ has its own probability distribution p_{μ_r} for every \mathbf{r} from which moments can be defined. These random variables belong to the same probability space P . The set $\mu(\mathbf{r}, \xi)$ is called an *ensemble* and *realisation* for a fixed ξ .

In order to fully describe a physical phenomenon represented by a process μ it is necessary to specify the distributions p_μ . There is a large list of probability distributions to describe physical phenomena. In [90], a vast list of probability distribution and their main properties are given. In particular, the Gaussian distribution would be of interest for modelling wave propagation in random media. As an example, the multivariable Gaussian distribution is presented. Let $x_1 = x(\mathbf{r}_1, \xi), \dots, x_n = x(\mathbf{r}_n, \xi)$ be n random variables thus its n -fold distribution is

$$p = \frac{1}{(2\pi)^{n/2} \sigma_1 \dots \sigma_n} \exp \left[-\frac{1}{2} \sum \frac{\Delta^2 y_i}{2\sigma_i^2} \right] \quad (3.1)$$

This probability distribution will be useful in obtaining the mean correlation of the field in forthcoming chapters. Here, y_i are arbitrary variables indicating that p is function in several variables. The parameters $\sigma_1^2, \dots, \sigma_n^2$ completely characterise the random variables $x_i(\mathbf{r}_i)$. These parameters are in fact the variance of the random processes x_i , which are defined below using the distribution Eq. (3.1).

The properties of a process, such as the mean defined below, are defined in terms of distributions. Such definitions can be found in any standard book on stochastic processes such as the ones already mentioned.

As matter of introduction the 1-point moment of order k is defined and denoted as

$$m_{\mathbf{r}\mathbf{r}'}^k = \langle \mu^k(\mathbf{r}, \xi) \rangle = \int \mu_{\mathbf{r}} p_{\mu_{\mathbf{r}}} d\mu_{\mathbf{r}} \quad (3.2)$$

Here $\mu_{\mathbf{r}}$ is a dummy variable. The first moments bear special names, $k = 1$ gives the mean value whereas $k = 2$ corresponds to the variance. These are the most important moments as many random process can be described solely by these two parameters. If one would like to extend the above definition for the 2-point or second moment, the definition will read

$$\langle \mu(\mathbf{r}, \xi), \mu(\mathbf{r}', \xi) \rangle = \int \mu_{\mathbf{r}} \mu_{\mathbf{r}'} p_{\mu_{\mathbf{r}} \mu_{\mathbf{r}'}} d\mu_{\mathbf{r}} \mu_{\mathbf{r}'} \quad (3.3)$$

Here $p_{\mu_{\mathbf{r}} \mu_{\mathbf{r}'}}$ denotes the two-fold probability density. In general $p_{\mu_{\mathbf{r}} \mu_{\mathbf{r}'}}$ is a interlinked

function of two variables that allows to calculate integral Eq. (3.3). It is difficult very often in practice to know an expression for $p_{\mu_r \mu_{r'}}$. A random processes is said to be statistically independent if its two-fold distribution splits as $p_{\mu_r \mu_{r'}} = p_{\mu_r} p_{\mu_{r'}}$. Analogously for any finite number $\mu_1 = \mu(\mathbf{r}_1, \xi), \dots, \mu_n = \mu(\mathbf{r}_n, \xi)$ of random processes, they become statistically independent if their n -fold distribution decompose as $p_{\mu_1 \dots \mu_n} = p_{\mu_1} \dots p_{\mu_n}$. Random processes of this type are easily handled especially if the $\mu(\mathbf{r})$ are Gaussian variables.

In forthcoming sections the above definitions on stochastic process will be used to describe the theory of elastic waves in polycrystalline materials. The stochastic process will be used without specifying a probability distribution.

3.2 Elastic waves in polycrystals

A polycrystalline material is any material that is composed of anisotropic grains with highly correlated elastic and geometric properties, e.g. aluminium. The grains have random orientation with respect to each other as well as random spatial distribution. Among other properties of grains in polycrystals, there is crystal plasticity and atomic lattice evolution of polycrystalline metals. Materials subjected to time dependent processes were not studied in this work, but good references on the subject are [73, 39]. In this thesis, the beginning is to describe elastic wave propagation in a given random spatial grain configuration.

The theory is based on the classical approach for elastic waves, the main difference being that the elastic moduli $c_{ijkl}(\mathbf{r})$, which are tensor functions that characterise the elastic properties of polycrystals, are assumed to vary randomly through space, [40, 49]. The theory is defined, in principle for any polycrystal. There are some constraints imposed on the polycrystals in order to simplify theoretical aspects of elastic waves. Here we reproduce some of the assumptions, which are very often used for theoretical prediction of waves modes in polycrystals, which appeared in [91].

1. Linear elasticity holds.

2. The anisotropy is small within individual grains or grains can be considered locally isotropic.
3. The grains are mainly convex regions and equiaxed. Equiaxed means that the diameter of the grain in each direction and the mean calliper diameter differ slightly.
4. The crystallographic axes of the individual grain has no preferred orientation; all orientations are equally likely.
5. The polycrystalline materials is single-phased with no voids or inclusions.

The aluminium samples analysed in this work, which are presented in chapter (6), hold condition (3), (5). The hypothesis (2) quite possible since aluminium shows relatively small elastic anisotropic behaviour. In this thesis an extra hypothesis or statement will be necessary in order to describe SAWs in polycrystalline materials. That is, the stochastic scalar approximation will suffice to describe SAWs. This is discussed in section (3.3.1) since it requires some explanation. From now on, the terms *inhomogeneous* or *heterogenous* media will be used as synonymous, and assumed to refer to any polycrystal or medium with random characteristics. Homogeneous is the opposite to inhomogeneous material, which is relative to wavelength. For instance, a polycrystal could be considered elastically homogenous if the wavelength is greater than the largest scale of grains within the polycrystals. A homogenous material at all scales relative to wavelength would be glass, for instance.

3.2.1 Linear elastic polycrystal

The theory of elastic waves in heterogeneous media is entirely analogous to the theory of linear elasticity for homogeneous solids. There is no surprise that the governing equation looks similar. In the discussion that follows, Einstein's summation convention is assumed; i.e. the summation over repeated indices is implied. Let us denote a point in the three dimensional space by $\mathbf{r} = (x_1, x_2, x_3)$, and the broken brackets $\langle \dots \rangle$ denote ensemble average.

The theory of elasticity in polycrystalline materials is based on the following model, known as *Hooke's law*:

$$\sigma_{ij} = c_{ijlm}(\mathbf{r})\epsilon_{lm} \quad (3.4)$$

where σ_{ij} denotes the stress tensor and ϵ_{lm} the strain tensor; c_{ijkl} is the tensor random field characterising the elastic properties of the medium. The obvious difference here to the stress-strain relationship for non-polycrystalline materials is that the *elastic moduli* c_{ijkl} is a random tensor field. The indices runs from 1 to 3 so one has 81 random process describing local elastic properties of the polycrystal as a linear elastic homogenous material.

The statement for linear elastic homogenous materials of Hooke's law is recovered by taking the c_{ijkl} to be independent of \mathbf{r} in Eq. (3.4). The macroscopic elastic properties of polycrystalline materials are measured by measuring the elastic moduli which can be found reported elsewhere for a great variety of materials. The microscopic elastic properties for polycrystalline materials, that is, taken into account microstructure, is obviously a much harder task since one would have to measure a random field; possibly by empirically specifying the probability distribution. One alternative for specifying the $c_{ijkl}(\mathbf{r})$ is to measured what is called the *effective parameters* based on certain spatial averages along grain orientations. Thus, the elastic moduli are specified as an average along grain orientation plus a fluctuating part. This is a very important point that will be discussed more broadly in section (3.2.2).

The effective parameters theory intended to explain the elastic response of polycrystals by homogenising the system. That is, replacing the overall elastic response for one that behaves as it were homogeneous. One of the difficulties is how to express the effective parameters as a function of the moments $\langle c_{ijkl}(\mathbf{r}) \rangle$, $\langle c_{ijkl}(\mathbf{r})c_{pqrs}(\mathbf{r}') \rangle$, ... of individual components of the elastic moduli. Some authors have found bounds for effective bulk modulus [92]. A brief introduction to the subject and list of references can be found in [26]. The effective parameter theory is not reviewed in this work but it will use some of the well established theoretical aspects for averaging the elastic

moduli based on the micro-characteristics of polycrystals.

3.2.2 The effective parameters

The effective parameters are important in specifying the elastic moduli $c_{ijkl}(\mathbf{r})$. These parameters are defined in terms of certain averages over the orientation. To avoid writing every time the sub-indices $ijkl$, the elastic moduli are also written by the single character $c(\mathbf{r})$.

Let us first review single grains characterised by assuming that the tensor $c(\mathbf{r})$ is constant. If a non-singular linear transformation T is applied to c , therefore changing their numeric values, the grain is said to be anisotropic. The transformation would be an axis rotation since the c are invariant under translations. Let us consider

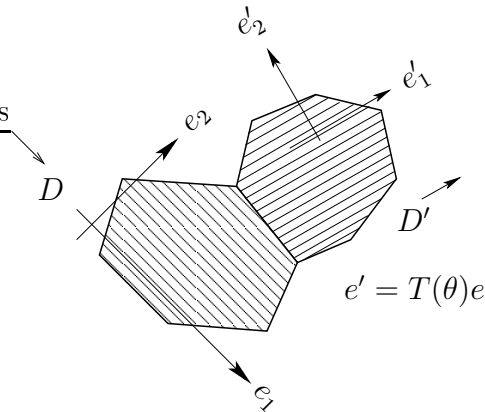


Figure 3.1: Anisotropy of polycrystalline materials

two adjacent grains belonging to a certain polycrystalline material. Denoting the stiffness by c in the coordinate system $\mathbf{e} = (e_1, e_2)$ attached to grain D and by c' in the new system \mathbf{e}' attached also to D' . The axes \mathbf{e} are called crystallographic axes that define a coordinate system within the grain. These axes are chosen in terms of the lattice and symmetries of the grain. In general, depending on the complexity of the grain, the crystallographic axes are not orthogonal systems and sometimes the number of axes needed exceed the dimension of the grain. Here for simplicity, two orthogonal axes define a coordinate system within the grain, Fig. (3.1).

If one performs the experiment of measuring c and c' independently in the direction indicated by the arrows on top of D and D' , Fig. (3.1) then $c = c'$. This is

because D, D' have identical elastic characteristics but different shape and different orientation relative to each other. Now, if one fixes a coordinate system, let say \mathbf{e} and $T(\theta)$ denotes the transformation between the coordinate system \mathbf{e}, \mathbf{e}' thus $c' = T(\theta)c$. What makes a polycrystalline material a special type of medium is that θ is a random variable, therefore one speaks of materials composed of anisotropic grains with random orientation. The macroscopic elastic response of polycrystalline materials is characterised by the effective parameters defined as $c^0 = \langle T(\theta)c(\mathbf{r}) \rangle_0$, where $\langle \cdot \rangle_0$ is the average over the orientation. The average could be well defined using Reuss's average Eq. (2.2). This, average or effective parameters, coincides with the elastic moduli for homogenous solids.

Based on this average, the elastic response of a polycrystalline material is modelled as random fluctuations with respect to c^0 , that is $c(\mathbf{r}) = c^0 + c'(\mathbf{r})$ where c' is a zero mean random tensor. Grains have their own symmetry, depending on their lattice that generates the grain itself. In terms of c^0 they are classified as: monoclinic, orthorhombic, cubic, etc., depending on the symmetry and form of c^0 . We shall take here, grains with cubic symmetry since aluminium can be considered to have this type of symmetry as an anisotropic solid. Then a grain having cubic symmetry is characterised with elastic moduli having the following form

$$c^0 = \begin{bmatrix} c_{11} & c_{12} & c_{12} & 0 & 0 & 0 \\ c_{12} & c_{11} & c_{12} & 0 & 0 & 0 \\ c_{12} & c_{12} & c_{11} & 0 & 0 & 0 \\ 0 & 0 & 0 & c_{44} & 0 & 0 \\ 0 & 0 & 0 & 0 & c_{44} & 0 \\ 0 & 0 & 0 & 0 & 0 & c_{44} \end{bmatrix} \quad (3.5)$$

Thus, three scalar random processes $c_{11}(\mathbf{r}), c_{12}(\mathbf{r}), c_{44}(\mathbf{r})$ are needed for an elastic description of a polycrystalline material with cubic symmetry.

3.2.3 The anisotropy of the grains

In theory the main contribution to of aberrations is the anisotropy of the individual constituents of the polycrystal. The degree of anisotropy of polycrystals shall be described in terms of the elastic moduli $c(\mathbf{r})$, where the non-fluctuating part c^0 will have the form Eq. (3.5). The anisotropy of each grain is given as [23, 24]

$$\beta(\mathbf{r}) = c_{11}(\mathbf{r}) - c_{12}(\mathbf{r}) - 2c_{44}(\mathbf{r}) \quad (3.6)$$

It is understood that all the quantities here depend on position including β , so it will not be written in the next paragraph. If grains within the polycrystalline materials were isotropic, i.e. $\beta = 0$ then $c_{44} = (c_{11} - c_{12})/2$, $c_{11} = \lambda + 2\mu$ and $c_{12} = \lambda$ where λ, μ are constants within grains which correspond to Lamé constants [36] for isotropic solids. Thus, in this case the overall aberrations or deviation of the acoustic field would come purely from scattering at grain boundaries with no contribution from the anisotropy of individual grains. In the same sense, if β is a small varying parameter, the polycrystalline materials are considered as being locally isotropic or weakly anisotropic.

The type of material studied in this thesis could be well considered as being macroscopically isotropic or that the anisotropy is weak from one region into another; it seems plausible to assume that $c(\mathbf{r})$ depends on only two scalar random fields $\lambda(\mathbf{r})$, $\mu(\mathbf{r})$, thus $c(\mathbf{r})$ could have the form [93, 26],

$$c(\mathbf{r}) = \lambda(\mathbf{r})\delta_{ij}\delta_{kl} + \mu(\mathbf{r})(\delta_{ik}\delta_{jl} + \delta_{il}\delta_{jk}) \quad (3.7)$$

where δ_{ij} is Kronecker's delta function.

This is the familiar form of the elastic moduli for isotropic linear elastic solids with λ, μ set to constants; which are termed Lamé constants or elastic constants for isotropic solids. The local isotropy or weak anisotropy will be useful for theoretical purposes since SAWs in polycrystalline materials can be reduced to scalar theory by using Eq. (3.5) for the elastic moduli [40].

3.2.4 The elastodynamics equations

In this section the elastodynamics equations are presented for a three dimensional body and later are specialised for SAWs. The displacement occurring in all directions of the body under stress are being denoted by U_i , $i = 1, 2, 3$. In the presence of external forces F the stress and strain tensors are dynamically related to the displacement $U_i(\mathbf{r}, t)$ occurring within the medium by

$$\sigma_{ij,j} + F_i = \rho \frac{\partial^2 U_i}{\partial t^2} \quad (3.8)$$

$$\epsilon_{ij} = \frac{1}{2}(U_{i,j} + U_{j,i}) \quad (3.9)$$

Combining Eq. (3.4), Eq. (3.8), Eq. (3.5) and assuming $U_i(\mathbf{r}, t) = u_i(\mathbf{r}, \omega)e^{-i\omega t}$, i.e. assuming that the displacement are monochromatic fields for simplicity, gives the governing equations for an polycrystalline material and no external forces as

$$\frac{\partial}{\partial x_j} (c(\mathbf{r}, \xi)u_{k,l}(\mathbf{r}, \xi)) + \rho\omega^2 u_i(\mathbf{r}, \xi) = 0 \quad (3.10)$$

The density ρ is assumed to be constant. This is equivalent to hypothesis (5) in section (3.2), where the polycrystal is assumed with to have no voids or inclusions. In Eq. (3.10) the following convention is used $\frac{\partial u_k}{\partial x_s} = u_{k,s}$ for short.

Equations Eq. (3.10) give the elastic displacement u_k , $k = 1, 2, 3$ in all directions in the polycrystal. This means, in terms of probability theory, finding the probability distributions which define entirely the displacements u_k as random fields. From these probability distributions, it is possible at least in theory, to calculate all moments of the random field u_k . This approach is beyond the scope of this thesis, so the solution is formulated in terms of moments of the random fields involved, which is described below.

Ultimately, the important part in the problem are the moments of the random field displacements, therefore the problem can be put in the following way: given the moments $\Gamma_{ijkl} = \langle c_{ijkl}(\mathbf{r}) \rangle$, $\Gamma_{pqrs}^{ijkl} = \langle c_{ijkl}(\mathbf{r})c_{pqrs}(\mathbf{r}') \rangle, \dots$ of elastic moduli or in terms of two scalar random fields $\lambda(\mathbf{r})$, $\mu(\mathbf{r})$ if c_{ijkl} is given by Eq. (3.7), $\Gamma_\lambda =$

$\langle \lambda(\mathbf{r}) \rangle, \Gamma_{\lambda\lambda'} \langle \lambda(\mathbf{r})\lambda(\mathbf{r}') \rangle, \dots, \Gamma_{\mu} = \langle \boldsymbol{\mu}(\mathbf{r}) \rangle, \Gamma_{\mu\mu'} = \langle \boldsymbol{\mu}(\mathbf{r})\boldsymbol{\mu}(\mathbf{r}') \rangle, \dots$, the problem is to find the corresponding moments $\Gamma_{u_k} = \langle u_k(\mathbf{r}) \rangle, \Gamma_{u_k u_r} = \langle u_k(\mathbf{r})u_r(\mathbf{r}') \rangle, \dots$ for the displacement in terms of $\Gamma_{ijkl}, \Gamma_{ijkl}^{pqrs}, \dots$ or $\Gamma_{\lambda}, \Gamma_{\lambda\mu}, \dots$. The most direct method in obtaining this relationship is to find a differential equation for all the moments $\Gamma_{u_k}, \Gamma_{u_k u_r}, \dots$ which has been proved to be an extremely difficult problem. Nevertheless, the authors in [93] derived an equation for the first moment Γ_{u_k} in terms of a infinite series which contained all the moments of the elastic moduli.

For the particular case of SAWs in polycrystalline material, the above formulation will be reduced to find the moments for the displacement in one single direction. Since this is a special case of a more general formulation, the SAW case is reformulated using the two dimensional stochastic wave in section (3.3). The above formulation applies equally to scalar theory governed by the stochastic Helmholtz equation in the sense that an equation for the correlation function can be obtained under certain conditions. This is explained in detail in chapter (5).

The anisotropy can also be described in terms of velocity variations within grains. Thus, locally the longitudinal and transverse velocity in terms of the elastic moduli are given [24] as $v_l(\mathbf{r}) = \sqrt{c_{11}(\mathbf{r})/\rho}$ and $v_s(\mathbf{r}) = \sqrt{c_{44}(\mathbf{r})/\rho}$, where v_l, v_s is the longitudinal and shear velocity, respectively in a polycrystalline material. The degree of inhomogeneity in the scalar description is also given in terms of these velocities as Rayleigh wave velocity is a function of the shear and longitudinal wave velocities. The development of this relationship is given in section (3.3.2).

The type of problem that concerns this work is two dimensional. The full wave theory would describe wave modes of any type as stated in Eq. (3.10), in particular SAWs. However, it is complicated to establish a solution under the boundary conditions for a SAW. A more precise meaning of the above problem formulation for SAW is given section (3.3).

3.3 SAWs in polycrystalline materials

In chapter (4) a theoretical description of SAWs is developed for the homogeneous medium, governed by Eq. (3.10) when $c' = 0$. A concise description of a SAW source and SAW devices is also presented. For the time being, an approximate solution for SAW is given below where the full wave is reduced to the stochastic Helmholtz equation in two dimensions.

The term SAWs has been used to stand for surface acoustic waves without stating precisely what they are. One would simply say that SAW is a two-dimensional wave travelling near or at the surface of a sample or half space as shown in Fig. (3.2). This wave emanates from a finite line source along x travelling in direction z . The

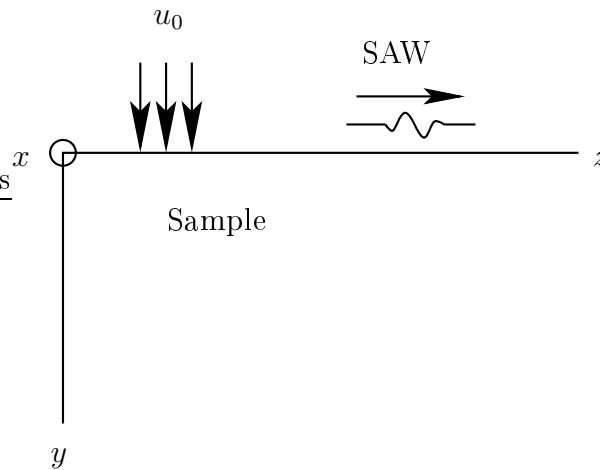


Figure 3.2: Geometry of SAW in polycrystals. The vertical arrows pointing downwards indicate the location of the initial field displacement u_0 . The horizontal arrow is indicating the direction in which a SAW propagates.

use of a finite line source is simply because the experimental setup uses a source of this type, but SAWs are not restricted to this geometry.

Formally, ultrasound on the surface is a Rayleigh wave. Thus, the particle motion is confined to the yz plane being motionless in x direction. Rayleigh waves, strictly speaking depend on depth, y in this case but decay rapidly [76]. In the type of SAW studied here, depth is unimportant but what is really important is the normal displacement to the plane xz , which shall be denoted by u_y or simply u . The Rayleigh wave motion is described simultaneously by the displacement in the other

directions which describe an elliptic particle motion.

The statement of the problem in general terms is to find a single random field that satisfies Eq. (3.10), with boundary conditions $u(x, y, 0)$ at $z = 0$. In fact, the main interest is the second order moment $\langle u(\mathbf{r})u(\mathbf{r}') \rangle$ and to the author's knowledge, it has not been reported in the literature. Many articles, however have written on the first moments of the field satisfying Eq. (3.10) for different wave modes and crystals symmetries [48].

Since one single field is needed to describe a SAW in the geometry of Fig. (3.2), it seems that scalar approximations would be appropriate for the present problem.

3.3.1 The scalar approximation

The boundary problem established in section (3.3) in elasticity terms is a lateral shear motion. That is, the particle motion is perpendicular to the plane xz . If one assumes local isotropy, that is the elastic moduli has the form Eq. (3.7), the mathematical formulation developed in [40] establish that SAW in polycrystals can be described by a stochastic scalar equation. That is, u satisfying Eq. (3.10) can be described by a single stochastic scalar equation. The author has reduced the problem to the parabolic version of the stochastic Helmholtz equation. There is no way of proving at present that Eq. (3.10) can always be reduced to a scalar equation for the normal displacement u , for polycrystals of general anisotropy, that is those polycrystals with elastic moduli not of the form Eq. (3.7). Therefore, the additional hypothesis to the ones introduced in section (3.2), is that a SAW can be described by a stochastic scalar equation which corresponds to the Helmholtz equation. From now on, $k_0 = 2\pi/\bar{\lambda}$ will denote a mean wave number where $\bar{\lambda}$ is the mean Rayleigh wavelength, Δ the Laplacian operator in two dimensions and \bar{v} is the mean Rayleigh wave velocity. Thus, SAW in a polycrystal for the geometry depicted in Fig. (2.1) can be described by

$$\begin{aligned}\Delta u(\mathbf{r}, \xi) + k_0^2 u &= -k_0^2 \boldsymbol{\mu}(\mathbf{r}, \xi) u(\mathbf{r}, \xi) \\ u(x, 0) &= w(x)\end{aligned}\tag{3.11}$$

where

$$k^2(\mathbf{r}, \xi) = k_0^2 \left(\frac{\bar{v}}{v(\mathbf{r}, \xi)} \right)^2 = k_0^2 (1 + \mu(\mathbf{r}, \xi))^2 \quad (3.12)$$

and μ would be a zero mean Gaussian random function that relates to the inhomogeneity of the medium. The boundary problem Eq. (3.10) has been reduced to the boundary problem Eq. (3.11) with initial boundary condition $w(x)$ in the plane x . u is a scalar that corresponds to normal displacement, in practice the displacement is a vector within plane components. Here, we neglect the effect of these on the basis that normal(scalar) displacements exhibit the statistical behaviour characteristic of the full displacement field.

Based on this model for SAW in polycrystals the problem will be to obtain an expression for the mean correlation function $\langle uu^* \rangle$, which is the subject of chapter (5). The first thing to do would be to construct an approximate solution to Eq. (3.11) based on a screen model. But first, one has to specify moments of the random process μ and certain conditions where it is possible to give an approximate solution of the boundary problem.

3.3.2 The degree of inhomogeneity

The scalar theory does not distinguish between the elastic properties of the grains. The grains, in this theory are considered random scatterers characterised by a wave number which is a random function of position and characterised by the stochastic equation, in particular the first and second moments. The wave number is modelled as fluctuations with respect to the background wave number, this is the mean along the ensemble of scatterers. The wave number, which is normally expressed in terms of a zero mean function μ in Eq. (3.12), which is the random fluctuations of the acoustic field. Those random fluctuations are quantified by the degree of inhomogeneity defined as

$$\sigma = \frac{1}{k_0} \sqrt{\langle [k(\mathbf{r}) - k_0]^2 \rangle} \quad (3.13)$$

Eq. (3.13) measures the random fluctuation with respect to the mean wave number k_0 . The brackets here denote an ensemble average. The average is taken along all realisations for the spatial grain configurations.

The ultrasound considered here is a SAW that travels with the Rayleigh wave velocity. It is well known that, this velocity in terms of the Poisson ratio ν is approximately given by [76]

$$\begin{aligned} v &= \frac{0.862 + 1.14\nu}{1 + \nu} v_s \\ &= p(\nu) v_s \end{aligned} \quad (3.14)$$

The velocity at which the SAW is travelling in a polycrystalline material can therefore be given as $p(\nu)v_s(\mathbf{r})$, where $v_s(\mathbf{r})$ is the velocity for shear waves previously defined for polycrystalline materials. Thus, the wave number in terms of v_s has the form

$$\begin{aligned} k(\mathbf{r}) &= \frac{\omega}{v(\mathbf{r})} \\ &= \frac{\omega}{p(\nu)v_s(\mathbf{r})} \end{aligned} \quad (3.15)$$

The inhomogeneity degree defined in Eq. (3.13) relates in an obvious way to the variance of process μ . The standard deviation for μ is defined as $\sigma = \sqrt{\langle \mu^2 \rangle}$; it shall be seen that σ is important in the correlation of the field. The second moments of k are defined in terms of this parameter. From now on, σ and the degree of inhomogeneity would mean exactly the same quantity. The parameter σ can be expressed in terms of the fluctuations of the elastic moduli in polycrystalline materials. Recalling that $v_s(\mathbf{r}) = \sqrt{c_{44}(\mathbf{r})/\rho}$ is defined in terms of the scalar process c_{44} , let c' denote the fluctuations with respect to the mean c_{44}^0 ; thus

$$c'_{44} = \frac{c_{44}(\mathbf{r}) - c_{44}^0}{c_{44}^0} \quad (3.16)$$

From Eq. (3.15), after inserting the definition for the velocity v_s the ratio $(k(\mathbf{r}) -$

$k_0)/k_0$ in terms of c_{44} and c_{44}^0 is given by

$$\begin{aligned}
 \frac{k - k_0}{k_0} &= \frac{\sqrt{c_{44}^0} - \sqrt{c_{44}(\mathbf{r})}}{\sqrt{c_{44}(\mathbf{r})}} \\
 &= \sqrt{\frac{c_{44}^0}{c_{44}(\mathbf{r})}} - 1 \\
 &= \frac{1}{\sqrt{c'_{44} + 1}} - 1
 \end{aligned} \tag{3.17}$$

If the fluctuations within a grain are small, that is $\|c'_{44}\| \ll 1$, the term on the right hand side in Eq. (3.17) is approximated by the linear term of its Taylor expansion around zero. In doing so,

$$\begin{aligned}
 \frac{1}{\sqrt{c'_{44} + 1}} - 1 &= \left(1 - \frac{1}{2}c'_{44} + \frac{3}{8}(c'_{44})^2 + \dots\right) - 1 \\
 &\approx -\frac{1}{2}c'_{44}
 \end{aligned} \tag{3.18}$$

Squaring both sides of Eq. (3.17) and inserting Eq. (3.18) in the expression, the standard deviation or degree of inhomogeneity σ in terms of the anisotropy fluctuation within grains is given by

$$\sigma \approx \frac{\sqrt{\langle (c'_{44})^2 \rangle}}{2} \tag{3.19}$$

The physical meaning of the standard deviation is now clear from Eq. (3.19). The standard deviation is half the standard deviation of one entry of the elastic moduli matrix. This entry accounts for wave velocity fluctuations with the grains. Thus, the standard deviation σ measures the overall degree of anisotropy of polycrystalline materials. The standard deviation can also be related to statistical geometrical characteristics of polycrystals via a correlation function of the wave-number. In the following section it will be seen in which way σ relates to the correlation function of k .

3.3.3 The statistical characteristics of the medium

Real materials can have very complicated microstructures, so an approximate description is potentially susceptible to large errors. In general, grains can be considered as randomly distributed spatially with preferred or random orientation, and macroscopically the material can be isotropic or anisotropic. “Randomly distributed” or just “randomly” is being used here as a generic word; so the spatial arrangement of grains may follow any probability distribution. Here, for theoretical simplifications the sample is considered as being composed of randomly oriented scatterers which are either isotropic or weakly anisotropic. This is a restrictive approximation but it appears to be justified as it explains many of the observed phenomena.

At this stage, no progress can be made without assuming statistical properties for μ . There is experimental evidence, which is the subject of chapter (6), to assume μ to be Gaussian and locally isotropic. By local isotropy (isotropy in the stochastic processes context), it means that $D_\mu = \langle [\mu(\mathbf{r}) - \mu(\mathbf{r}')]^2 \rangle$ depends only on the difference $r = \|\mathbf{r} - \mathbf{r}'\|$ and that the correlation of μ is invariant under translations. This assumption is necessary in order to give an approximated solution to $\langle u(\mathbf{r})u(\mathbf{r}') \rangle$.

Another important point is the grain shape, which can be described based on the scale length l . This length explicitly describes the form of correlation $\Gamma_k = \langle \mathbf{k}(\mathbf{r})\mathbf{k}(\mathbf{r}') \rangle$, which also fully describes μ . A single model is being used which characterises μ statistically in terms of σ and l . This is a fair representation of metals with equiaxed grains whose spatial distribution can be described by an isotropic random function. Complex structures such as inhomogeneous grain size distribution -elongated grains- will require a more sophisticated model. Micro-structures with grains elongated in a preferred direction can experimentally be investigated by propagating ultrasound at multiple directions.

Moreover, in what follows the second order moment $\Gamma_\mu = \langle \mu(\mathbf{r})\mu(\mathbf{r}') \rangle$ can take any form as long as it is a function of $\mathbf{r} - \mathbf{r}'$ only. But the exponential form $\Gamma_\mu = \sigma^2 \exp[-|\mathbf{r} - \mathbf{r}'|^2/l^2]$ has been shown to be useful in other areas to describe real physical phenomena, [47]. The function Γ_u will depend on two parameters in this approximation: the degree of anisotropy and a correlation length l . The correlation

l indicates the distance where two points bear no statistical correlation, that is for two points, such that $\|\mathbf{r} - \mathbf{r}'\| > l$ then $\Gamma_\mu \rightarrow 0$. This correlation distance is closely related to the mean diameter of the grains. They are, in fact the same quantity as shown in section (3.3.3) below, where a precise meaning of the diameter of the grain is also introduced.

Mean grain size

The mean grain size or more general geometric features of microstructure are important parameters in material characterisation. There is no simple method or even a simple number that best describes geometrical features of grains. There are several standards for measuring grain size used in industry. One very popular among metallurgists that uses a statistical estimation of mean grain diameter by laying out line segments of random length on a micrograph and counting the number of grain boundary intersections [94] within segments.

Many other important stereological methods are available to describe geometric features for a given configuration of microstructure which are reviewed in [34]. The mean calliper diameter \bar{b} is discussed, for any geometric object $X \subset \mathbb{R}^2$, defined as

$$\bar{b} = \frac{1}{\pi} \int_0^\pi b(X_\theta) d\theta \quad (3.20)$$

where $b(X_\theta)$ is the projection of X_θ onto the y axis, see Fig. (3.3). X_θ is the same object X but rotated an angle θ around zero, that is $X_\theta = M \cdot X$ is a rotation of X around the origin. The integral in Eq. (3.20) averages the length of all lines that connect two points in ∂X that are diametrically opposed with respect to M . The symbols ∂X stand for the boundary of the object X . For a polygonal X with vertices $v_n = \{z_n \mid z_n \in \mathbb{C}\}$, $M = e^{i\theta}$ and $M \cdot X$ becomes the convex hull of $\{e^{i\theta} v_n\}$. The convex hull of $\{v_n\}$ is the minimum closed polygon containing the points v_n . The mean calliper diameter is a measure of the ‘‘average’’ diameter of a shape. It is determined by taking the average, over angle (or solid angle), of the distance between two limiting lines (or planes) bounding the extremities of the shape as the

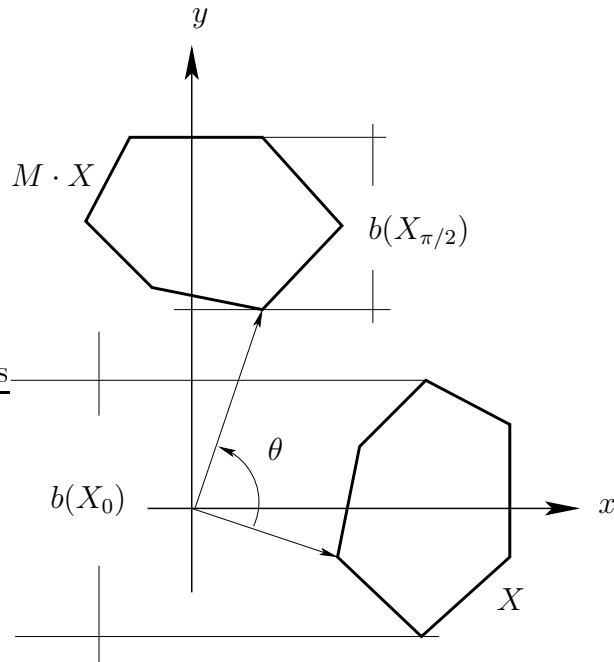


Figure 3.3: Rotation of object X around zero, which represents grain around. The matrix M rotates X by an angle θ , the calliper diameter is the distance between the points intersecting the vertical axis as indicated by $b(X_0)$ and $b(X_{\pi/2})$.

shape is rotated, see Fig. (3.3). Therefore, \bar{b} is defined as the average of \bar{b} over the number of shapes X . If X is convex $L(X) = \pi\bar{b}(X)$ where $L(X) = \int_{\partial X} ds$ is the length of the boundary ∂X . The above is a good theoretical definition, and it was used to characterise the aluminium samples for the experimental work. The connection between the correlation length l and the mean calliper diameter is done by simulating grain spatial configuration using Voronoi cells as will be shown in section (3.3.4).

3.3.4 Simulating the microstructure of polycrystals

In order to generate realisations of the phase variation ϕ one needs to know precisely the properties of the polycrystal. This, as has been discussed in section (3.3.3) is difficult in general. The wave number k was expressed as mean k_0 plus a fluctuating part μ in Eq. (3.12), and some assumptions were introduced for the process μ , such as the correlation function Γ_μ to describe the medium. Realisations of the process ϕ can be given if Γ_μ is known as explained below. Another method is by simulating

the actual microstructure of the polycrystals by using Voronoi cells. This method will be explained first by introducing the Voronoi cells.

The simulation of microstructure is a common practice in the area of material characterisation for theoretical and practical reasons [44, 34]. One of the most widely used not only for its mathematical simplicity but for its closest resemblance to real microstructure is the Poisson Voronoi tessellation. Here, in this chapter only brief introduction of its potential is given. The aim here was to simulate wave velocity variations within the material as well as to investigate the relationship between the mean grain size Eq. (3.20) and the correlation length l of the process μ introduced earlier in section (3.3.3).

The Voronoi cells

The Voronoi tessellation is based on a Poisson random process in space. This process places a number of random points that serve as seeds for the regions that define the tessellation of the space. To begin with, consider a domain $B \subseteq \mathbb{R}^2$ in the two dimensional Euclidean space. A Poisson process $N(B)$ in the domain B is a random process that generates N pairs of points within B , with Poisson statistics. In fact, $N(B)$ gives the number of regions in which B is going to be divided thus the average size of each region. This implies that the size distribution and mean size of each region is a statistical estimation that depends on how the seeds are generated.

The starting point to generate the seeds in B that predetermine the tessellation is by generating samples of the random variable $N(B)$. Let us generate a number $N(B)$ with Poisson statistics. The seeds in B are obtained by generating $N(B)$ points in B , that is $(x_1, y_1), \dots, (x_{N(B)}, y_{N(B)}) \in B$, where x_k, y_k are uniformly distributed random variables. The pairs $\{x_k\}, \{y_k\}$ are arbitrary random variables and to ensure all the points belong to the domain B , a simple linear transformation is applied.

The statistical properties of the random variable $N(B)$ are weighted via a constant λ and the volume of the cells but can be generalised with λ as a function of position. Thus, the first moment takes a simple form, i.e. $\langle N(B) \rangle = \lambda v_B$, see [39] for more details. In the case of the generalised Poisson process, that is when $\lambda(\mathbf{r})$,

$\mathbf{r} \in B$, the seeds cluster together on specific regions in B depending on the form of λ . This type of process is particularly useful if one is interested in an inhomogeneous distribution of the regions. For simplicity we have taken λ to be constant since it serves to our purposes.

In order to define Voronoi tessellation from samples of $N(B)$, $N(B)$ uniformly distributed points $b_1, \dots, b_{N(B)}$ in B are generated.

The regions that define the Voronoi tessellation as subsets of the Euclidean space are defined as the open convex sets

$$B_k = \{x \in \mathbb{R}^2 \mid \|x - b_k\| < \|x - b_l\|, k \neq l\} \quad (3.21)$$

Geometrically the regions B_k that tile the entire space are constructed by finding the line perpendicular to the segment that connects two adjacent seed point b_k . This construction is also valid for generation of polytopes in three dimensions where planes are to be found instead of lines. By definition of tessellation $B_k \cap B_l = \emptyset$ for $k \neq l$. The above construction is the simplest version of Voronoi tessellation but it

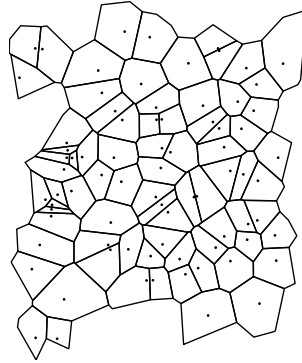


Figure 3.4: The Poisson Voronoi tessellation simulating microstructure of polycrystals. Only a few regions are being showed for illustration purposes. The dots inside the regions are the seeds from which regions are grown.

can be generalised almost arbitrarily [34], where a full range of statistical estimators of geometrical features is also reviewed. It is a simple task using open source software¹ to generate Voronoi tessellation. Fig. (3.4) shows the regions tessellating the set $B = [0, 1] \times [0, 1]$ by generating $N(B)$ uniformly distributed random variables

¹qhull <http://www.qhull.org/>

$b_k = (x_k, y_k) \in B$. By construction, almost everything is known using this numerical technique for microstructure simulation, namely area and size distribution of the regions and also their statistical properties. The unitary polytope has been chosen because real areas can always be normalised.

The simulated microstructure had two purposes: (1) phase screens were designed to obtain the representation for the acoustic field in chapter (3). (2) it has helped in making a better first estimate for the correlation function Γ_μ characterising the inhomogeneities as well as the relationship between the correlation length and the mean grain size for real microstructure.

Wave velocity variations

The idea is to replace the continuous model for velocity variation for a discrete version, the two being statistically equivalent in the second order sense, that is, two processes that have same or similar correlation function. Let σ^2 be the variance of μ and let us simulate the wave number in simulated media as follows: If B_n are the polygons tiling randomly the entire space and c_n are independent zero mean Gaussian variables with variance 1, hence k can be simulated as

$$k(\mathbf{r}) = k_0 + k_0\sigma \sum c_n \mathbf{1}_{B_n}(\mathbf{r}) \quad (3.22)$$

Here $\mathbf{1}_{B_n}$ denotes the function

$$\mathbf{1}_{B_n} = \begin{cases} 1 & \mathbf{r} \in B_n \\ 0 & \text{otherwise} \end{cases} .$$

The wave number defined in this way relates directly to the defining microstructure. The regions B_n were generated using Voronoi tessellation enabling samples for the wave number to be reproduced by the algorithm presented in appendix (A.4). The algorithm gives the coordinates of the vertices defining the polytope of the simulated microstructure and this can be used to fill the regions with normal random variables using Eq. (3.22).

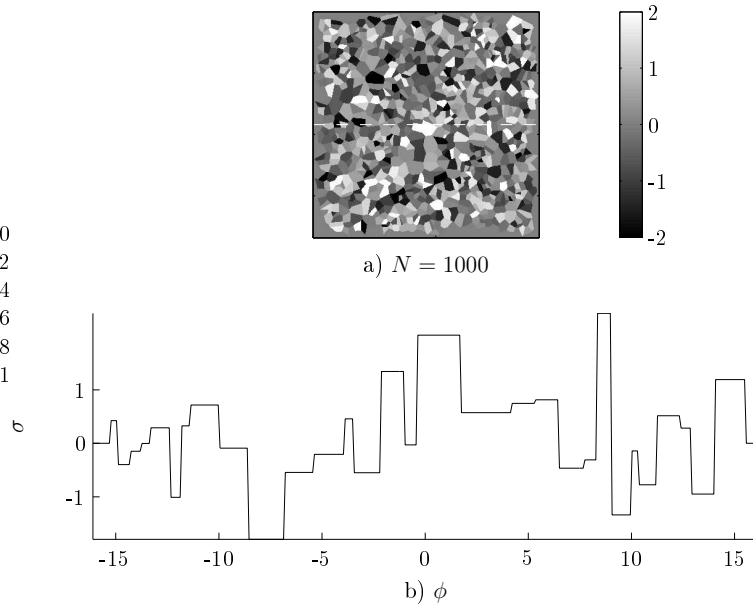


Figure 3.5: a) Realisation of the wave number k in a simulated microstructure showing deviations from mean value in arbitrary units. b) A realisation of ϕ generated using Eq. (3.22) by generating the Gaussian variables c_n .

The spatial correlation of grain distribution

At this point nothing has been said about the correlation length l of the process μ and its relationship to the mean grain size of polycrystalline microstructure.

The process in Eq. (3.22) depends on two random processes simultaneously, namely the Poisson variable $N(B)$, the uniform variables giving the actual position of the seed and finally the Gaussian process that models velocity fluctuation within the grains. This dependence complicates the calculation of the correlation Γ_μ defined in this form. One would be tempted to compute an exact expression but that is not as straightforward as it may look. For the purpose of simulating the acoustic field this was not necessary but one needs to find a relationship between the mean grain size and correlation length for the process defining the inhomogeneities where the wave is to propagate. This relationship is found by the two-dimensional Fourier transform of Eq. (3.22) and fitting an appropriate function to the result.

Using the well known Wiener-Khinchine theorem which says that the autocor-

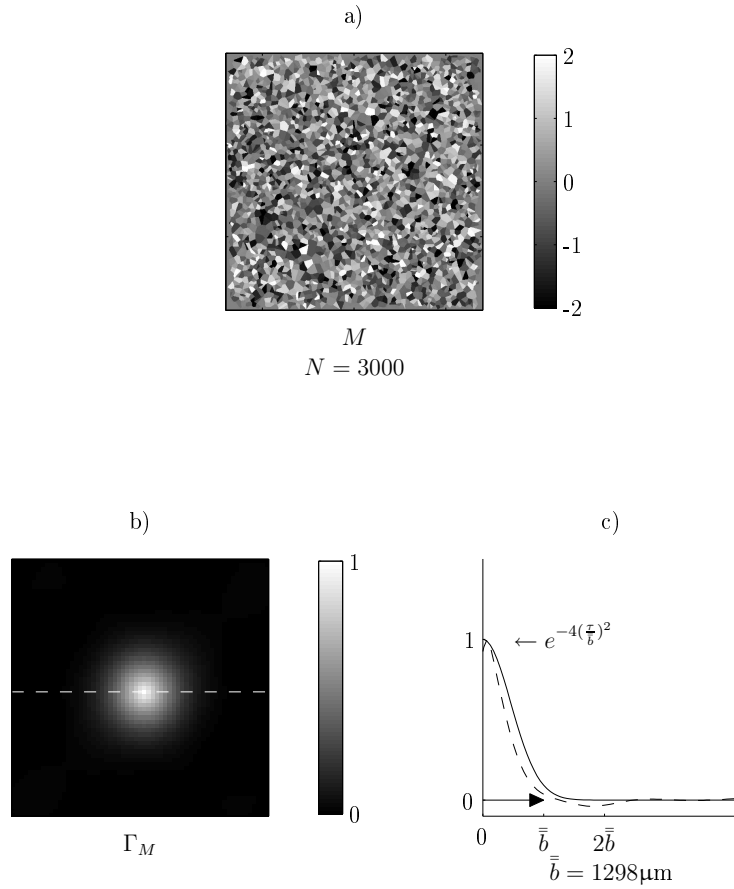


Figure 3.6: a) Simulated microstructure using Voronoi cells. b) The two-dimensional Fourier transform of M normalised to maximum value. c) Comparison of the transverse correlation function Γ_M as indicated by the dashed line in (b) to $\Gamma_\mu = e^{-4\frac{r^2}{\bar{b}^2}}$ to obtain l or \bar{b} .

relation is the inverse Fourier transform of power correlation,

$$\Gamma_M = \int MM^* e^{-i\mathbf{r}t} dt \quad (3.23)$$

Here $M = \cup_k B_k$ is the union of the region that composed B . This method directly measures the correlation that two points $\mathbf{r}_1, \mathbf{r}_2 \in M$ may have, that is Γ_μ shows whether or not $\mathbf{r}_1, \mathbf{r}_2$ are in the same region. Γ_μ turned out to be symmetric with respect to zero as it can be seen in Fig. (3.6)(b).

The Fig. (3.6)(a), shows a simulated grain structure with N regions. Fig. (3.6)(b) is the two dimensional Fourier transform of M , i.e. Γ_M which is a symmetric function that clearly resembles an exponential function. The size of the spot of Γ_M is

proportional to the mean caliper diameter of the regions as shown on the right hand side of Fig. (3.6)(c).

This simulation shows that for microstructure with equiaxed grains the exponential function $\Gamma_\mu = e^{-\frac{4r^2}{l^2}}$ can be used as a good approximation for the correlation function of the process accounting for the wave velocity fluctuations. The mean calliper diameter \bar{b} was obtained from M and substituted into Γ_μ showing the result in Fig. (3.6)(c).

3.4 Concluding remarks

A theoretical description of SAWs in polycrystalline materials has been presented based on the full wave theory for elastic polycrystals. The normal displacement given by the full theory was reduced to a scalar description as a limiting case. The advantages of the scalar description over the full vectorial theory is the simplified mathematical description of SAWs in polycrystalline materials. In this description, velocity variations within grains can be simply described by a single stochastic process avoiding the complicated expression arising from tensor processes. The degree of inhomogeneity and correlation length in the scalar approach have a direct physical meaning in relation to microstructure of the polycrystal.

The description of SAWs in polycrystals using a scalar theory has been done within the paraxial approximation; this appeared a very restrictive approximation but it will be seen that most of the experimental phenomena observed can be explained within the framework of this approximation.

The anisotropy or degree of anisotropy is described in terms of the elastic moduli but it has been related to the standard deviation of the wavenumber in the scalar description in such a simple way that the standard deviation has clearly a physical meaning. The correlation length of the wavenumber could also be directly related to the mean grain size of the polycrystal. This relationship is not so obvious as with the standard deviation because it uses the hypothesis that the random wave velocity fluctuation is an isotropic random process with a Gaussian correlation func-

tion. This assumption appears very restrictive since real microstructures may be far more complicated. To support this idea, a Voronoi model for simulating real microstructure was used to investigate the correlation function of the wave velocity fluctuation in polycrystalline microstructures. The results showed that for polycrystals with mainly convex equiaxed grains the assumption of Gaussian correlation is a good approximation. The relationship between the correlation length of the process modelling the characteristics of the medium was also numerically investigated. This was necessary to corroborate that the correlation length is in fact proportional to the mean grain size.

Chapter 4

SAW waves in polycrystalline materials

Introduction

In chapter (3) was stated that SAW in inhomogeneous media can be described by the stochastic wave equation to a good approximation. This chapter is the continuation of the statement in that an approximate solution to the stochastic equation is presented. The solution is given in two stages. The first one will comprise the propagation of SAWs in homogenous media. This will follow from theory for SAW in isotropic solids by means of Green's function theory. The acoustic field on the homogenous half-space is approximated using the angular spectral expansion for fields that satisfy the Helmholtz equation in a homogeneous half space with no boundaries. This result is used in the second stage in conjunction with a phase screen model for waves in random media to give an approximate solution to the stochastic wave equation.

The idea of using the phase screen model is to approximate the variations of the acoustic field caused by the microstructure using a simple model rather than solving the stochastic wave equation. This approximation considerably reduces the mathematical calculations involved and gives a direct way for obtaining the correlation function of the field. The aberrations of the field strongly depend on the charac-

teristics of the medium. These, were described in section (3.3.3) by the stochastic process that characterises wave velocity fluctuation; thus phase screens and wave velocity fluctuations are functionally interlinked. This functional dependency, comes naturally since the phase screen model and the Helmholtz equation in its parabolic form are related.

The overall approach is to divide the region of interest, a slab in this case, along one of the axes, and into many layers of equal thickness thus approximating the field within each layer by means of a phase screen and half space propagation. The total acoustic field is then given as a multiple integral. The objective and convenience of this integral representation is to facilitate or be able to calculate second order moments of the field. These calculations are part of chapter (5) and will not be discussed here.

At the end of this chapter some numerical implementations are discussed as part of the overall development. Generation of realisations of the acoustic field in random media implies necessarily generation of a realisation of the process accounting for the aberrations. The numerical implementation of phase screens is done by using two methods. The first one has already been introduced in section (3.3.4) as part of microstructure simulation. The second one, which is used in this chapter, generates realisations by using the correlation Γ_{μ} of process μ , discussed in chapter (3.3), by means of the Fourier transform. A brief discussion of the development of a SAW from a series of straight lines evenly distributed is also presented. This type of source is related to the instrument used in the experimental work presented in chapter (6). A more detailed description of ultrasound generation from this type of source is included in the appendix.

4.1 Propagation in random media

The full wave theory presented in chapter (3) includes SAWs in inhomogeneous as well as homogeneous media. The homogeneous media is included in the theory by setting the fluctuating part c' to zero of the elastic moduli in the stress-strain rela-

relationship Eq. (3.4). The homogeneous medium, in principle, includes both anisotropic and isotropic materials, but to a good approximation in this thesis the theory is only considered for the isotropic case. Thus, from the elasticity Eq. (3.10) it is possible to describe SAWs in a homogeneous isotropic material. This is done by providing explicitly the Green's function of Rayleigh waves developed in [17] for the point source expansion. The explicit description of SAWs in homogeneous media is important for the approximation of SAWs in the inhomogeneous case, so it will be developed first. An important point, which will be demonstrated, is that SAWs can also be given as a solution of the Helmholtz Eq. (3.11) in the homogeneous half space. From this, and some intuition, it is possible to conclude that SAWs in the inhomogeneous case are also given by Eq. (3.11) using the phase screen model. Although, a mathematical justification is not as simple as for the homogeneous case, it is important to show that a description of SAWs in inhomogeneous media can also be given by the stochastic equation, Eq. (3.11). This is because second order moment or correlation function theory of the scalar acoustic field is mostly based on Eq. (3.11). Most of the mathematical development in this chapter is left for an appendix, specially the calculations of the field using phase screens.

4.1.1 Displacement from a line source in the half space

The theoretical development presented in this section by means of Green's functions applies to any type of sources for SAW generation. The Green's function is independent of the source utilised for SAW generation. In this section however, the normal displacement depends on a laser profile. The reason for that is because the mathematical development to represent point sources has been done within the framework of SAW generation by thermal expansion using lasers in [17]. This could have been removed for the sake of generality in this thesis but it is important to keep it that way because experimental work is mainly concerned with laser ultrasonics. The descriptions of line sources are required because the instrument to carry out the experimental work uses a line source for SAW generation. But again, the approach is not confined to line sources.

The source S is assumed to lie within the plane xz and finite in the x, z axis as depicted in Fig. (4.1). Thus, the $(x, y, z > 0)$ coordinate system will represent the half-space of a homogenous or inhomogeneous material. The elastic wave Eq. (3.10) give as a result the displacement in every direction. For the geometry being considered, the SAW will be the normal displacement to the xz plane. This is the displacement in direction y .

The position of the source is in the plane xy at $z = 0$. The source region S is represented by a different set of coordinates (α, β) and its dimension is completely determined by a, b . The additional coordinate system (α, β) is necessary to integrate all the contributions from point sources contained within the region S generating the SAW. In the geometry of Fig. (4.1) particles within the material are supposed to be

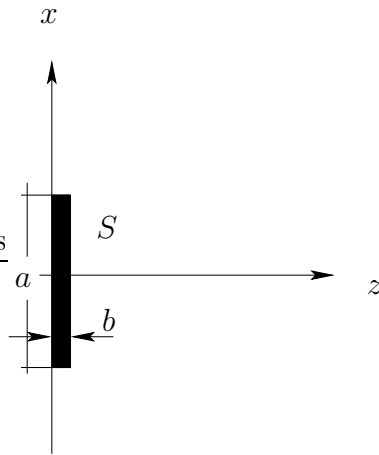


Figure 4.1: Geometry of SAW on the half-space generated by a line source S .

motionless along the x -direction. The only motion that matters in SAW waves is the direction of propagation along z and the upwards and downwards particle motion along y -axis. In the general case one would have displacement in all directions and the boundary problem is solved by giving an appropriate Green's function that represents displacements in each direction.

Let u_{y0} be the normal displacement given by solving equations Eq. (3.10) of a point source for the geometry shown in figure Fig. (4.1). The Green's function for a linearly elastic isotropic material from a point source is developed in [17], thus the

normal displacement u_{y0} due to a point source is given by

$$u_{y0}(\mathbf{r}, t) = Aq(t) \otimes \frac{H(t - s_R R)}{\sqrt{t^2 - s_R^2 R^2}} \quad (4.1)$$

where A is a constant that depends on the material properties. All the constants involved in defining A are given in appendix (A.6). The function $q(t)$ is the laser envelope used to generate a point source on the surface of the materials. H is the step function and $s_R = \frac{1}{c_R}$, with c_R being the mean Rayleigh wave velocity. Here, the variable t represents time.

Adding all the contributions emanating from each point with the region occupied by the source S is equivalent to integrating u_{y0} over the region S weighted with an appropriated function representing the spatial energy distribution. Let $w(\alpha, \beta)$ be that spatial laser profile, then the displacement, denoted by $u_y(\mathbf{r}, t)$ at $\mathbf{r} = (x, z)$ away from the source is

$$\begin{aligned} u_y(\mathbf{r}, t) &= \iint_S w(\alpha, \beta) u_{y0}(R, t) d\alpha d\beta \\ &= \iint_{-\infty}^{\infty} \Pi_{ab} w(\alpha, \beta) u_{y0}(R, t) d\alpha d\beta \end{aligned} \quad (4.2)$$

where $R = \sqrt{(x - \alpha)^2 + (z - \beta)^2}$. In order to be able to integrate Eq. (4.2) it is necessary to know w explicitly. A very detailed discussion of the function w is given in section (4.1.5) where u_y will be plotted in the frequency domain.

The integration over the source was changed to infinity and this is possible, only in this case that S is a line, because of the introduction of the step function in two dimensions, that is

$$\Pi_{ab} = \begin{cases} 1 & |\alpha| \leq a \\ 1 & |\beta| \leq b \\ 0 & \text{otherwise} \end{cases} \quad (4.3)$$

where a , b is the width and length of S , respectively.

A further step in this development is to substitute the expression for u_{y0} in the above integrals and transformed into the frequency domain. The transformation

from the temporal to the frequency domain is both for mathematical convenience and also because the experimental work was carried out at a single frequency. Therefore, the displacement is transformed into the frequency domain by taking the Laplace transform on both sides of Eq. (4.2). The transformation is simplified by using the convolution theorem. In doing so one has

$$\mathcal{L}[u_{y0}] = A\mathcal{L}[q]\mathcal{L}[g] \quad (4.4)$$

where \mathcal{L} is the symbol denoting the Laplace transform and $g = \frac{H(t-s_R R)}{\sqrt{t^2 - s_R^2 R^2}}$.

Before proceeding any further let us recall that the Laplace transform of the Green's function is the modified Hankel function $H_0^{(1)}$, hence

$$\mathcal{L}[g(x, z; \alpha, \beta)] = \frac{i\pi}{2} H_0^{(1)}(\bar{k}R) \quad (4.5)$$

where $\bar{k} = \frac{\omega}{c_R}$, see [78] page 288.

Denoting the Laplace transform of u_y by u and applying the Laplace operator \mathcal{L} to both sides Eq. (4.2) after inserting Eq. (4.4), Eq. (4.5) gives

$$u(\mathbf{r}, \omega) = A\mathcal{L}[q(t)] \iint_S w(\alpha, \beta) \mathcal{L} \left[\frac{H(t - s_R R)}{\sqrt{t^2 - s_R^2 R^2}} \right] d\alpha d\beta \quad (4.6)$$

$$= \frac{i\pi A}{2(i\omega\tau + 1)^2} \iint_S w(\alpha, \beta) H_0^{(1)}(\bar{k}R) d\alpha d\beta \quad (4.7)$$

Note that $\mathcal{L}[q(t)] = \frac{1}{(s\tau + 1)^2}$, with $s = i\omega$ and ω is the angular frequency.

The above representation for the displacement can be easily evaluated since the Hankel function has been numerically implemented elsewhere. However, a better representation for numerical evaluation is to expand $H_0^{(1)}$ in plane waves.

This can be accomplished by recalling that $H_0^{(1)}$ can be expanded in plane waves in the same manner as u . After the insertion of this expansion for the Hankel

functions u becomes

$$\begin{aligned} u(\mathbf{r}, \omega) &= \frac{i\pi A}{2(s\tau + 1)^2} \iiint \Pi_{\alpha\beta} w(\alpha, \beta) \frac{e^{i\bar{k}(x-\alpha)p + i\bar{k}(z-\beta)\sqrt{1-p^2}}}{\sqrt{1-p^2}} d\alpha d\beta dp \\ u &= \int a(p, \omega) e^{i\bar{k}xp + i\bar{k}z\sqrt{1-p^2}} dp \end{aligned} \quad (4.8)$$

where

$$a(p, \omega) = \frac{i\pi A}{2(i\omega s\tau + 1)^2} \iint \Pi_{\alpha\beta} w(\alpha, \beta) \frac{e^{ik\alpha p + ik\beta\sqrt{1-p^2}}}{\sqrt{1-p^2}} d\alpha d\beta \quad (4.9)$$

and the variable p denotes spatial frequencies. The function a looks complicated because of the double integration over the weight function w and plane waves. This apparent complication can be overcome by simply realising that

$$u(x, 0, \omega) = \int a(p) e^{i\bar{k}p} dp \quad (4.10)$$

In other words, the angular spectral representation is the Fourier transform of the initial displacement evaluated at the spatial frequencies $\bar{k}p$. In summary, the calcu-

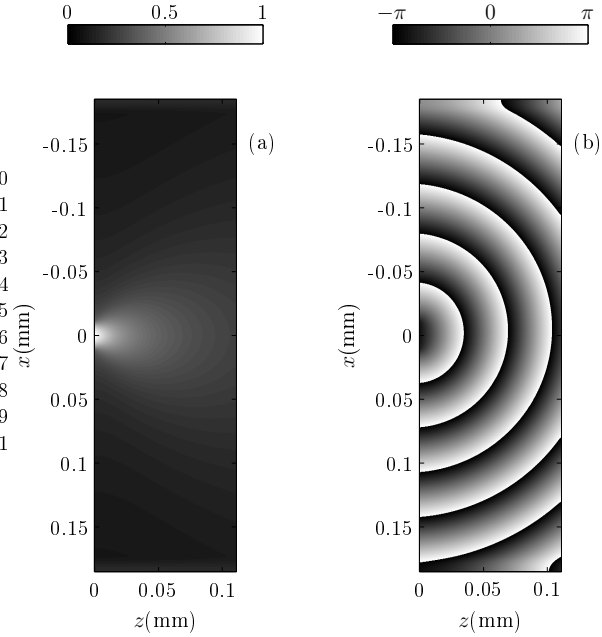


Figure 4.2: a) Amplitude of the complex normal displacement (arbitrary units). b) Phase distribution (radians)

lation of the normal displacement from a line source has been reduced to the angular

expansion of the field and the frequency components of the laser are the frequency components of the displacements. As it can be seen the important quantity here is the initial displacement at $z = 0$. In the experimental setup the idea was to propagate a plane wave but because of the finite size of the source it becomes a truncated plane wave. Thus, ideally the normalised initial displacement would be

$$u(x, 0, \omega) = \begin{cases} 1 & x \in [-\frac{a}{2}, \frac{a}{2}] \\ 0 & \text{otherwise} \end{cases} \quad (4.11)$$

Using this in Eq. (4.8) the resulting displacement of the field is shown in Fig. (4.2). Fig. (4.2)(a) is the amplitude of the normal displacement and initial displacement given by Eq. (4.11) whereas Fig. (4.2)(b) shows the phase. The wave propagates from left to right.

It is now easy to recognise that the last expression in Eq. (4.8) is the angular spectral representation of the normal displacement $u(\mathbf{r}, \omega)$, as developed in [70]. It is straightforward to check that $u(\mathbf{r}, \omega)$ satisfy Eq. (3.11) since $e^{ikxp+ikz\sqrt{1-p^2}}$ is a plane wave satisfying the Helmholtz equation.

4.1.2 Propagation through a random thin layer

In section (4.1.1) the normal displacement or SAW was developed for homogenous isotropic materials. This result is used in the present section for SAWs in inhomogeneous media. Specifically, an approximation for the acoustic field will be given in the slab ($x, 0 \leq z \leq L$) containing inhomogeneities. In order to achieve that, the region of interest is divided in layers of equal thickness δz along the propagation distance, in this case the z axis. Thus, the geometry will be as in (4.1.1), figure Fig. (4.1).

The displacement $u(\mathbf{r}, \omega)$ in Eq. (4.8) is frequency dependent. In this thesis, a single frequency will be needed for comparison with the experimental work. The description of the SAW in this section therefore will be in the frequency domain. The frequency will be dropped from the notation for the rest of the chapter as it

will be understood that the displacement depends on it. The first step in achieving

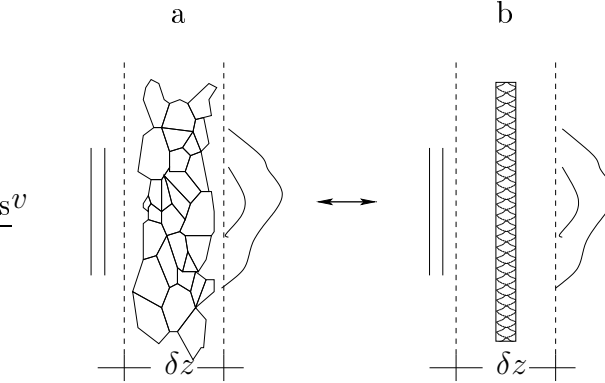


Figure 4.3: Schematic representation of ultrasonic propagation in a random medium using phase screen theory.

propagation in a random slab is to consider a thin layer of thickness δz and incident field $v = u(x, 0)$ to the layer, as shown in Fig. (4.3)(a). Some assumptions have to be made in order for this approximation to work. Firstly, that forward scattering within the layer is stronger than backward scattering so it can be neglected to a good approximation. As a result, the phase of the field will be the only one affected leaving the amplitude unchanged. Secondly, the layer is thin enough for all points belonging to the wavefront of the field to follow approximately straight lines. This means that the phase changes can be represented by a phase screen. Essentially, a phase screen is a complex number $e^{i\phi}$ where ϕ is a random process representing the characteristic of the medium. Below, it will be seen how the process ϕ is related to process μ accounting for wave velocity fluctuations, which was first mentioned in section (3.3.1).

Let us consider the situation as shown in Fig. (4.3). The idea is to substitute the field within the inhomogeneous region Fig. (4.3)(a) by the incident field to the layer times a complex number or phase screen that depends on the characteristics of the medium. The phase screen is located in the middle of the layer as shown in Fig. (4.3)(b). The approximation is as follows: instead of solving Eq. (3.11) within the random layer, the incident field v is propagated in a half space using Eq. (4.8) to a distance $\frac{\delta z}{2}$, then the resultant field is multiplied by a phase screen $e^{i\phi}$, which gives the normal displacement $u(x, \frac{\delta z}{2})$ behind the screen.

Let us denote by u_{in} the field from 0 to $\frac{\delta z}{2}$ in half space having v as source at $z = 0$, thus the field behind the screen can be written as

$$u(x, z) = u_{in}(x, z)e^{i\phi(x)} \quad (4.12)$$

The inhomogeneous medium has been replaced by a phase screen that modifies the phase leaving the amplitude unchanged. The situation is depicted in Fig. (4.3)(b) where the screen is being represented by a thin box. The phase screen has been allocated in the middle of the slab but it could have been at the entrance of the layer.

In the continuous model v is expected to follow random paths which depend on the statistics of the medium, in this case the process μ , whereas in the present situation, the implicit assumption is that those paths are indeed straight lines. The phase ϕ , therefore, has the following functional dependence [95, 57, 60] as

$$\phi(x) = \frac{k_0}{2} \int_0^{\delta z} \mu(x, z') dz' \quad (4.13)$$

The Eq. (4.13) indicates that the overall phase change experienced by the field is in fact the integrals of all possible changes induced by the inhomogeneities within the layer. Again, the reason for the appearance of the process μ in Eq. (4.13) is because it has been assumed that u within the layer is approximately given by solving the stochastic Eq. (3.11). It has to be said, that the functional dependency Eq. (4.13) is only valid in case of weak backscattering or equivalently if the field is given by the parabolic form of Eq. (3.11), see [60].

To end this, the field u in Eq. (4.12) is again propagated in the half space to a distance $\frac{\delta z}{2}$. Thus, by taking the Fourier transform with respect to x of Eq. (4.12) and using Eq. (4.8), and reverting back again to the spatial domain by performing the inverse transform gives the angular representation for u in a random medium as follows:

$$u(\mathbf{r}) = \int [\hat{v}(p)h(p, \frac{\delta z}{2}) \otimes \hat{s}(p)]h(p, \frac{\delta z}{2})e^{ipx} dp \quad (4.14)$$

Here \hat{v} , \hat{s} denote the spatial Fourier transform of v and $s = e^{i\phi}$, respectively. The following substitution has been made, $h = e^{i\bar{k}px+i\bar{k}z\sqrt{1-p^2}}$ to represent the function propagator to simplify Eq. (4.14). The symbol \otimes stands for spatial convolution between two functions. A field propagating through an inhomogeneous layer has therefore been approximated by distorting the phase of its elementary components by ϕ . In order to extend the above development to the entire domain ($x, 0 \leq z$) the field is expressed in the Fourier domain by relabelling the field to indicate the number screens and their precise location within the region ($x, 0 \leq z$). This is explained in great detail in the following section.

There is an important point to bear in mind. The thickness δz is taken to be of the order of the correlation length of $k(\mathbf{r})$, see section (3.3.3) for a precise meaning of the correlation length.

4.1.3 Propagation through many layers

Let us divide the slab $D = (x, 0 \leq z)$ in N layers of thickness δz and let us assume, for the sake of symmetry, that the screens are located at $\frac{\delta z}{z}$. The phase change for each screen is relabelled as $\phi_n(x)$, let \hat{s}_n be the Fourier transform of $s = e^{i\phi_n(x)}$. The situation within the n th layer is schematically showed in Fig. (4.4). In order to approximate the field within the slab D formulation Eq. (4.14) is applied recursively for each layer. As the incident field v is propagated from one layer into another the phase screen recursively multiplies as well as the function h . Because u has been expressed as a integral as well as a convolution, equation Eq. (4.14), the final expression would be given as a multiple integral. To express the long representation in a single expression let us label the field with each layer by u_n , thus u_n represents the field at distance $n\delta z$ away from the source. For each layer, one needs a set of different dummy variables to represent the field as in Eq. (4.14), thus let p_n be that variable and making $h_{p_n} = h(p_n, \frac{\delta z}{2})$.

Assuming that v propagates to a distance $n\delta z$, and taking into account that

$$\mathcal{F}[u_n(x, n\delta z)e^{i\phi_n(x)}] = \hat{u}_n(p_n, n\delta z) \otimes \hat{s}(p_n) \quad (4.15)$$

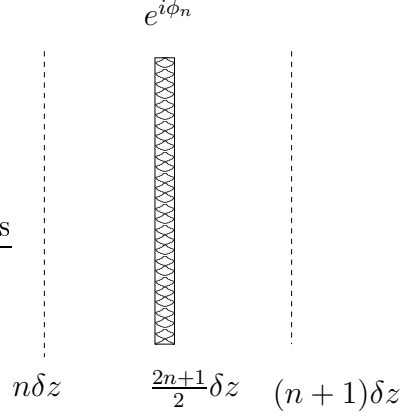


Figure 4.4: Schematic representation of the n th layer replaced by the phase screen system. The screen $s = e^{i\phi_n}$ is being allocated in the middle of the layer.

where \mathcal{F} is the Fourier transformation operator, by using Eq. (4.14), the field in the frequency domain at the exit of the n th layer can be expressed as

$$\begin{aligned}\hat{u}_{n+1} &= [\hat{u}_n h_{p_n} \otimes \hat{s}_n] h_{p_{n+1}} \\ &= h_{p_{n+1}} \int \hat{u}_n(p_n) h_{p_n} \hat{s}(p_{n+1} - p_n) dp_n\end{aligned}\quad (4.16)$$

The convolution is the operation of propagating the field through a random screen and multiplication again by $h_{p_{n+1}}$ propagates $\hat{u}_n h_{p_n} \otimes \hat{s}_n$ to the entrance of the next screen thus becoming the new incident field. In appendix (A.2), it is shown how to express the field in the following multiple integral representation by substituting the recurrent integral representation Eq. (4.16) for u_n , thus the total field $u = u_{n+1}$ can be expressed as

$$\begin{aligned}u(x, z) &= \int \cdots \int \hat{v}(q_0) \prod_{n=0}^{n-1} h_{q_j}^2 \hat{s}(q_{j+1} - q_j) \\ &\quad \times e^{ik_0 q_n x} dq_0 \cdots dq_n\end{aligned}\quad (4.17)$$

Equation Eq. (4.17) represents the ensemble of acoustic fields in a random medium. The dependency on s makes u a random process that depends on the statistical properties of μ because of the functional dependency Eq. (4.13). Equation Eq. (4.17) will serve as a basis to calculate the second moments $\langle uu^* \rangle$ of the field. It is a

multiple integral and there are as many integrals as there are screens used for the approximation, however it is computationally efficient as these can be implemented using the FFT algorithm.

The field u is a random process that depends entirely on the statistical properties of the process ϕ ; thus generation of realisations of the field within the slab D will follow from the realisation of ϕ . The realisation of ϕ in turn depends on the statistics of μ via the relation Eq. (4.13). The construction of the realisation for ϕ is based on a given correlation function for μ which is discussed in the next section. A realisation of u will then be given by evaluating Eq. (4.17) by substitution of the appropriate realisation of screens.

4.1.4 Realisation of phase variations

The realisation of the field u depends on the process ϕ accounting for phase variations. This process depends directly on the properties of the medium, which is being represented by the process μ earlier introduced in section (3.3.3).

In section (3.3.4) a method was then introduced to generate realisations of the process ϕ . It was based on simulation of wave velocity variations within microstructure by constructing a process μ that depends on geometric characteristics. The correlation function of μ was also investigated, with the conclusion that as a good approximation it could well be considered to have an exponential form. This is the starting point to generate a realisation of the phase ϕ in this section. That is, it will assume a known correlation function for μ and from this the required phase realisations will be generated by using the Fourier transform method.

Fourier method for phase generation

Let us start by assuming the process μ has the known correlation function Γ_μ , having the exponential form $\sigma^2 e^{-|\mathbf{r}|^2/l^2}$, where again σ^2 is the variance of μ and l is the correlation length. Therefore, generation of realisations of ϕ is equivalent to the generation of realisation of the process μ by means of correlation Γ_μ and relation Eq. (4.13). Although, not essential for the present development, it is important to

mention that, in chapter (5), the relationship between the structure function of ϕ and the correlation function Γ_μ is investigated.

The Fourier method for generating a realisation of a process is as follows: Let us denote the power correlation of μ by S_μ and let $W(\omega)$ be complex white noise, i.e. a complex zero Gaussian process with correlation $\langle W(\omega)W^*(\omega') \rangle = \delta(\omega - \omega')$. Then μ admits the following spectral representation

$$\mu(x) = \int W(\omega) \sqrt{S_\mu(\omega)} e^{ix\omega} d\omega \quad (4.18)$$

Thus, realisations are simply given by taking the Fourier transform of the product of a Gaussian noise and the square root of the power correlation of μ . This method has the advantage of being easily implemented by using the discrete Fourier transform. Generation of realisation from Eq. (4.18) acts as a filter for W giving a smooth realisation compared to Eq. (3.22), in Fig. (3.5). The fact that the process μ has Γ_μ as correlation function follows from the Wiener-Khinchine theorem for random process, thus

$$\begin{aligned} \langle \mu(x)\mu(x') \rangle &= \iint W(\omega)W(\omega') \sqrt{S_\mu(\omega)S_\mu(\omega')} e^{ix\omega - x'\omega'} d\omega d\omega' \\ &= \iint \delta(\omega - \omega') \sqrt{S_\mu(\omega)S_\mu(\omega')} e^{ix\omega - x'\omega'} d\omega d\omega' \\ &= \int S_\mu(\omega) e^{i\omega(x-x')} d\omega \\ &= \Gamma_\mu(x - x') \end{aligned} \quad (4.19)$$

In chapter (3) it was stated that a good approximation in representing microstructure of certain polycrystals is when Γ_μ has exponential form. Taking this into account, realisations for ϕ are generated using the discrete Fourier transform from Eq. (4.18). Fig. (4.5) shows the correlation Γ_μ (top graph), a single realisation of the white noise $W\sqrt{S_\mu}$ and a superimposed plot of the profile $\sqrt{S_\mu}$. On the bottom of Fig. (4.5), is shown a realisation of ϕ using this method.

In section (3.3.4) we showed how to generate microstructure using Voronoi tessellation. This method also give a straightforward way to generate realisations of the

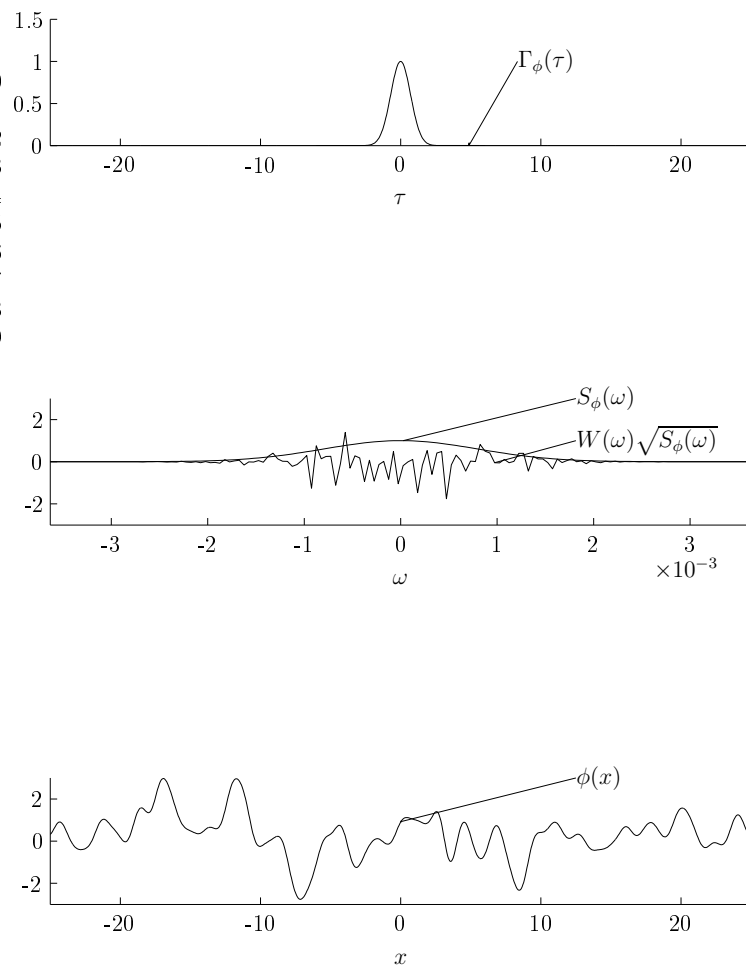


Figure 4.5: Generation of realisation of ϕ

process ϕ , as shown in the same section. It was also shown that the autocorrelation of the generated microstructure is an exponential function. Therefore, the Fourier method with exponential autocorrelation and the one described in section (3.3.4), for generating realisation of the process ϕ are equivalent. In the former, it is only necessary to calculate the Fourier transform of a known function whereas in the latter it is necessary to build the tessellation and colour the regions. Colouring the regions in this context means specifying the velocity variations within regions, as explained in section (3.3.4). The algorithm for tessellating the space and definition of wave velocity variations within the regions is a slow process. This is why the Fourier method was preferred, since it is simple and fast. This method will be used for the rest of the thesis for generating realisations of the process ϕ .

4.1.5 Realisation of the acoustic field

Before showing a realisation of the field based on Eq. (4.17) it is necessary to specify the incident field. It was said in section (4.1.1) that the Fourier transform of the incident field is the angular spectrum of u . But the angular spectrum a , Eq. (4.9) is an integral over a laser spatial profile $w(\mathbf{r})$ which was not specified. Here for completeness a Gaussian profile is presented, although already mentioned in section (4.1.1), it is not necessary to specify the incident field. The (4.6) shows a plot of $\Pi_{ab}(\mathbf{r})w(\mathbf{r})$; note that $\Pi_{ab}w$ is rounded on top, this is because w has been assumed to be a Gaussian profile, i.e. $w = e^{-|\mathbf{r}|^2/c^2}$, where c is a parameter defining the width of w . Many lasers have Gaussian distribution [64], so w can fairly be described with a Gaussian profile. Here, again for practical purposes the incident field is taken to be of the form Eq. (4.11). Thus, by using Eq. (4.17) and realisations of ϕ already generated in section (4.1.4) is possible to give a realisation of the field u which is shown in Fig. (4.7). Fig. (4.7) shows the amplitude distribution numerically implemented from Eq. (4.17). It is a truncated plane wave propagating in the simulated inhomogeneous medium characterised by standard deviation $\sigma = 0.02$. As the wave travels from left to right (z -direction) the phase is being altered by screens placed to approximate the field within a layer. The overall phase is distorted as well

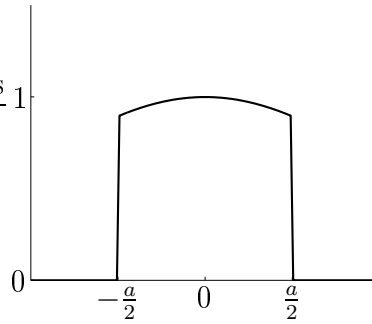


Figure 4.6: Plot of the transverse light distribution $\Pi_{ab}(\mathbf{r})w(\mathbf{r})$, where w has a Gaussian envelope.

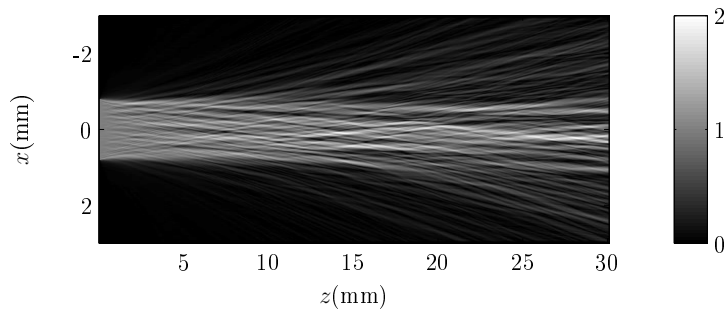


Figure 4.7: Amplitude distribution according to Eq. (4.17). The simulation is based on real parameters and a numerical procedure. This can be compared with the experimental amplitude distribution shown in Fig. (1.1).

as the amplitude distribution breaking up as it can be seen in the Fig. (4.7). This shows what to expect to happen to the acoustic surface waves propagated in real polycrystals, which can be compared to Fig. (1.1) showing aberrations in aluminium.

4.1.6 Solids in general

So far the theory just developed applies mainly to isotropic solids. The angular spectrum representation is a powerful tool that can even be extended to more general type of solids.

In the article [96], a paraxial theory for ultrasonic beams was developed for anisotropic solids. The integral representation of the field is basically an angular expansion based essentially on Taylor series expansion of the slowness surface. The argument in the exponential function of the integrand in Eq. (4.9), however, involves crossed and quadratic terms leading to a complicated angular expansion. The advantage of that formulation is that the isotropic case is easily obtained as a limiting case.

Here, for simplicity the isotropic case was only considered since the anisotropic parameter is lost in polycrystalline materials as part of a random effect from microstructure.

4.2 Conclusions

A model that accurately represents line sources for ultrasound generation has been presented. The mathematical development uses the method of Green's function to express the elastic response of a homogenous medium. This mathematical formulation gives explicitly the Green's function of the normal displacement for a thermoelastic point source. By integrating the Green's function across the area occupied by a line on the sample surface, an expression for the normal displacement is given as a plane expansion. This representation was later used in section (4.1.2) to approximate the field in an inhomogeneous medium using a phase screen model.

One of the parameters directly involved in the description of screens to ap-

proximate the field is the standard deviation. This parameter in the scalar model developed in section (3.3.2) is directly related to the anisotropy of the grains which in turn describes the strength of the screens.

The expression obtained for the field is given as multiple integrals that can be efficiently implemented using the FFT. The other important property of this representation is the possibility of calculating the second order moments of the field by using Eq. (4.17), which is developed in great detail in chapter (5).

It is believed that the representation Eq. (4.17) is a fair approximation since it explains most of the observed phenomena in polycrystalline materials with microstructure characterised by an exponential correlation function. Naturally, this must be combined with the general assumption listed in section (3.2).

The representation (4.17) is assessed by comparison via the second order moments of the field in chapter (6).

Chapter 5

Propagation of correlation function

Introduction

This chapter describes the theory of propagation of the correlation function or, in terms of stochastic process, the second order moments. The aim is to determine an expression for the ensemble average $\Gamma_u = \langle u(\mathbf{r})u^*(\mathbf{r}') \rangle$, where u is the process representing the acoustic field. The correlation function is important since it is directly related to the geometric characteristics of the medium. In chapter (3.2), grain structure was described via the correlation function of the wave number. This correlation will be seen to be directly related to the correlation Γ_u of the field by calculating the ensemble average using Eq. (4.17), in the first place.

The propagation and the determination of this function through random media have been given in the literature [70, 97, 47]. In these papers, many constraints are imposed on processes defining the medium in order to approximate $\langle u(\mathbf{r})u^*(\mathbf{r}') \rangle$. The assumptions introduced here are not that different from the ones proposed in the literature, in particular that μ is isotropic in transverse directions and almost delta correlated in the direction of propagation. By definition a process μ is delta correlated if its correlation is of the form $\Gamma_\mu = \delta(z - z')f(x - x')$, where δ is the Dirac delta function and f is an arbitrary function. Other assumptions have been already introduced in the previous chapter (3), sections (3.3.2) and (3.3.3) and they will continue to hold.

The expression for $\langle u(\mathbf{r})u^*(\mathbf{r}') \rangle$ is given by two different points of view that differ in the way the ensemble average is obtained. The first one is a direct application of phase screens to obtain an approximate solution to Γ_u using the integral representation for the field Eq. (4.17).

The assumption on the process μ of the inhomogeneity fluctuations, is that the phase fluctuations ϕ are Gaussian. This property is used to calculate the ensemble average of the field based on a standard result in multivariate statistics that is valid for the Gaussian stochastic processes. The correlation, however, is calculated transversally, which is defined as the ensemble average $\langle u(x, z)u^*(x', z) \rangle$ for each z . The variable z here denotes propagation distance.

The second point of view uses the Helmholtz equation to approximate Γ_u , which satisfies a differential equation derived in the literature [47]. There are some technical problems within the phase screen technique that cannot easily be solved. The strong assumption that rays do not bend considerably within a layer not only restricts the suitability of the method but also the correlation function depends on the number of screens used to approximate the field within the slab.

To remedy this in some way the correlation function of the field, based entirely on the stochastic equation, is given in a heuristic manner in section (5.2). This alternative approximation would also justify the feasibility of the phase screen method in approximating the correlation function since the two coincide.

One of the reasons for obtaining the correlation function of the field is to relate it to the correlation of the medium. The grains are assumed to be equiaxed, thus a measure in any direction would give a reliable quantification of the mean grain size.

The importance of the correlation function Γ_u is that aberrations can be quantified by means of this function, which is determined by two main parameters defining the medium. These are the correlation length and the standard deviation of μ that measures the degree of inhomogeneity.

5.1 Moments of the acoustic wave field

The second moment of the acoustic field by definition is the ensemble average $\langle u(\mathbf{r})u^*(\mathbf{r}') \rangle$, where $\mathbf{r} = (x, z)$ will denote a point in the two dimensional coordinate. The second moment for any stochastic process will be denoted by Γ_u if u is the process being considered. Thus, for instance the second moment for the process μ is already defined and necessary in what follows

$$\Gamma_\mu = \langle \mu(\mathbf{r})\mu(\mathbf{r}') \rangle \quad (5.1)$$

The rest of the notation necessary for the mathematical development will be introduced within the text.

5.1.1 Initial correlation function

The starting point in calculating the correlation function is to introduce the correlation of the incident field v to a slab as in the boundary problem Eq. (3.11). This initial value for the field at $z = 0$ could, in principle, be a random process with prescribed statistical properties. What is needed here in order give an approximation to Γ_u is the initial form of Γ_v . The process $v(x)$ can be non-stationary or a wide sense stationary random process. If v is non-stationary, the correlation function Γ_v will not be independent under translation, specifically $\langle v^*(x)v(x + \tau) \rangle$ will depend in general on the point x in space, where $\tau = x - x'$. Thus, Γ_v is defined as the energy correlation function of a random process as

$$\Gamma_v(\tau) = \int_{-\infty}^{\infty} v^*(x)v(x + \tau)dx \quad (5.2)$$

It is well known that under stationary conditions the average Γ_v is infinite. In this case it is meaningless to consider Eq. (5.2); the power correlation function

$$\Gamma_v = \lim_{X \rightarrow \infty} \frac{1}{X} \int_{-X}^X v^*(x)v(x + \tau)dx \quad (5.3)$$

has to be considered, instead. The integral in Eq. (5.2), is known as the autocor-

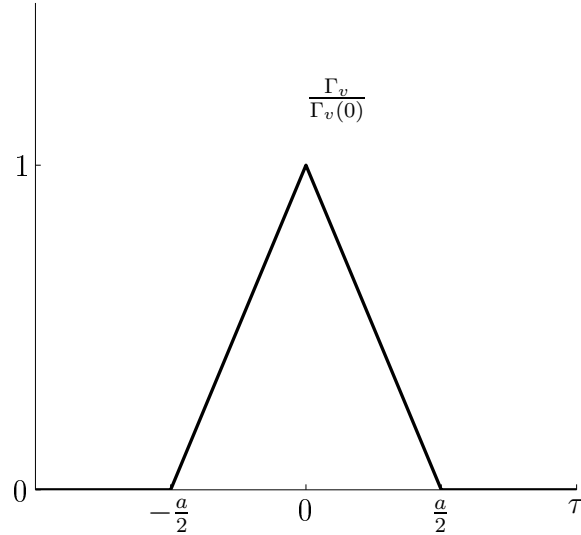


Figure 5.1: Idealised correlation function of the field at $z = 0$. The width a determines the size of the source

relation function in signal processing for complex signals. For comparison with the experimental work it is sufficient to give the initial form of Γ_v as a function of τ only. This function will be the autocorrelation of the initial displacement Eq. (4.11) considered in section (4.1.1). Thus, Γ_v has a triangular form as shown in Fig. (5.1).

5.1.2 The structure function of the medium

The structure function of a process is of great importance in optics and atmospheric calculations [47]. Here it is introduced as it arises in the calculation of the correlation function.

The statistical characteristics for the process μ have already been introduced in chapter (3) where it was needed for building ensembles of the process. The correlation Γ_μ was then used to build realisations of the phase fluctuations ϕ . The structure function of ϕ is introduced as it will be used for the calculations of Γ_u in the following section. This is defined as the ensemble average of the squared difference of ϕ at two different points in the transverse axis of coordinates, thus

$$D_\phi = \langle [\phi(x) - \phi(x')]^2 \rangle \quad (5.4)$$

The process ϕ has a functional dependence on μ , equation Eq. (4.13), and hence one would expect to be able to express D_ϕ in terms of μ . This can only be done if μ holds certain properties. Let us suppose that Γ_μ can be split as $\Gamma_\mu = f(x, x')g(z, z')$ where f, g are arbitrary functions that depend on $x - x', z - z'$, respectively. The reason for splitting Γ_μ in the above form comes from the fact that in the end an exponential for Γ_μ is taken since it could accurately represent the measured correlation of the acoustic field. The exponential form would trivially satisfy this condition. It is clear from the above definition that f is the correlation of two points along the axis x , whereas g is the correlation of μ at two arbitrary points along axis z . The functions f and g in general would be determined by different correlation lengths that determine the scale of the grains along x, z axes, respectively. Earlier in chapter (3), the grains were assumed to be equiaxed, and so to speak of two different correlations is meaningless at this point.

Here, the process ϕ has the same meaning as in Eq. (4.13) but without the factor $k_0/2$ and the limits of integration are from 0 to z , hence

$$\phi = \int_0^z \mu(x, z') dz' \quad (5.5)$$

Inserting Eq. (5.5) in definition Eq. (5.4) after using the assumption on Γ_μ the structure function D_ϕ is given by

$$\begin{aligned} D_\phi &= \iint \langle [\mu(x_1, z') - \mu(x_2, z')][\mu(x_1, z'') - \mu(x_2, z'')] \rangle dz' dz'' \\ &= \iint f(x_1, x_1)g(z', z'') - f(x_1, x_2)g(z', z'') \\ &\quad - f(x_2, x_1)g(z', z'') + f(x_2, x_2)g(z', z'') dz' dz'' \end{aligned} \quad (5.6)$$

Since f depends on the difference at two different points it follows that $f(0) = f(x_1, x_1) = f(x_2, x_2)$, $f(x_1, x_2) = f(x_2, x_1)$ and is obviously independent of z', z'' , thus the structure takes the final form

$$D_\phi = 2[f(0) - f(x_1, x_2)]\Psi(z) \quad (5.7)$$

where $\Psi(z) = \int_0^z \int_0^z g(z', z'') dz' dz''$.

The integrals defining Ψ can only be calculated in a specific form if g is assumed. In the paragraphs below D_ϕ is specified for the case when g bears an exponential form. To be consistent with notation for the rest of the calculation f is again denoted by Γ_μ , even when it only represents transverse correlation.

The exponential correlation

Ultimately, the final form of Γ_μ used for comparison with the measured correlation function has the following form $\Gamma_\mu = \exp[-\frac{(x-x')^2+(z-z')^2}{l^2}]$, thus $g(z, z') = \exp[(z - z')^2/l^2]$ and Ψ after substitution of g following a change of variable $l\xi = z' - z''$, $l\eta = z' + z''$ takes the form

$$\begin{aligned} \Psi(z) &= \iint_0^z e^{-(z'-z'')^2/l^2} dz' dz'' \\ &= \frac{l^2}{2} \iint_0^{\frac{2z}{l}} e^{-\xi^2} d\xi d\eta \\ &= \frac{\sqrt{\pi}lz}{2} \operatorname{erf}\left(\frac{2z}{l}\right) \end{aligned} \quad (5.8)$$

The function $\operatorname{erf}()$ introduced in the last step above is the familiar error function, which is basically Ψ up to some constant factors. Substituting the above integral in Eq. (5.7) one gets

$$D_\phi = \sqrt{\pi}lz \operatorname{erf}\left(\frac{2z}{l}\right) [\Gamma_\mu(0) - \Gamma_\mu(x_1, x_2)] \quad (5.9)$$

The relationship between the structure function of the process ϕ and material properties is evident from Eq. (5.9). As presented in section (3.3.3), the correlation Γ_μ directly characterises properties of the medium, which defines the structure function D_ϕ of the process ϕ in Eq. (5.9). A plot of D_ϕ is shown in Fig. (5.2) at arbitrary distances. The shape is given by the normalised correlation function

$$\gamma_\mu = 1 - \frac{\Gamma_\mu(\tau)}{\Gamma_\mu(0)} \quad (5.10)$$

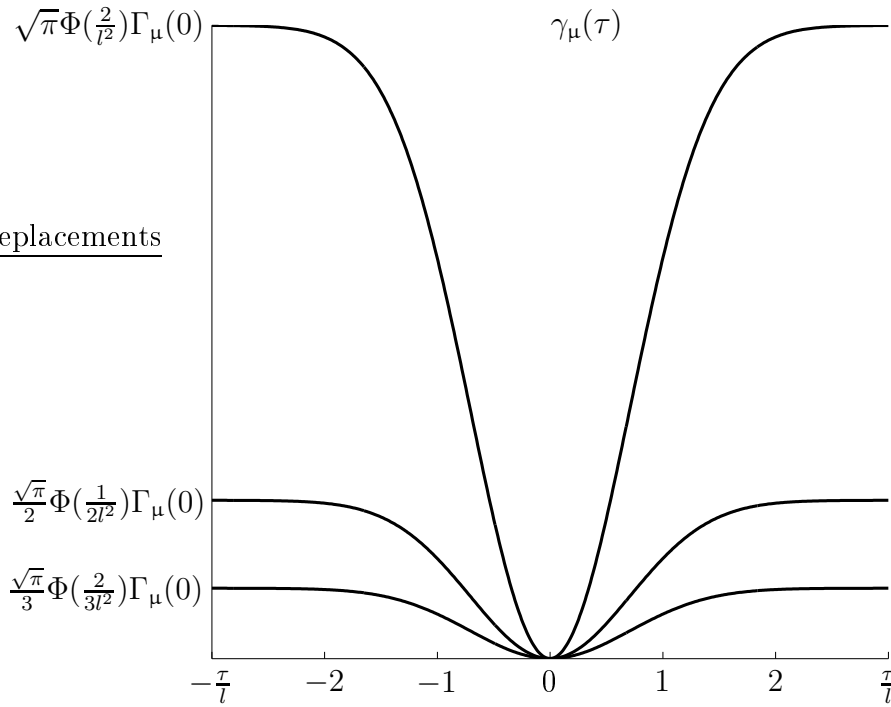


Figure 5.2: The structure function D_ϕ plotted over the normalised axis $\frac{\tau}{l}$ propagation distances $z = 1/3l, 1/2l, 1/l$.

As shown in the graph the function γ_μ narrows as the multiplicative factor $\sqrt{\pi}lz\Phi(\frac{2z}{l})\Gamma_\mu(0)$ increases for different $z = 1/3l, 1/2l, 1/l$. The values for z were chosen arbitrarily. The behaviour of this function is dictated mainly by the parameters $l, \Gamma_\mu(0)$ that are kept constant in plotting this graph. As we shall see these parameters will completely define the correlation function of the field Γ_u .

5.1.3 Multiple screens

The calculation of the correlation Γ_μ requires integration on several variables, so an independent coordinate system is attached to each screen. Since the correlation involves the averages at two arbitrary points in the transverse coordinates let us denote them by \mathbf{x} and \mathbf{y} leaving \mathbf{z} for the direction of propagation as before. Let $\mathbf{x} = (x_0, \dots, x_n)$, $\mathbf{z} = (z_0, \dots, z_n)$ and denote their coordinate differences by $\mathbf{x}^- = (x_1 - x_0, \dots, x_n - x_{n-1})$; the same definition would apply for \mathbf{y}^- and \mathbf{z}^- as well. The phase variations at each screen are labelled by sub-indices to indicate which screen they

belong to. If $\phi_0(x_0), \dots, \phi_n(x_n)$ are the phase variation at each screen, then

$$D_s(\tau_s) = \langle [\phi_s(x_s) - \phi_s(y_s)]^2 \rangle \quad (5.11)$$

will denote the structure function for phase variations at each screen. An extra variable \mathbf{y} is needed since the structure function is calculated at two different points in the transverse direction. In general D_s is not a function of the difference $\tau_s = x_s - y_s$ but one has to assume this in order to calculate Γ_u . This point has already been discussed in section (5.1.2). The D_s , $s = 1, 2, \dots$ are essentially the same function but defined on different coordinate systems for technical reasons.

Following this notation and according to phase screen approximation the multivariate screen would be

$$s(\mathbf{x}) = e^{i \sum_s \phi_s(x_s)} \quad (5.12)$$

The process of propagating v from one screen into another according to Eq. (4.14) is that every time the field is distorted by a screen the phase variation adds up resulting in Eq. (4.17) if written in several variables. One could call s a multivariable screen; s is a random process determined completely by the processes ϕ_s . In the case when the ϕ_s are Gaussian processes, it is possible to obtain the second moment of s as a function of the structure functions D_s . In appendix (A.1) it is shown how the ensemble average $\langle s(\mathbf{x})s^*(\mathbf{y}) \rangle$ is related to the structure function Eq. (5.4) by using a standard result in multivariate statistics [64]; in doing so

$$\langle s(\mathbf{x})s^*(\mathbf{y}) \rangle = e^{-\sum_s D_s(\tau_s)} \quad (5.13)$$

The average Eq. (5.13) will be in the end an exponential function but it will be seen that for calculating Γ_μ it suffice for D_s to depend on the difference $x_s - y_s$; processes with this property are called locally isotropic.

5.1.4 Correlation function by averaging over the ensemble

The field at the entrance of each screen shall be denoted by u_n and the Fourier transform for all the functions considered here is denoted by the hat symbol, so for instance \hat{u}_n is the Fourier transform of u_n .

In general, u_n may be statistically related to ϕ for a single layer, because as v propagates from layer to layer, u_n depends on ϕ . It will be shown that it is possible, at least mathematically, that the energy correlation of the field can be calculated if the medium is statistically independent of the incident field.

The Green's parabolic function

The Green's function for the Helmholtz equation is well known, and in appendix (A.3) the Green's function for the Helmholtz equation in the paraxial approximation is given and has the following form

$$g(x - x', z - z') = (1 + i) \sqrt{\frac{k}{4\pi(z - z')}} e^{ik \frac{(x - x')^2}{2(z - z')}} \quad (5.14)$$

The Eq. (4.17) is written in the spatial frequency domain and the actual calculation of Γ_μ is performed in the spatial domain. Hence rewriting Eq. (4.17) in the spatial domain the function g arises acting as a propagator. For a derivation of the Green's function g from the angular representation of the field see [64].

As in the case of the screens, the multiple propagation through screens results in multiplicative functions if written using several variables. That is, at each screen, let us say the s -th screen, one has to consider the following product $g(x_s - x_{s-1}, z_s)g^*(y_s - y_{s-1}, z_s)$. Multiplied altogether one has to define a multivariable Green's function.

The function propagator in several variables or the multivariable Green's function is simply the multiplication of the Green's function Eq. (5.14) by its conjugate

evaluated at every single coordinate x_s , thus

$$G(\mathbf{x}, \mathbf{z}) = \prod_{s=1}^n g(x_s^-, z_s^-) \quad (5.15)$$

where $x_s^- = x_s - x_{s-1}$. The function G is a deterministic function bearing no relation with the ensemble average but the fact that it is a multidimensional Gaussian function considerably simplifies the integration. This is one of the reasons in making the parabolic approximation since it is possible to give a simple expression for the correlation function.

Calculation of Γ_μ

To calculate the transverse correlation of the field, i.e. $\Gamma_u(x, x', z) = \langle u(\mathbf{x}, z)u^*(\mathbf{x}', z) \rangle$ at distance z away from the source, is necessary to take the ensemble average of Eq. (4.17) in the spatial domain. In achieving this, let us set $H(\mathbf{x}, \mathbf{y}) = G(\mathbf{x}, \mathbf{z})G^*(\mathbf{y}, \mathbf{z})$ and define the ensemble average of vs as $f = \langle v(\mathbf{x}_0)v(y_0) \rangle \langle s(\mathbf{x})s^*(\mathbf{y}) \rangle$, the ensemble splits because v and s are statistically independent. Thus the ensemble average $\langle u_n(x_n)u_n^*(y_n) \rangle$ using Eq. (4.17) is given by

$$\Gamma_u = \int \cdots \int f(\mathbf{x}, \mathbf{y})H(\mathbf{x}, \mathbf{y})d\mathbf{x}d\mathbf{y} \quad (5.16)$$

To be able to integrate Eq. (5.16) one would need to calculate the average f but this is not necessary as long as f is a function of the difference $\mathbf{x} - \mathbf{y}$ only. This is a consequence of ϕ being a Gaussian and locally isotropic process. Thus, using Eq. (5.13), f takes the form

$$f = \langle v(\mathbf{x}_0)v(y_0) \rangle e^{-\sum_{s=1}^N D_\phi(x_s - y_s)} \quad (5.17)$$

To continue the evaluation of integral Eq. (5.16) more notation is introduced to shorten the length of the equations. Let $\Lambda_s^- = \frac{2(z_{s-1} - z_s)}{k}$ and $r_s = (x_s - x_{s-1})^2 - (y_s - y_{s-1})^2$ be with obvious definition in vectorial form. Then Eq. (5.16) can be

rewritten as

$$\Gamma_u = b \int \cdots \int f(\mathbf{x}, \mathbf{y}) \prod_{s=1}^N \left\{ \frac{\exp[-i \frac{r_s}{\Lambda_s^-}]}{\Lambda_s^-} \right\} dx dy \quad (5.18)$$

where $b = (-\frac{1}{\pi})^N$. A step further in calculating the above integral follows by making the following change of variables: $2\mathbf{x} = \mathbf{p} + \mathbf{q}$, $2\mathbf{y} = \mathbf{q} - \mathbf{p}$, therefore $r_s = (p_s - p_{s-1})(q_s - q_{s-1})$ or $r_s = p_s^- q_s^-$. Thus, Γ_u in the new coordinate system is

$$\Gamma_u = b \int \cdots \int f(\mathbf{p}, \mathbf{q}) \prod_{s=1}^N \left\{ \frac{\exp[-i \frac{p_s^- q_s^-}{\Lambda_s^-}]}{\Lambda_s^-} \right\} d\mathbf{p} d\mathbf{q} \quad (5.19)$$

Now, using that, Eq. (5.17) depends only on the difference of its coordinates, f would be a function of \mathbf{p} only, and so it is possible to integrate with respect to \mathbf{q} . Recognising, that the function to be integrated in Eq. (5.19) is the Fourier transform of the identity thus resulting in a product of delta functions. But first, let us express the term appearing inside the exponential function as

$$-i \frac{p_s^- q_s^-}{\Lambda_s^-} = i \sum_s \left[\frac{p_s^-}{\Lambda_s^-} - \frac{p_{s+1}^-}{\Lambda_{s+1}^-} \right] \quad (5.20)$$

with $p_1^- = p_{n+1}^- = 0$, since we have added extra terms for convenience. After inserting Eq. (5.20) in Eq. (5.19) and performing integration with respect to \mathbf{q} , except for the single variable q_0 , we have

$$\Gamma_u = \int f(\mathbf{p}, q_0) \prod_{s=1}^N \Lambda_s^- \delta \left(p_s^- - \frac{\Lambda_s^- p_{s+1}^-}{\Lambda_{s+1}^-} \right) \prod_{s=2}^N \frac{1}{\Lambda_s^-} d\mathbf{p} dq_0 \quad (5.21)$$

where δ is the Dirac function delta. In the above expression N is an even integer otherwise one would have to multiply the term on the right by $(-1)^N$.

Finally, integration can be completed by noting that if $\Lambda_s^- = \Lambda_{s+1}^-$ for all s , i.e. all screens are allocated at equal distance in space then we have

$$f(\vec{p}_N, q_0) \prod_{s=2}^N \Lambda_s^- = \int f(\mathbf{p}, q_0) \prod_{s=1}^N \Lambda_s^- \delta \left(p_s^- - \frac{\Lambda_s^- p_{s+1}^-}{\Lambda_{s+1}^-} \right) d\mathbf{p} \quad (5.22)$$

Here, $\vec{p}_N = (p_N, \dots, p_N)$. The final expression for Γ_u is obtained by inserting Eq. (5.17) and Eq. (5.22) into Eq. (5.21), in doing so

$$\begin{aligned}\Gamma_u &= e^{-ND_\phi(p_N)} \int \langle v(\frac{p_N + q_0}{2}) v^*(\frac{p_N - q_0}{2}) \rangle dq_0 \\ &= e^{-ND_\phi(p_N)} \Gamma_v(p_N)\end{aligned}\quad (5.23)$$

where D_ϕ is given in Eq. (5.9) by changing to the new variable $p_N = \tau$. The above calculations show that the energy function at distance L is equivalent to the product of individual energy functions at the exit of each layer. Letting N tend to ∞ Γ_u approximates to a continuous solution of second order moment of the Helmholtz's equation. An approximate solution for the second order moment of Eq. (3.11) is given in [70] and closely coincides with Γ_u . An expression for the correlation function of the backscattering field is also given in that paper. An example of the energy correlation over a distance corresponding to several grains, as calculated according to Eq. (5.23), is illustrated in Fig. (5.3). The decay and width as it propagates is determined by σ and l , respectively. As a reminder, σ is the standard deviation of the process μ characterising microstructure and l is correlation length proportional to grain size in polycrystalline materials.

The extreme case, i.e. for a highly aberrated medium, that is, $\sigma \rightarrow 1$ and small l -small grains- then the function Eq. (5.23) decays rapidly having a narrow tail. The ideal case occurs when $\mu = 0$, that is a homogeneous medium, Γ_u so does not change with the propagation distance.

The chart shows a series of images of the correlation function for different values of σ and l . From the chart one can observe the behaviour of this function as the parameters are varied. The very first row shows the correlation of the field in a homogeneous medium. The row on the bottom line shows the behaviour of Γ_u for larger values, that is $\sigma \rightarrow 1$ and $l \rightarrow \infty$ which represent a medium with strong anisotropy and large mean grain size.

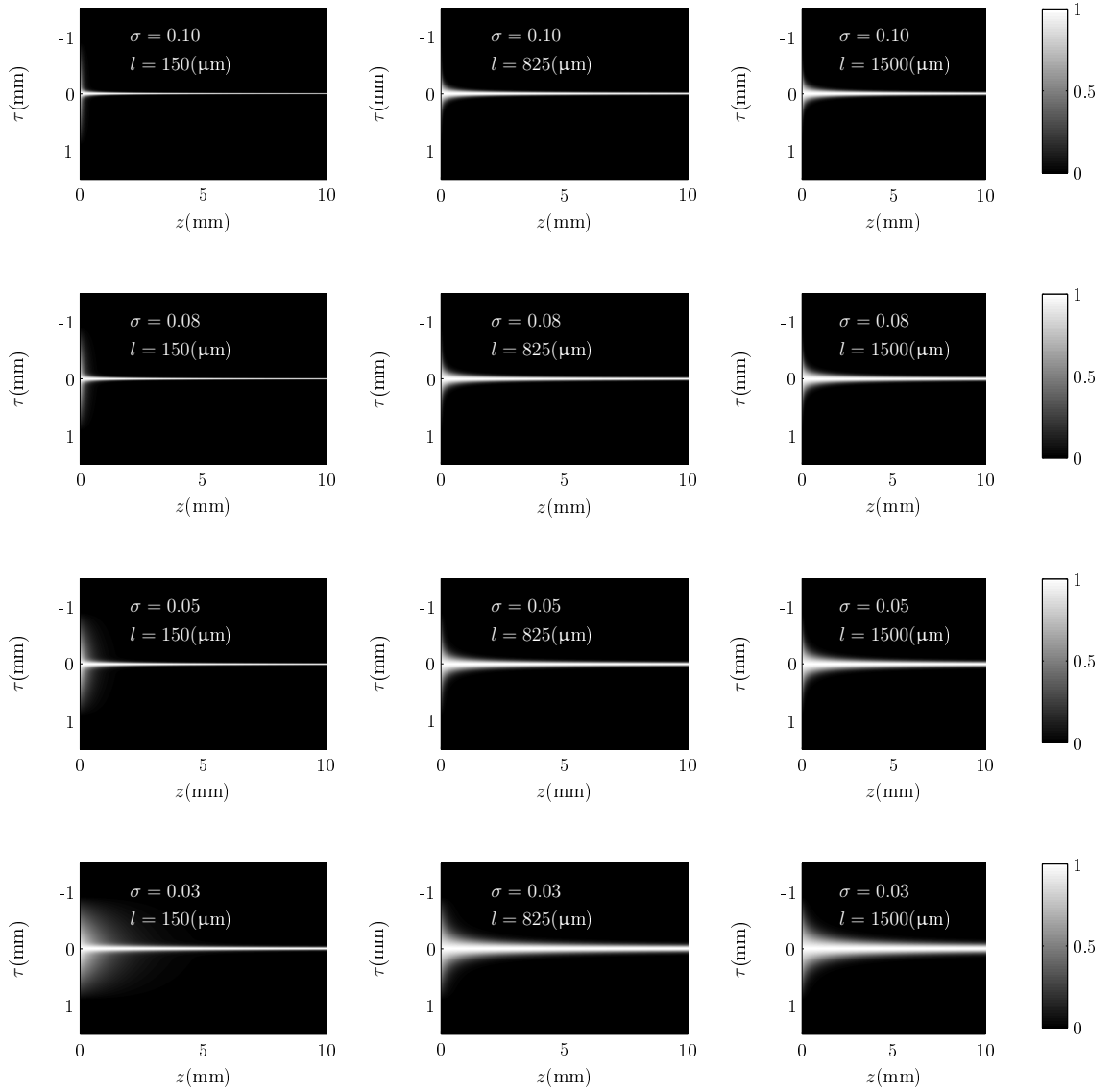


Figure 5.3: Images of the energy correlation propagating in a random medium - z -direction- as a function of σ and l , Eq. (5.21). The correlation function has been plotted in arbitrary normalised units.

5.2 Using a derived differential equation

The calculation of the second order moment of the field in a random medium is not straightforward as the last section has shown. Even for the case of single scattering. Many authors had dealt with second order moments, [70, 59, 49, 40, 98, 97, 24, 60], of solutions of the stochastic wave equations with applications to different areas, such as optics, and acoustics as well as elasticity. Some have given approximate solutions under the assumption that the random process characterising the medium is delta correlated in the direction of propagation, or the Markov approximation as it is also known. In references [47, 46], an equation for the second order moment is obtained and its solution is shown under the Markov approximation. It was found that this solution is basically the second moment previously obtained in (5.1.4), using the spectral representation of the field.

5.2.1 Equation for the second moment

The equation derived in [47, 46], is presented with the aim of giving an alternative approximation to $\Gamma(x, x', z)$ already given in the previous section.

Following the development in [47, 46], although it is easy to derive from Eq. (3.11) in its paraxial version, the equation for $Z(x, x', z) = u(x, z)\bar{u}(x', z)$ is given by

$$2ik\partial_z Z + [\Delta_x - \Delta_{x'}]Z + k^2[\mu(x, z) - \mu(x', z)]Z = 0 \quad (5.24)$$

Note that the ensemble average has not been taken yet, which means that the equation for second moment is far from complete. In order to find an equation for $\langle Z \rangle$ the average of the third term in Eq. (5.24) has to be calculated. But this is difficult, without assuming that μ is delta correlated, that is, its correlation satisfies $\langle \mu(x, z)\mu(x', z') \rangle = \delta(z - z')f(x - x')$, f an arbitrary function and δ the Dirac delta function. Using this condition, and the assumption about the incident field, which is that its correlation function depends only on its difference, it is possible to define a random process that satisfies Eq. (5.24) after taking the mean.

Let the following process

$$Z_\gamma(x, x', z, \xi) = Z_0(x, x', \gamma) e^{\frac{ik}{4}g(\mathbf{r}, \xi)} \quad (5.25)$$

be where $g(x, x', z, \xi) = \int_0^z [\mu(x, z', \xi) - \mu(x', z', \xi)] dz'$ and $Z_0 = v(x, \gamma)\bar{v}(x', \gamma)$. Since v is fixed it is obvious that g must meet certain conditions so $Z_\gamma(x, x', z, \xi)$ is a solution of Eq. (5.22) for all ξ . One could try to find those conditions but since the important quantity here is the mean over an ensemble, that will not be necessary. The initial condition at $z = 0$ is indicated with the product of the incident random processes $v(\cdot, \gamma)$ and its conjugate. The γ is aimed to indicate that v belongs to a different ensemble which implies that $Z_\gamma(\cdot, \xi)$ has to be averaged twice. This does not represent a problem since the process v and μ are statistically independent.

Taking the average in Eq. (5.24) results in

$$2ik\partial_z \langle Z_\gamma \rangle + [\Delta_x - \Delta_{x'}] \langle Z_\gamma \rangle + k^2 \langle [\mu(x, z, \xi) - \mu(x', z, \xi)] Z_\gamma \rangle = 0 \quad (5.26)$$

One still has to find a random process that satisfies Eq. (5.26) and there is no way to prove that process Eq. (5.25) satisfies Eq. (5.26). Obviously

$$2ik\partial_z \langle Z_\gamma \rangle + k^2 \langle [\mu(x, z, \xi) - \mu(x', z, \xi)] Z_\gamma \rangle = 0 \quad (5.27)$$

is satisfied for the process of the form Eq. (5.25)). Therefore, the solution to Eq. (5.26)) reduces to finding processes of the form Eq. (5.25)) that satisfy the condition

$$[\Delta_x - \Delta_{x'}] \langle Z_\gamma \rangle = 0 \quad (5.28)$$

The realisations of the process Z_γ are defined by the realisations of the process μ . This means that the mean $\langle Z_\gamma \rangle$ is completely determined by the statistical properties of μ . In principle, all processes satisfying Eq. (5.28) would solve Eq. (5.26) but the derivation here is in more elementary terms. One of the assumptions is that μ is a

Gaussian process, besides being transversally isotropic, and almost delta correlated in the direction of propagation, thus the mean $\langle Z_\gamma \rangle$ is a function of the mean $\langle g^2 \rangle$.

Let us first average Z_γ with respect to ensemble γ , that is, using the same letter to average the initial condition one has $Z_0(x - x') = \langle v(x, \gamma) \bar{v}(x', \gamma) \rangle_\gamma$. Hence the average $\langle Z \rangle$ over the ensemble is equivalent to obtaining $\langle e^{\frac{ik}{2}g(x, x', z)} \rangle$, which is something that can be achieved if g is a Gaussian process.

The process $g(x, x', z, \xi)$ is Gaussian since μ is a Gaussian process. It is well known that for any Gaussian process g

$$\left\langle e^{\frac{ik}{2}g(x, x', z)} \right\rangle = e^{-\frac{k^2}{8}\langle g^2 \rangle} \quad (5.29)$$

so it remains to calculate $\langle g^2 \rangle$. Now, the mean $\langle g^2 \rangle$ is in fact the structure function D_ϕ already introduced in section (5.1.2) for Gaussian statistics. After inserting Z_0 and $\langle g^2 \rangle$ into Eq. (5.29) the ensemble average $\langle Z(x, x', z, \xi) \rangle$ of Eq. (5.25) is

$$\langle Z(x, x', z, \xi) \rangle = Z_0 e^{\frac{\sqrt{\pi}k^2}{4}lz[\Gamma_\mu(0) - \Gamma_\mu(x - x')]} \quad (5.30)$$

Now, expression on the right hand side of Eq. (5.30) is a function of the difference $x - x'$ so is $\Gamma = \langle Z(x, x', z, \xi) \rangle$. It is now straightforward to check that Eq. (5.28) holds true by substituting Eq. (5.30) in Eq. (5.28). Therefore, processes $Z(x, x', z)$ of the form Eq. (5.25) satisfy equation Eq. (5.26).

In this section a random process has been derived such that its 2-point correlation satisfies Eq. (5.26) and this coincides with Eq. (5.23) previously developed in section (5.1.4) using a different method.

5.3 Concluding remarks

The calculation of the average correlation function of the field has been given first by the phase screen method and derived from a differential equation in a separate section. The integral representation given in chapter (4), Eq. (4.17) was used to approximate the average correlation function, by directly calculating the cross average

of the field. The paraxial assumption allowed us to integrate the resulting multiple integral. The average of the multiple phase screen in the integrand of Eq. (5.16) could have been calculated because of the Gaussian assumption on the process μ , that follows from a standard result for multivariate Gaussian processes. It is possible that in the future these conditions could be removed so as to include processes with more general characteristics, thus representing other types of polycrystals.

The resulting correlation depends on the number of screens used to approximate the field, thus giving a discrete approximation of the correlation. The section where we have derived the correlation from an differential equation was intended in a way to alleviate this limitation. The resulting correlations are essentially the same if one uses an exponential function for the process μ . It has to be observed that the same result is obtained if one assumes from the beginning that u is statistically independent, under which condition the operator $[\Delta_x - \Delta_y]$ is eliminated from the equation. At any rate, any of the Eq. (5.23) or Eq. (5.30) can be used for theoretical purposes as will be seen in chapter (6).

Chapter 6

Experimental methods and results

Introduction

In the previous chapters a theoretical model for SAWs in polycrystals was developed. The aim was to derive a correlation function for the field which relates the statistical properties of the medium to the statistical properties of the field. This correlation was the transverse correlation of the field and was dependent on the degree of inhomogeneity and the correlation length of the medium. In this chapter this is investigated experimentally by imaging the deviation of an plane acoustic wave on the surface of the polycrystal. Aluminium and titanium were used as media because they have relevance to industrial measurements and exhibit well defined properties.

In order to measure the correlation function, which is stochastic, it is necessary to measure an ensemble of independent samples of the medium. So multiple measurements were carried out on the surface of the samples to get an experimental ensemble of the acoustic field. A procedure based on the estimator of the mean correlation for a finite sequence is given to study the acoustical ensemble statistically. From this analysis a transverse correlation function can be measured for each sample with the aim of comparing it to the theoretical correlation to obtain the degree of inhomogeneity and the mean grain size of the samples. Material characteristics, such as mean grain size, are obtained by numerically solving a nonlinear fitting problem for the measured and theoretical correlation function.

The instrumentation is briefly introduced describing the main characteristics of the OSAM system on which the experiments were carried out. Part of the experimental work was the selection and preparation of the samples and their metallographic characterisation. This is explained in detail as is their characterisation by the direct measures of the grain size from photomicrographs.

The results comparing the theoretical and measured correlation function of the ultrasonic ensemble are presented at the end of this chapter together with some conclusions.

6.1 Sample selection

Two different metals were selected, aluminium and titanium. Aluminium was selected because is extensively studied in the literature, both ultrasonically as well as mechanically. The other reason was because of the well understood technique to produce samples with different grain sizes and a certain degree of spatial randomness of the grains. Aluminium naturally shows grain structure as shown in Fig. (6.1). The photomicrograph, clearly shows huge elongated grains and the regions have certain degree of spatial orientation. From theoretical and experimental points of view these types of samples were not of interest for the present research, mainly because of the elongated grain shape, which is extremely difficult to model. The microstructure of aluminium in Fig. (6.1) can be modified by adding a refiner. Using the refiner the grains tend to become mainly convex, and spatially distributed at random.

Titanium metal was selected mainly because of increasing interest in determining its properties non-destructively in industry. The titanium sample, widely used in aeroplane, engines was provided by Rolls Royce.

6.2 Sample preparation

Three different aluminium samples were created, *A*, *B* and *C*, each with a different mean grain size, and one block of titanium. The grain size distribution in aluminium

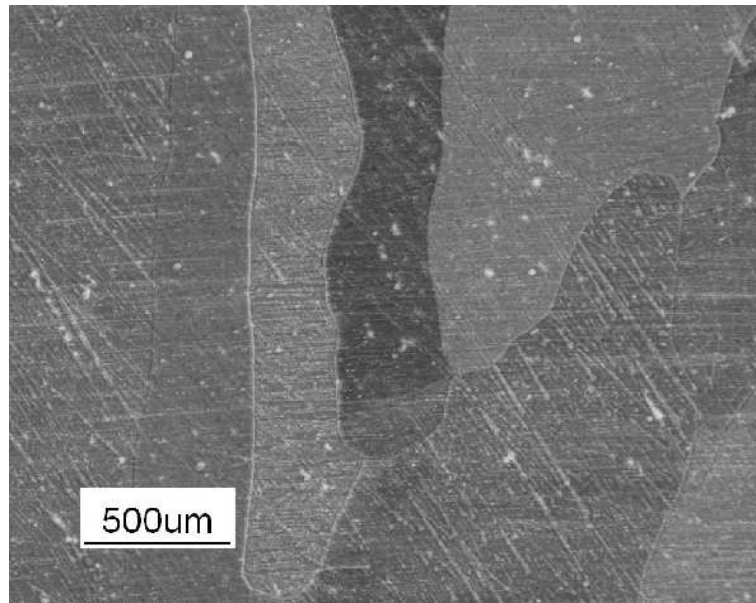


Figure 6.1: Photomicrograph showing individual elongated grains in an aluminium sample. The photomicrograph was obtained in a conventional microscope under cross-polarised light.

was selected by varying the concentration of the refiner. The procedure is similar for all of them so only a detailed description for one sample is described here.

6.2.1 Procedure for refining grains in Al

An Al (99.9%) charge of 500gr, contained in a clay bonded SiC crucible, was heated to 730°C in a muffle furnace. After melting the Al charge and in order to obtain a lightly refined Al ingot, 0.2wt.% of an Al-titanium-B commercial grain refiner was added and dissolved into the melt. Prior to removal of the oxide skin from the surface of the molten metal, the melt was cast into a rectangular steel mold in which it was allowed to solidify naturally. The Al ingot was released from the mold and sectioned with a band saw. Due to the geometry of the steel mold, a coarse columnar grain structure is expected in the top part of the Al ingot. For this reason, that section was removed and four useful blocks were obtained. Owing to the symmetry of the ingot, only three blocks were used; one for the counter part for metallographic characterisation and the third was subjected to *macro etching* to reveal the overall grain structure. The macro etching is simply the immersion of the sample in a

solution to reveal the microstructure and to be able to observe it with the naked eye. Samples for metallography were taken from one block and were mounted, ground and polished down to $1\mu\text{m}$ following standard polishing procedures. The same preparation was given to the counter face of the other block. To reveal the grain structure, the Al block was repeatedly immersed into a solution (38% H_2O , 45% HCl , 15% HNO_3 and 2% HF) and washed until a good contrast was achieved. Also, the Al polished samples were anodised in a 2% solution of KBF_4 in water for 1 min at 25V [31]. After washing and drying, the samples were viewed and imaged in an optical microscope, equipped with a digital camera, under cross-polarised light.

The idea with this technique was to create samples with different grain sizes, mainly convex grains and spatial random distributions [31], by refining the grain size by adding small quantities of the refiner, Al-Ti-B, to the aluminium. This technique did work well for high concentrations of Al-Ti-B in the mixture which has produced samples, identified as M_B , M_C below, with the required characteristics. The technique is probably not suitable for producing samples with those characteristics and grain mean sizes bigger than $1000\mu\text{m}$, as it was the case for the other two samples.

Finally, the samples were polished to a mirror-like finish for ultrasonic inspection using standard techniques.

Ti preparation

One single block of titanium was prepared for ultrasonic inspection. The metal block was polished to a mirror-like finish for inspection. Immediately after the ultrasonic experimentation was complete a small piece of the corner, $1\text{cm}\times 1\text{cm}$ in size, of the sample was cut-off for metallographic characterisation. This small section was etched with the purpose of revealing the microstructure, but most of the standard techniques did not reveal clearly the microstructure as with the aluminium samples. Nevertheless, a photomicrograph is presented in section (6.3.1) where it can be appreciated that the microstructure of the Ti sample is complicated.

6.3 Metallographic characterisation

Characterisation of a metal, in particular Al, means more than just measuring the grain size of the microstructure. Other properties inherent to metals like mechanical, optical or physical characteristics, to mention just a few, are beyond the scope of this work. However, the optical properties of the surface of the sample are important since this technique requires samples with well polished surfaces for laser ultrasonic analysis. The metallographic analysis or characterisation of samples means, in this context, the estimation of the grain size distribution expressed in terms of a mean grain size and a standard deviation. The unit chosen for these quantities was the micrometre.

The characterisation of the aluminium is presented first, followed by the titanium sample.

6.3.1 Digital characterisation

The grain size distribution was measured directly from a digital image for each block. The image corresponding to block A will be referred as M_A , M_B for block B and so on.

Using open source software¹ the perimeter was measured for each region contained within each micrograph and stored in a file for mean estimation. The mean calliper diameter, as defined by Eq. (3.20), was obtained by dividing the mean diameter of each region [34] by π .

Characterisation of block A

For block A , M_A is not a single image but several pictures stitched together. This procedure was necessary due to the optical limitation of the microscope used at the time of imaging the samples. The image in Fig. (6.2) does not contain a sufficient number of grains for statistical estimation. A sensible number in the population of the grains would be at least fifty.

¹ImageJ <http://rsb.info.nih.gov/ij/>

To minimise the error, software was used to identify similar points of adjacent images and it was possible to stitch them together. In this way an image containing more than enough regions for metallographic characterisation was created. The im-

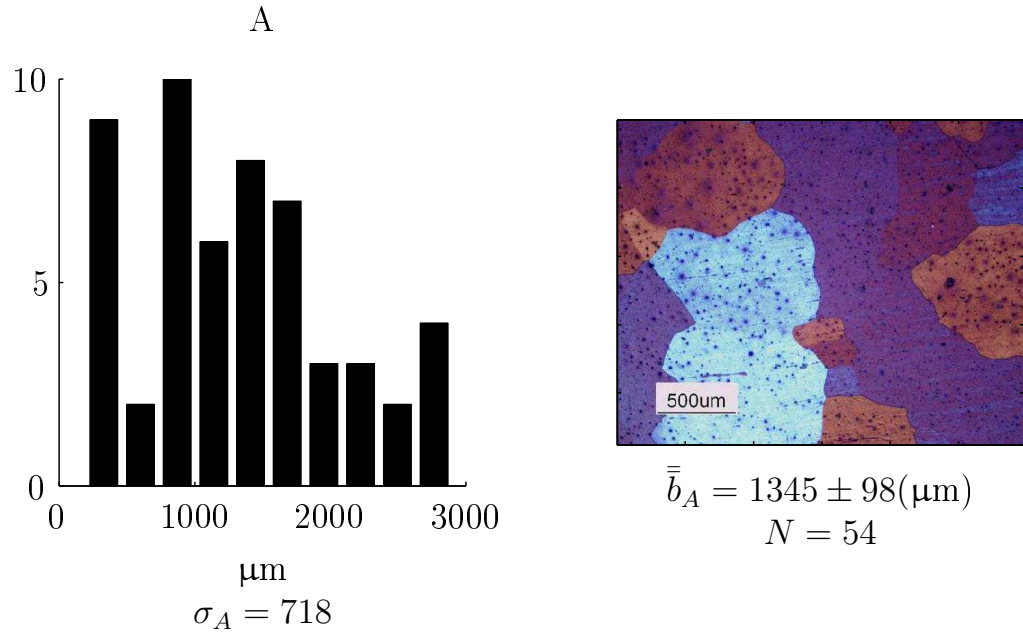


Figure 6.2: A histogram of the grain size distribution for M_A is showed on the left hand side, where σ_A is the standard deviation of the grain size distribution. To the right hand side, the photomicrograph of the aluminium sample is shown, under-cross polarised.

age M_A corresponding to block A has a more complicated microstructure compared to M_B , M_C , in that it contains non-convex regions. The other problem was that the contrast in some regions of the etched surface was very poor, so quite a few grains were merged into one. Additionally, some of the grains were completely embedded within larger grains, in which only the big ones are counted. This feature made characterisation difficult.

The complication with grain characterisation can be seen in Fig. (6.2), where the distribution does not uniformly accumulate around a central value. Nevertheless, the results were approximately $\bar{b}_A \approx 1345\mu\text{m}$ for the mean grain size, standard deviation $\sigma_A = 718$, and the number of grain considered was $N_A = 54$. The mean calliper diameter number was roughly checked with a different method by measuring the number of visible grains within an square and dividing the area of the square

by number of grains, results were comparable with both techniques.

Characterisation of block B

For the second piece a similar procedure was applied as described in previous paragraphs, but the number of regions present in one image was far greater than in M_A in Fig. (6.3). The difference with M_B is that it has a homogeneous distribution of mainly convex grains. In the sense that the size distribution is more evenly distributed, unlike A , making the estimation of the length of the boundary for each region easier. Strictly speaking, neither M_A nor M_B have microstructure completely populated with convex regions. To make characterisation easier, grains which are mainly concave are being thought as convex when estimating the mean calliper diameter. On average grains mainly convex outnumber grains mainly concave for aluminium sample M_B . Fig. (6.3) shows the results of measuring grain size distribu-

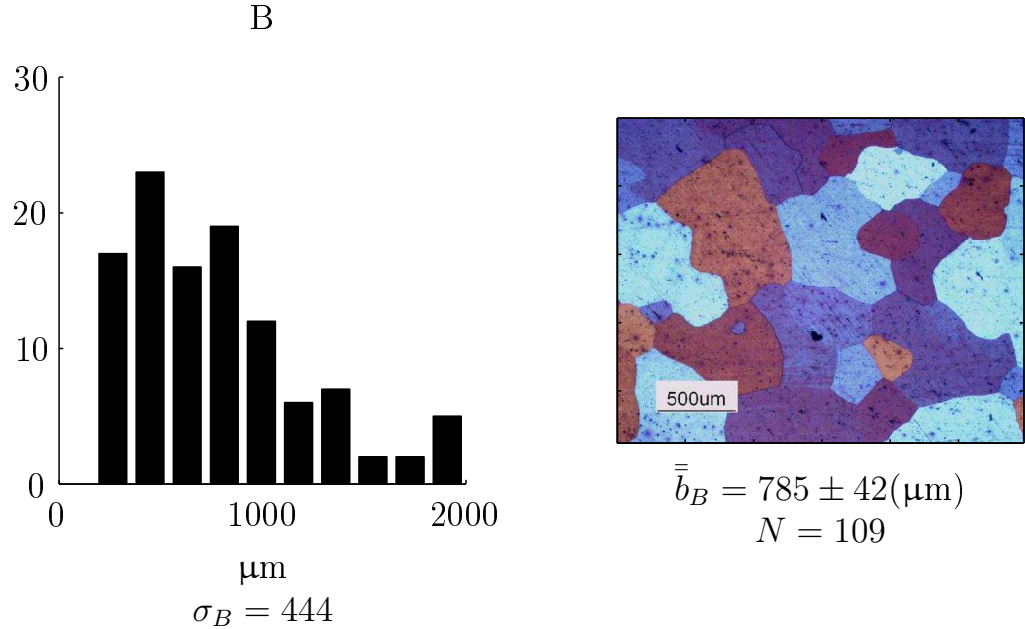


Figure 6.3: A histogram of the grain size distribution for M_B showed on the left hand side, where σ_B is the standard deviation of the grain size distribution. To right hand side, the photomicrograph of aluminium sample is shown, under-cross polarised.

tion for each region by measuring their perimeters. The mean calliper diameter was obtained under similar conditions from equation Eq. (3.20) with an approximate

value of $\bar{b}_B \approx 785\mu\text{m}$. The numerical values for the standard deviation σ_B and the number of regions N_B considered in this case are also shown in Fig. (6.3).

Characterisation of block C

A third sample aluminium M_C was characterised with encouraging results. This sample has the smallest grain sizes compared to the other two so one could see high number of grains in a single image. It was not necessary to take several images and stitch them together. The interesting feature of this sample is the evenly distributed grain configuration. The frequency of grains of size of approximate mean value

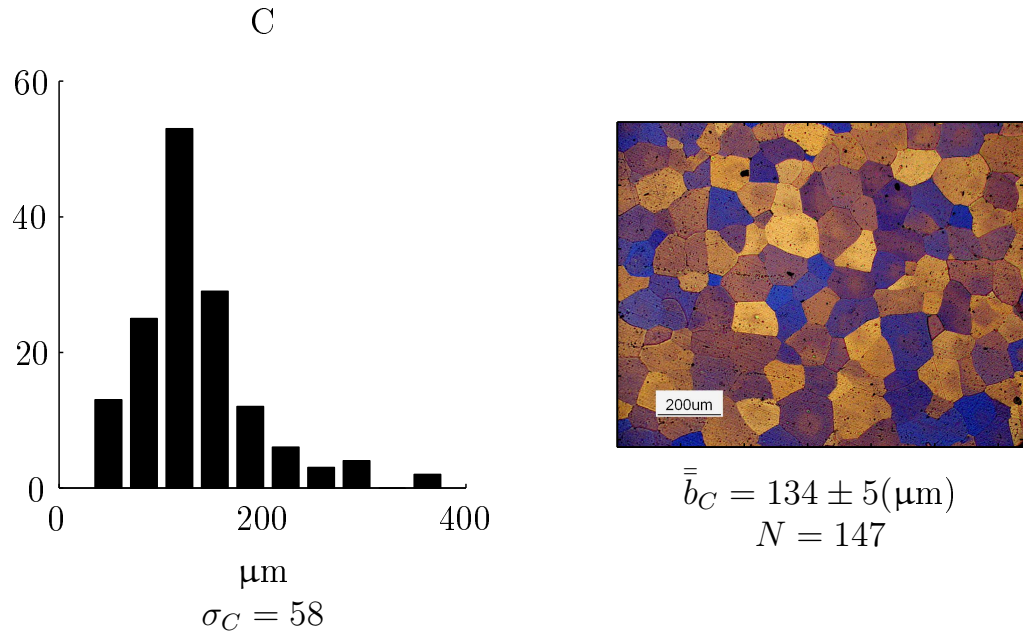


Figure 6.4: A histogram of the grain size distribution for M_C showed to the left hand side, where σ_C is the standard deviation of the grain size distribution. To right hand side, is the photomicrograph of the aluminium sample showing, under-cross polarised light the grain for block M_B .

$\bar{b}_C \approx 134\mu\text{m}$ is high, making a good distribution as shown in the histogram in figure Fig. (6.4). The high contrast between regions in this sample made perimeter measurement easier, considerably reducing the error.

Characterisation of Ti

The characterisation of this sample was difficult. At the beginning it was thought it was titanium but most of the standard techniques for etching titanium to reveal the microstructure did not show the expected result, so an alloy must have been present. Below, in figure Fig. (6.5), is shown the photomicrograph of a section of titanium sample etched to reveal the microstructure. It was obtained in a standard microscope equipped with a digital camera after etching the surface of the metal with standard techniques. There are certain regions that could correspond to grains

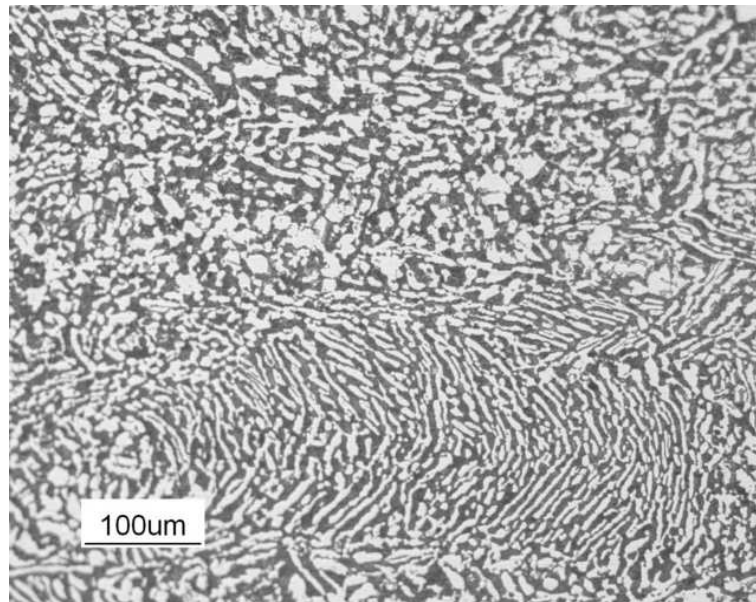


Figure 6.5: Photomicrograph of the surface of titanium etched by standards procedures to reveal the microstructure.

but it is difficult to conclude that they actually correspond to grains. Therefore, the estimation of the mean grain size was not possible for this particular sample. The complicated microstructure made the discussion about the observed aberrations in this sample difficult as well.

6.3.2 Error in characterisation

The perimeter was measured by using graphical interpretation using the open source software as before. A source of error is then how accurately a normal human being

can measure the perimeters of regions composed entirely of pixels with the aid of a computer mouse. The other possible source of error is in the procedure of taking several digital pictures by mechanically moving the sample to a different position, with the possibility of the microscope being out of focus.

A more quantitative error is given in terms of the standard deviation and the number of regions considered for each block, i.e. $E_s = \sigma_s / \sqrt{N_s}$ where $s = A, B, C$, showed in Fig. (6.2), Fig. (6.3) and Fig. (6.4). This is the *standard error* [99], which measures the difference between the estimated and the true values for the diameter of the grains. The units of the standard deviation σ_s are the units used for estimating the mean size distribution, therefore the units of E_s . The mean grain distribution was estimated in micrometres.

6.4 Experimental setup

Over the past few years an Optical Scanning Acoustic Microscope (OSAM) has been developed [89]. This highly flexible instrument can be fully automated and is capable of performing multiple acoustic measurements over the surface of a sample. Advantages has been taken of these capabilities to build up an ensemble of the acoustic field over the surface of aberrating materials.

6.4.1 SAW generation systems

Two different type of devices were used for SAW generation in the experimental work. The first one is a spatial light modulator (SLM) being part of the OSAM system, which is briefly presented below, and a 10MHz transducer, which replaced the SLM as source of SAWs for the titanium sample.

The OSAM system

The main components of the OSAM are shown in Fig. (6.6). It uses a Q-switched mode locked Nd-YAG laser for SAW generation, by using a spatial light modulator

(SLM) to image any desirable pattern—typically a set of arcs or straight lines—onto the surface of the material under investigation. This image, illuminated by the pulsed laser, acts as the source of the surface waves. The fundamental frequency at which the OSAM generates ultrasound is 82MHz, but multiples of that frequency can be also generated.

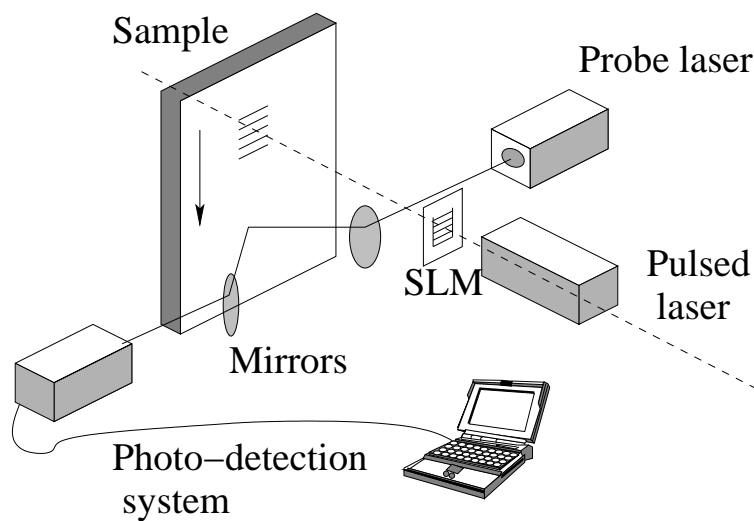


Figure 6.6: A pattern generated by a spatial light modulator is imaged onto the sample using a pulsed laser. This pattern acts as the source of the surface acoustic waves. The waves are detected by another laser, using an optical beam deflection technique [19].

SAW generation using a transducer

The ultrasonic inspection of titanium was performed by generating SAWs using a standard 10MHz transducer. In this experiment, the SLM was replaced by the transducer as the source to generate SAWs on titanium as shown in Fig. (6.7). The same probe and capabilities of the OSAM were used, so it uses the mechanical and optical setup of OSAM system to detect SAWs in titanium. Two things were taken into consideration for changing devices for SAW generation. Firstly, and most important, is that it was not possible to launch a SAW in titanium at 82MHz, which is the fundamental frequency of the OSAM and actively uses the SLM to achieve it. Secondly, the idea was to have a broadband source to test the microstructure of titanium at different scales relative to the wavelength. The transducer was a 10MHz

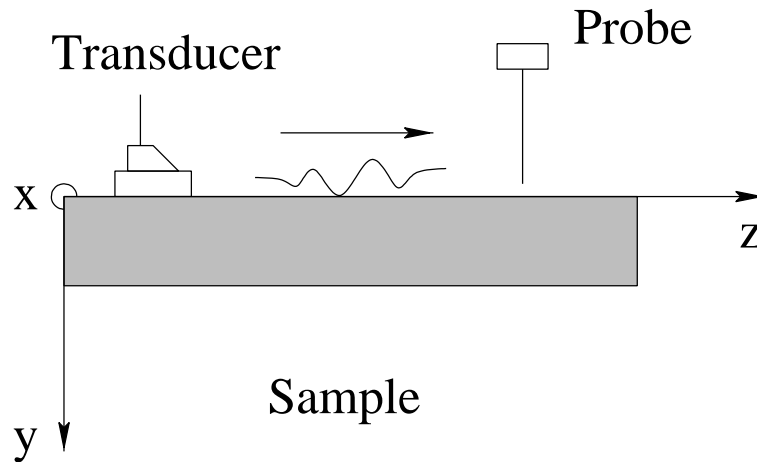


Figure 6.7: Sample and transducer array for SAW generation. The probe and the whole detection system in this experimental setup correspond to the OSAM system.

[Panametrics, A544S-SM], so one can take the amplitude and phase measurement above and below this frequency to see how it interacts with the grain structure of the material. The bandwidth of the transducer allowed one to measure frequencies $\pm 2\text{MHz}$ from the centre frequency. The frequency of the transducer was selected simply on the basis that the transducer was readily available, although it would have been interesting to experiment with other frequencies; unfortunately there was no time for more experiments.

6.4.2 Detection system

A continuous wave laser is used to detect the propagating surface waves using an optical beam deflection technique. Both the detection system and the sample are mounted on computer-controlled automated stages, and so the OSAM is capable of rapidly imaging, due to the analogue data capture system, the propagating wavefront at any position on the sample. A comprehensive overview and technical details are given in [89].

A complete set of software and electronics has been developed for gathering information at high speed. Typically, an amplitude and phase c-scan over an area of $1.5\text{cm} \times 1.5\text{cm}$ with a resolution of $10\mu\text{m}$ can be taken within a matter of minutes.

6.5 Measurements

The ultrasonic investigations on aluminium and titanium samples are presented in this section as a fundamental part of the experimental work. In order to measure the mean correlation function, it is necessary to have multiple independent measurements of the acoustic field across the ensemble of the sample. Fig. (6.8) shows the schematics of the multiple location on the surface of the sample where multiple measurements were performed. It is important to highlight here that the procedure is fully automated so it was only necessary to create a single script in order to perform all the measurements. The materials tested were aluminium blocks, labelled M_A ,

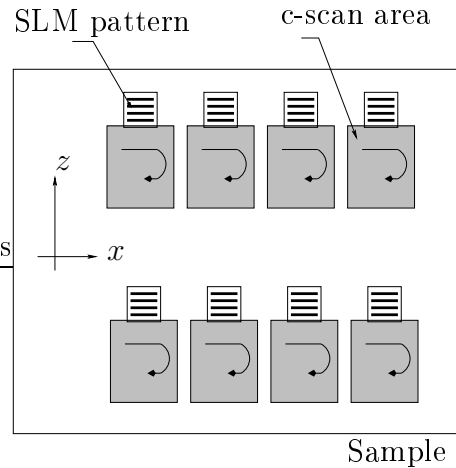


Figure 6.8: Schematic representation of scanning area and source locations to built up an ultrasonic ensemble. At each position of the SLM, marked with a series of black and white stripes, a c-scan was performed across x and z direction. The direction of propagation is along the z axis.

M_B and M_C already introduced and titanium. The measured fields are labelled at each location by u_n^A where A indicates the block it belongs to, in this case to block A , n is the number of c-scans performed in that particular block.

The dimensions of each metal block were approximately $6\text{cm} \times 4\text{cm} \times 1\text{cm}$, which gives sufficient room for multiple measurements since the scanning area is typically $3\text{mm} \times 10\text{mm}$. This area was chosen so the size of the SLM or equivalently the width of the source as well as the spread of the ultrasonic beam was entirely scanned as the SAW propagates in the material. The length of 10mm along the propagation distance was also carefully chosen so to be able to detect SAWs until the acoustic

field became undetectable or the knife-edge was detecting only noisy signals.

The images are presented separately since the grain size distributions are different for each block to give different aberration patterns. In all cases, the SLM was programmed to project a series of straight lines onto the surface of the sample, each line separated from its nearest neighbour by a distance equal to the mean Rayleigh wavelength in aluminium. The waves are generated at 82MHz, which is the fundamental frequency of the excitation laser in the OSAM system, which corresponds to a line spacing of approximately $37\mu\text{m}$ in this material. For the titanium sample a

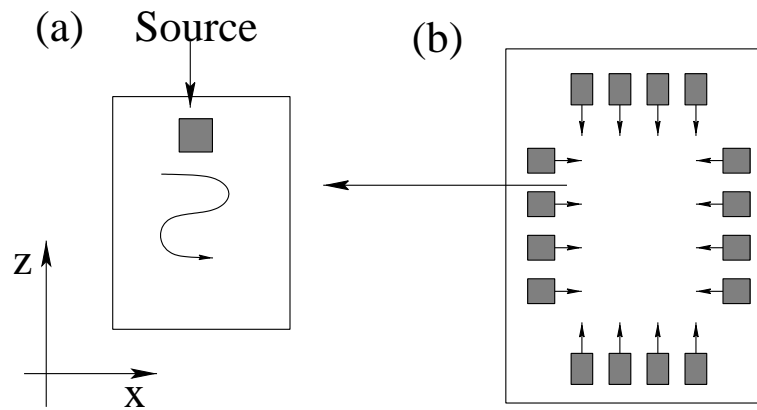


Figure 6.9: (a) Area in xz plane which c-scan has been performed. (b) The black square represents the multiple positions where the transducer has been located to perform a c-scan according diagram (b); whereas arrows indicate the direction of propagation.

similar procedure was carried in order to obtain multiple measurements. The only difference was in the areas chosen within which to perform the scanning. This was mainly because the transducer could only physically be fitted to the edge of the sample. The situation of the scanning areas chosen for this particular experiment is schematically represented in Fig. (6.9)(b). Fig. (6.9)(a) shows the source and the area to perform c-scan for each black square in Fig. (6.9)(b).

The relocation of the source was done manually by moving the transducer to a new location and making sure the contact medium was in good condition at all times. The contact medium was a water based couplant that dries very quickly, so the c-scan had to be done very quickly before the couplant became hard, changing the pattern. The effect of dried couplant could not entirely be avoided, and this can

be noticed in the measured fields which will be presented at the end of this section.

In both experiments, the location of the source is unimportant as long as the areas chosen do not overlap, and the detected acoustic fields remain independent. This was to ensure that every SAW propagated in the samples travelled through different samples of the ensemble of local microstructures. The basic assumption is that each area chosen to perform the scanning represents an independent realisation of the microstructure ensemble which is equivalent to having many independent samples with the same statistical properties.

Case A

Block *A* has large grains compared to mean Rayleigh wavelength, and so they have a relatively small effect on the wave in the direction of propagation. In this particular case, the acoustic field could not be measured until it became uncorrelated because of mechanical limitations of the system. This can be seen in Fig. (6.10), where the signal at 6mm remains strong in some cases and so could have propagated even further. Thus the effect of microstructure on the acoustic field could only be partially observed. Fig. (6.10) shows the amplitude and phase distributions of a plane wave travelling from left to right on different locations in sample *A*. The images show the deviations caused by the microstructure to the wavefront of the acoustic wave. The transverse size of the field is determined by the size of the SLM. The propagation resembles an optical diffraction pattern through a slit since the SLM has a finite aperture. The effects of the corners of the SLM are not observed in this particular experiment.

The images have a typical plane wave pattern propagating in a medium with inhomogeneities such as polycrystals. The wavefront breaks up due to aberration caused by the grain structure, leading to transverse variations in the amplitude. The same effect can be observed in the phase distribution; the wavefront is not flat as one would expect in a homogeneous medium.

One possible cause for the relatively small effect in this experiment is that the grain size is reaching the size of the SLM ($\approx 2\text{mm}$), so the beam behaves as it was

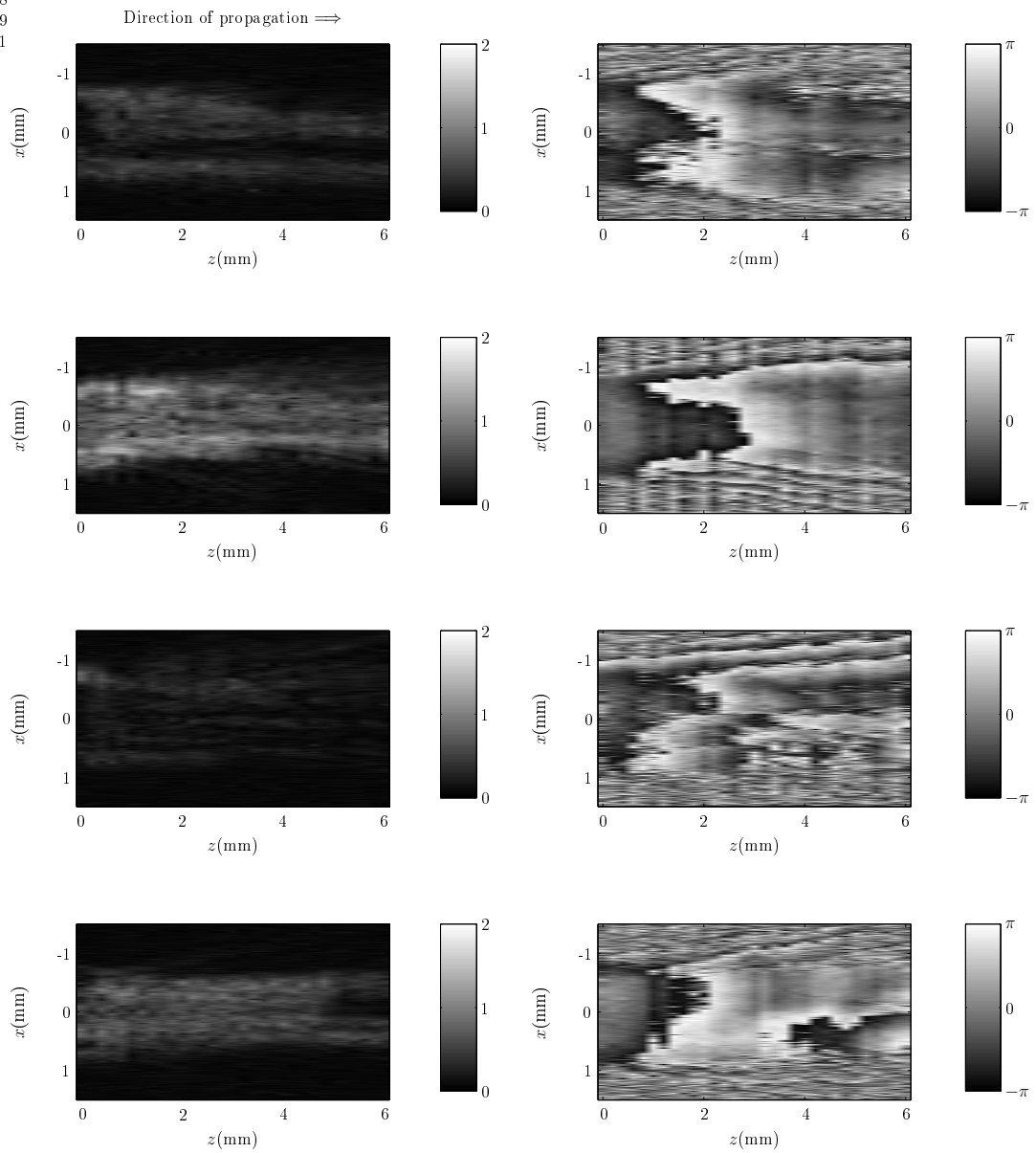


Figure 6.10: The first column is the plot the amplitude distribution of u_n^A at different instances across the sample. The second column shows the phase distribution for each field on the left. The wave propagates from left to right as indicated by the arrow on top of the first column.

propagating in a homogeneous medium.

By comparing the different amplitude images in Fig. (6.10), one can observe that they are different from each other. As the source changes location, one is in fact measuring the acoustic field in a different realisation of the microstructure ensemble. The source position was chosen in such way that the scans of adjacent areas were not overlapping, see Fig. (6.8); thus the family $\{u_n^A\}$ for different n is an ensemble of acoustic fields since different scanning areas correspond to different realisations of the microstructure.

Case B

Under similar experimental circumstances as with block A , the sample B was investigated. Block A and B have similar dimensions, grain size being the only difference between them. The ensemble of acoustic fields was built up by moving the source at different locations and performing a c-scan every time. Fig. (6.11), shows a number of phase and amplitudes images, once again at different locations on sample B . The mean wavelength is still smaller than the grain size distribution, but the grains are smaller compared to the previous case. In this case, it is expected that there would be a stronger interaction between SAWs and grains compared to the one observed previously with sample A . This can be observed as the amplitude decays faster and the field becomes diffuse at propagation distances less than 6mm. By diffuse we mean that the energy of the wave has spread transversally due to aberrations and the acoustic field becomes uncorrelated in the sense that the transverse correlation function tends to a delta function. The phase changes are slightly more difficult to observe here because of the resolution limitations. A comparison can be made with Fig. (1.1) in chapter (1), where the scanning was performed at higher resolution in both directions.

Case C

Finally, sample C was also ultrasonically investigated showing the amplitude and phase distributions of a number of realisations of the acoustic ensemble in Fig. (6.12).

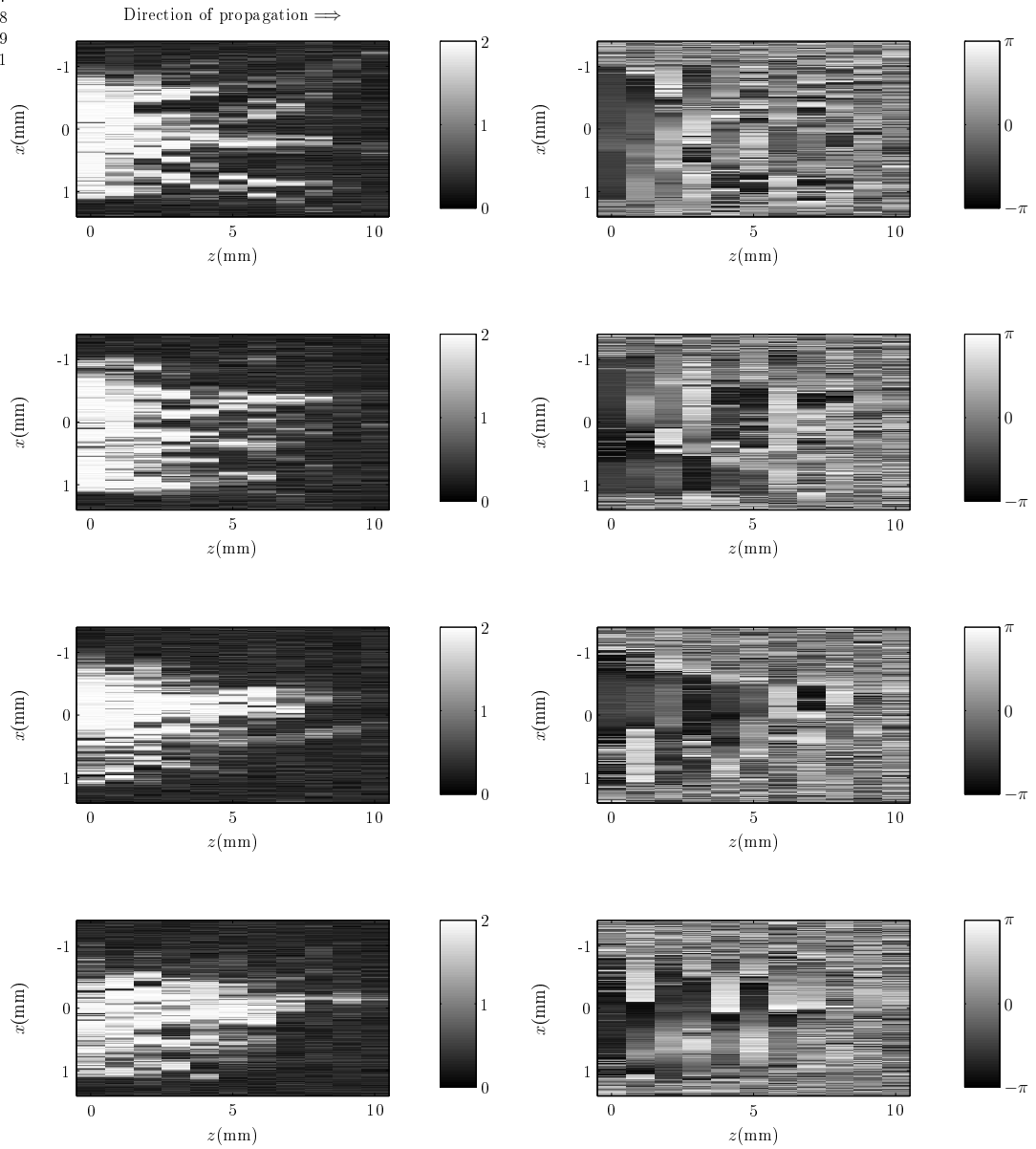


Figure 6.11: The first column is the plot the amplitude distribution of u_n^B at different instances across the sample B . The second column shows the phase distribution for each field on the left. The wave propagates from left to right as indicated by the arrow on top of the first column.

As expected, the wave became diffuse very quickly due to multiple interactions with the grains.

Summary on the values obtained and used previously

The following table summarises the various values obtained and used in the whole experiment.

Aluminium	$\bar{b}(\mu\text{m})$	$\bar{\lambda}_R(\mu\text{m})$	n	$p_x \times p_z(\mu\text{m} \times \mu\text{m})$
M_A	1345 ± 98	35.5	54	5×200
M_B	785 ± 42	35.5	118	5×2000
M_C	134 ± 5	35.5	56	5×100

Table 6.1: Summary of some of the values used and obtained for mean caliper diameter \bar{b} , mean Rayleigh wavelength λ_R , and the number of images n in aluminium samples at 82MHz. p_x, p_z denotes pixel size in x and z , respectively.

The low resolution chosen in the direction of propagation (z -axis) in comparison to the transverse axis is partly due to the relatively small variations of the correlation function field for short propagation distances. So for instance, block M_B has a resolution of $2000\mu\text{m}$ giving as a result a total of eleven slices of the field along the axis of propagation. This is why aberrations cannot visually be observed in Fig. (6.11). The resolution on the rest of samples was increased only for aesthetic purposes to show the variations of the wavefront. It is believed that a minimum of three slices along the propagation direction would be sufficient to observe the overall behaviour of the correlation function. It was important to keep the transverse resolution high since the width of the correlation function will be an estimator of the mean grain size, which is presented in section (6.6). As regards the number n of fields measured, it is believed that $n \geq 50$ would be a sensible number for obtaining an average correlation function. The procedure for obtaining the average correlation is explained in detail in section (6.6). To make sure this was the case, n was increased to 118 for block M_B , making a small difference on average for the correlation function. The other reason, perhaps less important, in keeping n around 50 in blocks M_B and M_C was to speed up the process of gathering data.

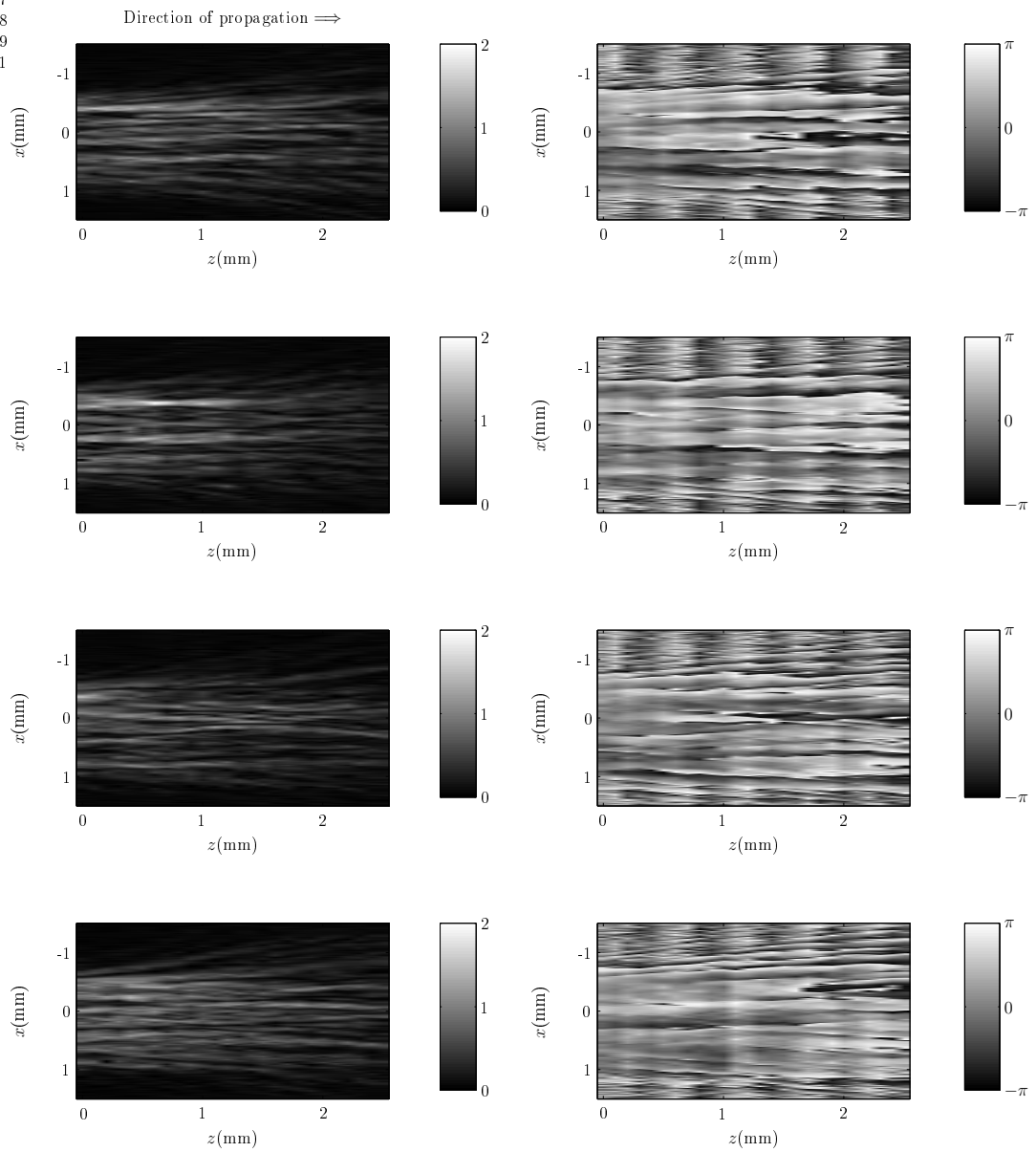


Figure 6.12: The right column is an image of the amplitude distribution of u_n^C at different instances across the sample C . The second column shows an image of the phase distribution for each field to left. The wave propagates from left to right as indicated by the arrow on top of the first column.

The values for the mean wavelength are only approximations for aluminium. The OSAM system is wavelength tunable in order to generate ultrasound so a value of $35.5\mu\text{m}$ for the Rayleigh wavelength, gave the maximum signal that could be observed using a standard oscilloscope for the normal displacement signal.

6.5.1 Measurements in Ti

This section discusses the experiment carried out in the titanium sample; the procedure is similar to the one for the aluminium specimen already discussed. The experimental setup and SAW generation as well as the procedure for the experiment has been discussed in section (6.4). The important point here is to observe how the amplitude breaks up with distance as well as the phase variations. The propagation is from left to right. As it can be observed the speckle patterns are slightly different to each other as the acoustic field interacts at different frequencies with the grains. The purpose of this experiment was to make the ultrasonic field interact with different grain sizes and to build an ensemble of the acoustic field at multiple frequencies. Therefore, for each point $\mathbf{r} = (x, z)$ and fixed source position a time waveform, $u(\mathbf{r}, t)$, for the normal displacement was obtained. The waveform $u(\mathbf{r}, t|\gamma)$ has been transformed to the frequency domain using the Fourier transform,

$$u(\mathbf{r}, \omega|\gamma) = \int u_y(\mathbf{r}, t|\gamma)e^{-i\omega t} dt \quad (6.1)$$

where γ represents a sample of the acoustic ensemble across a microstructural ensemble.

The fundamental frequency of the transducer is 10MHz so analysis of the speckle pattern at that frequency was expected to provide the most accurate estimation of the material characteristics.

In Fig. (6.13) there are some noticeable deviations of the acoustic field that are possibly not to due to the interaction of the acoustic field with the microstructure. These latter observations, by looking at images in Fig. (6.13), were partly due to the observed microstructure, shown in Fig. (6.5) after etching the titanium sample

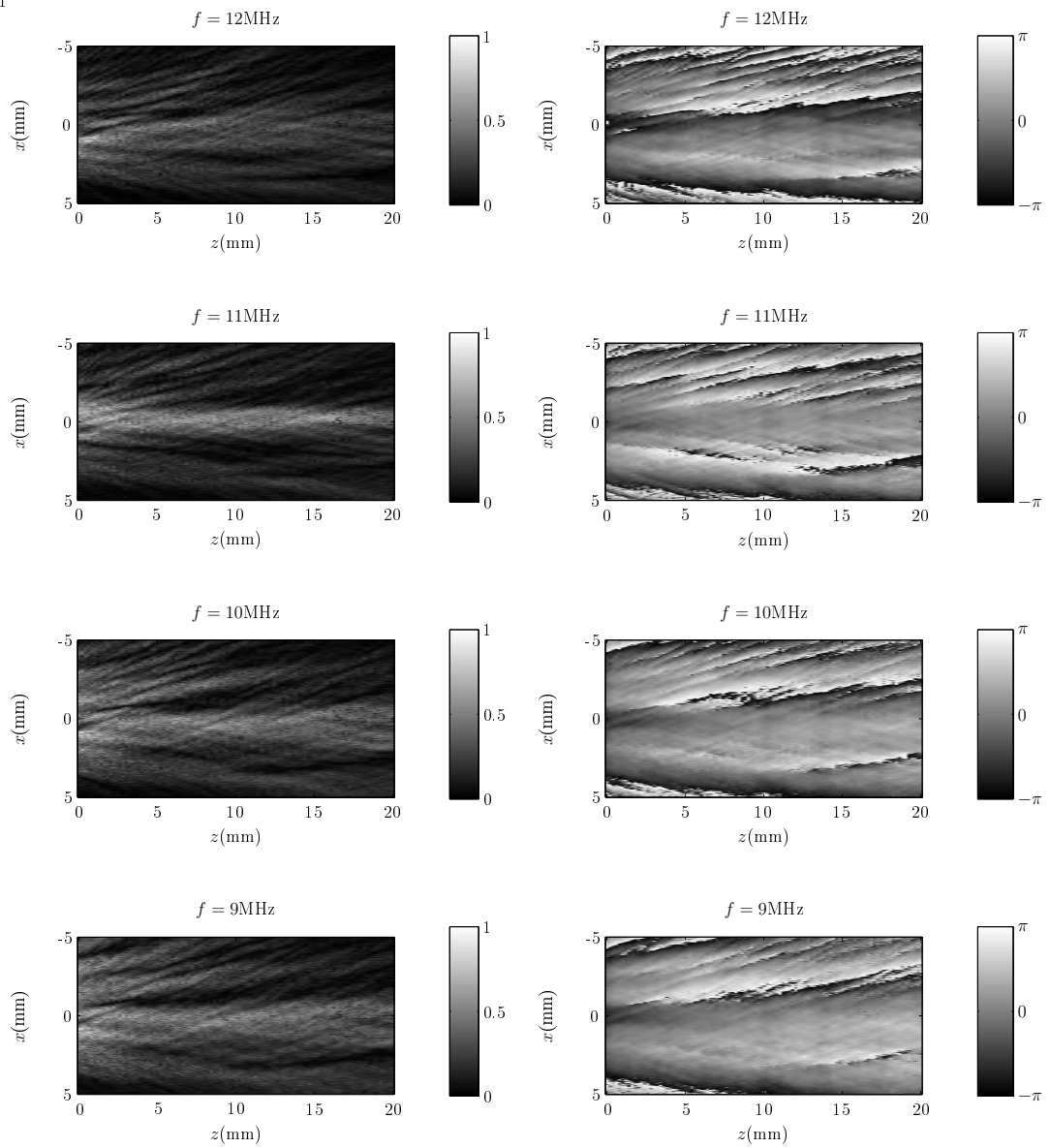


Figure 6.13: Amplitude and phase distribution of the acoustic field $u(\mathbf{r}, \omega|\gamma)$ showing aberrations in titanium at different frequencies. The propagation is from left to right. The right side column shows the amplitude of the field whereas the other column the residual phase.

for characterisation. To assess and to make sure that those deviations were caused by the interaction with the microstructure an experiment in a homogenous isotropic medium was carried out. The findings are presented in the next section for glass. It was found that the couplant was partly responsible for the deviations.

The acoustic field in a homogeneous medium

The purpose of this experiment was to assess the output of the transducer in a non-polycrystalline medium and experimentally assess the weak contributions of the microstructure to the aberrations caused in the acoustic field. The resultant acoustic field is shown in Fig. (6.14) below. Comparisons can be made with the

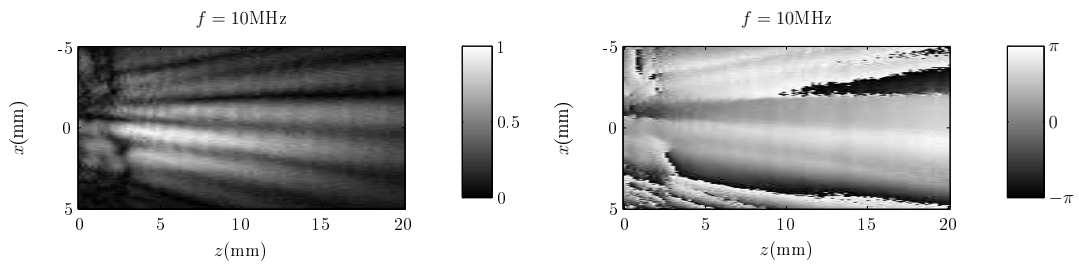


Figure 6.14: Amplitude and phase distribution of the acoustic field at 10MHz on an ideal sample (Glass) with no microstructure. The transducer output is not a single beam as one might expect.

amplitude and phase in Fig. (6.13). It can be clearly seen in Fig. (6.14) the effect that the couplant is having to the beam. This problem could have been avoided by using a different couplant but this was learned later on that there was not time to repeat the whole experiment. Nevertheless, by comparing Fig. (6.13) and Fig. (6.14) there are some deviations to the wavefront that can be observed but turned out to be very weak. This is assessed by looking at the correlation function of the field in section (6.6).

6.6 Analysis of experimental data

6.6.1 Procedure for spatial correlation

The statistical analysis of aberrations was made on the basis of statistical concepts such as the second order moment or energy correlation function for finite sequences. Notation is introduced to explain some of concepts and be able to compare them with the theory earlier developed in previous sections of chapter (5).

The measured acoustic field in all the samples is being denoted by u_{xz}^n . Thus, u_{xz}^n will represent any of the fields shown in Fig. (6.10), Fig. (6.11), Fig. (6.12) and Fig. (6.13). The acoustic field is a two dimensional scan in the xz axis, so $x = 1, \dots, K$, where K is the number of measurements in the x direction whereas $z = 1, \dots, L$ being L the number of measurements in the z direction. The numbers K and L are determined by the resolution of the c-scan taken in both directions. The index runs as $n = 1, \dots, N$, where N is the number of c-scans performed on each sample.

The aberrations are being quantified by the transverse correlation of the field. Hence, the transverse correlation is calculated from the acoustic ensemble at each plane along the direction of propagation.

We define the cross-correlation as $\langle u_{xz}^n u_{x'z}^{n*} \rangle$ where $\langle - \rangle$ denotes the ensemble average for finite sequences. The estimation of the ensemble average of $Z_{xx'z}^n = u_{xz}^n u_{x'z}^{n*}$ is rather complicated since there is little statistical information about u_{xz}^n . Instead, two different averages will be performed. By making $\tau = x - x'$, $Z_{xx'z}^n$ can be rewritten as $Z_{x(x+\tau)z}^n = u_{xz}^n u_{(x+\tau)z}^{n*}$. Since there is a transverse waveform for each τ , the average over x is performed as well as the ensemble average, leading to

$$Z_{\tau z} = \frac{1}{NK} \sum_{n=1}^N \sum_{x=1}^K Z_{x(x+\tau)z}^n \quad (6.2)$$

The average Z is an average transverse correlation for each measured realisation of the acoustic field. The discrete function Z remains a complex function so its modulus will be considered, and it will be termed correlation or the energy correla-

tion function. The average correlation function is denoted by Γ_e where sub-index e indicates measurement, thus

$$\Gamma_e(\tau, z) = \|Z_{\tau z}\| \quad (6.3)$$

The average Eq. (6.2) is simply the arithmetic average of the discrete correlation for each realisation of the acoustic ensemble measured on each sample. As pointed out in section (6.5), if $N \geq 50$ Eq. (6.3) would give a good estimation for Γ_e .

6.6.2 Results

The estimated correlation function is presented in this section. It has been numerically estimated using Eq. (6.3) for one instance of the acoustic field. The main properties of this function are described in the next section where it will be compared to Eq. (5.23). Only a single image of the correlation function, in particular for aluminium, will be presented as they all look similar. A more detailed version for both aluminium and titanium will be described in section (6.7).

The correlation Γ_e in a aluminium sample numerically implemented is shown in Fig. (6.15). The function has been normalised so the value of each transverse correlation at 0 along the propagation axis is 1. The important characteristics of this function will be the width of the central tail which will be related to the mean grain size. The second most important characteristic of the correlation function is that it decays away from the source. This decay is also directly related to the strength of the aberration measured via the standard deviation that characterises the degree of inhomogeneity. The correlation function at $z = 0$ has a wide base and tail (brightest areas in Fig. (6.15), near 0), but narrower away from the source. The base corresponds to the non-zero values of the correlation function. The width of the base is completely determined by the size of the source, in the case of aluminium, the size of the SLM. As the correlation function propagates away from the source, it decays so the base disappears as can be seen in Fig. (6.15) at distance $z = 8$, for instance. The reason for that to happen is because the acoustic field at those propagation distances

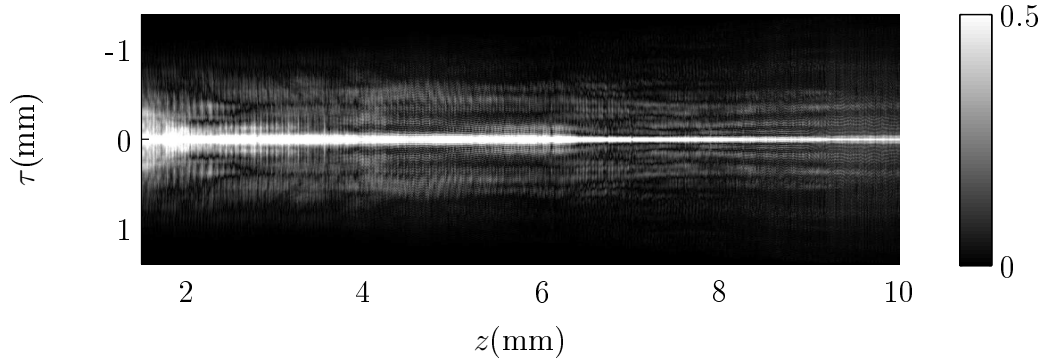


Figure 6.15: One single instance of measured correlation function in aluminium sample according to Eq. (6.2). The width of this function is an estimator of the mean grain size in polycrystals.

is transversally uncorrelated, thus giving as a result almost a delta correlation. This transverse property of the field depends entirely on the microstructure of the sample under investigation. Therefore, the correlation function behaves differently on samples with different microstructural properties. In theory, each specimen would correspond to a unique correlation function, each one being characterised by two parameters such as correlation length and degree of inhomogeneity. For instance, the correlation function is expected to have small variations both on the decay and width for aluminium sample M_A compared to M_B and M_C at equal propagation distance away from the source. This is because M_A has larger grains relative to the wavelength compared to M_B and M_C . In the latter case there is a greater number of interactions between grains and the acoustic field and so the field becomes rapidly uncorrelated.

In order to have a global behaviour of the correlation function in both directions, transverse and in the direction of propagation, the field was observed until it became vanishingly uncorrelated or diffuse, that it is $\Gamma_e \rightarrow 0$. These properties are discussed in the next sections, which is dedicated to correlation of the acoustic field and its relation to the theoretical counterpart.

6.7 Comparison

This section presents the main results concerning the measured correlation function on aluminium and titanium samples. The statistical analysis of the acoustic fields measured on each sample was performed according to analysis described in section (6.6.1), which culminates in the estimation of an average correlation function for each sample. So, the main result is the comparison between theory and the measured correlation function. The averaged measured correlation function for each case, that is for A , B , C and the titanium sample, was estimated from Eq. (6.2) in all cases for comparison to Eq. (5.21). From this comparison, two parameters characterising the overall behaviour of the correlation function are estimated. These, as it will be seen, correspond to the degree of inhomogeneity and the mean grain size. To continue with the same order as in previous sections the results for aluminium are presented first.

6.7.1 Comparison for Al

The experimental data acquired by the OSAM instrument were processed in the way described in section (6.6.1) which discussed correlation for finite sequences, and comparisons are made between the measured Γ_e and predicted Γ_u in Eq. (5.21); these are the energy correlation functions at various propagation distances. Fig. (6.16) shows the comparison of the measured Γ_e and predicted Γ_u energy correlation functions—where Γ_u is shown as solid lines—for samples A, B and C. In each case, it is shown at three different propagation distances, in order to illustrate the decay of the correlation function with distance.

The dashed lines in Fig. (6.16) represent the measured energy correlation function on the samples at the same propagation distances, derived from the acoustic ensemble in samples A, B and C. There is good agreement for samples B and C.

There are two parameters which are free in Eq. (5.23), being σ and l . These

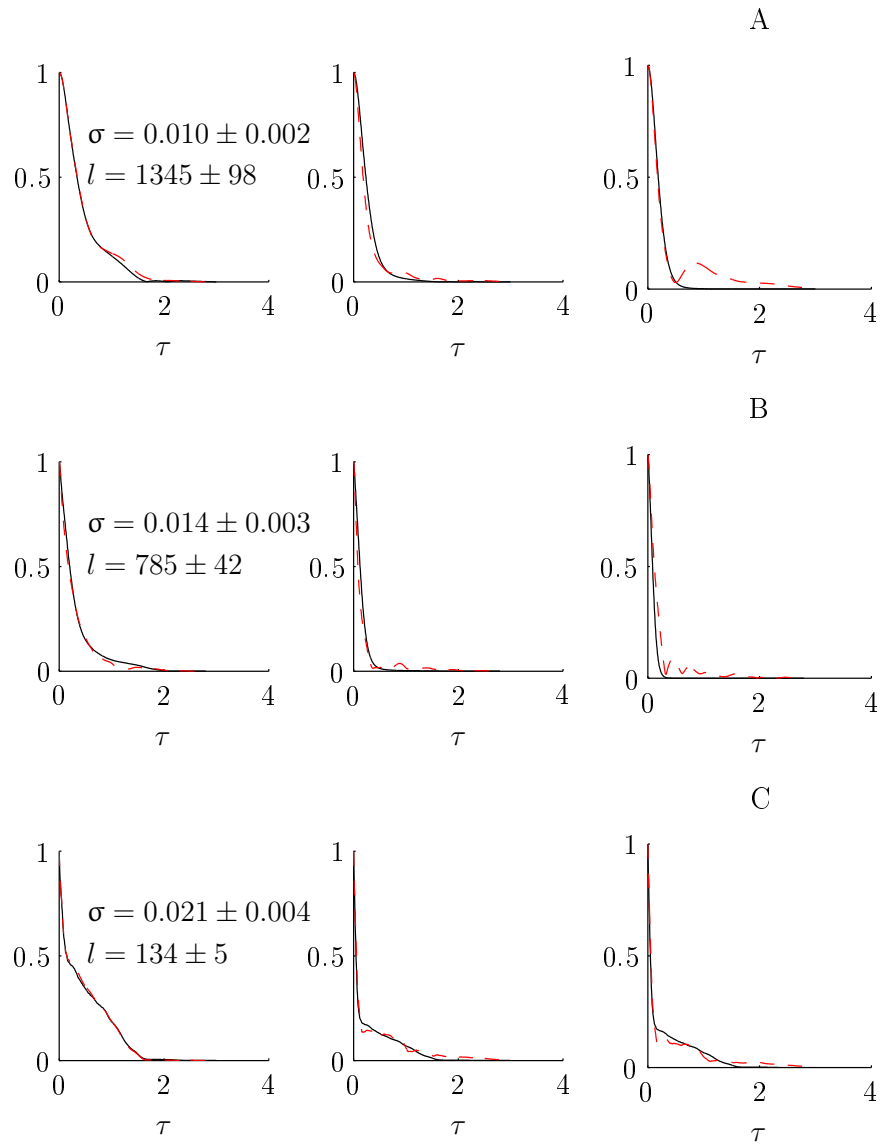


Figure 6.16: Comparison of theoretical and experimental correlation functions, Γ_u and Γ_e for the three blocks *A, B, C* of aluminium. The dashed lines is Γ_e at several distances whereas the continuous line is Γ_u at same distances. The half-width of the plotted functions is proportional to mean grain size. The numerical values for σ and l are given for each of the three cases.

have been obtained by fitting Γ_e to Γ_u by minimising the following function

$$\chi^2(\sigma, l) = \sum_{x_k, z_l} [\Gamma_e - \Gamma_u]^2 \quad (6.4)$$

The values obtained for σ and l from Eq. (6.4) were obtained by nonlinear minimisation of the square difference between the experimental and predicted correlation function. The above non-linear fitting problem is numerically implemented elsewhere. The standard deviation which measures the velocity variations from grain to grain, Eq. (3.19), used in Fig. (6.16) for comparison; average this $\sigma \approx 0.015$, which is a value that one would expect for aluminium [23]. For comparison between Γ_u and Γ_e in Fig. (6.16), the values for the correlation length l were taken as the mean grain size from the characterisation of the specimens in section (6.3). This is to illustrate that the theoretical correlation Γ_u , is indeed reproducing the measured correlation function using real values.

The estimated values σ and l from Γ_e obtained by minimising Eq. (6.4) are shown in table (6.2). It should be remembered that the standard deviation σ , and the

	M_A	M_B	M_C
σ	0.010 ± 0.002	0.014 ± 0.003	0.021 ± 0.004
l	686 ± 137	678 ± 136	165 ± 33

Table 6.2: Experimental values for σ , l obtained by minimising Eq. (6.4) for the aluminium samples A, B, C. The spread in both quantities σ , l indicates that they are to be found within a 20% accuracy.

correlation length l in table (6.2), have no relationship with the standard deviation and mean calliper diameter \bar{b} in Fig. (6.2), Fig. (6.3) and Fig. (6.4). It would be desirable, however, that l and \bar{b} have the same value, so the correlation length is a good estimation of the mean grain size. The definition and physical meaning of σ or degree of inhomogeneity has been given in detail in section (3.3.2). The spread in both quantities, σ and l in table (6.2) indicates that they are to be found within a 20% accuracy according to analysis presented in section (6.8) for the best fitting.

The estimation of σ is reasonable in all cases, compared to the value reported in [23], however, the estimated correlation length for sample A is significantly different

from the values obtained visually, which are approximately $1345\mu\text{m}$, $785\mu\text{m}$ and $134\mu\text{m}$, as shown in Fig. (6.10), Fig. (6.11) and Fig. (6.12), respectively.

Possible reasons for this are as follows. Firstly, due to mechanical limitations in the OSAM instrument, the acoustic field on sample A could not be mapped in its entirety. This effectively truncated the available dataset from which an estimation could be made. Secondly, we note that the measured mean grain size ($1345\mu\text{m}$), is approaching the width of the acoustic source ($\approx 2\text{mm}$). This is significant, because Γ_e is influenced more by the acoustic aperture in this case than by the correlation length. Finally, as noted in section (6.3.1), the large grains in sample A have complicated form in that many of the grains are non-convex.

6.7.2 Comparison for Ti

The analysis of the ensemble acoustic field was identical to that of aluminium, in the sense that the energy correlation function was obtained using the same method. The results for some representative frequencies are presented in table (6.3) below Fig. (6.17) shows a comparison of the predicted and measured power correlation

$f(\text{MHz})$	8	9	10	11	12	13	
σ	0.024	0.025	0.028	0.028	0.026	0.027	$\pm 0.15\sigma$
$l(\mu\text{m})$	351	399	368	428	424	424	$\pm 0.15l$

Table 6.3: Parameter values used for comparison of the predicted and measured correlation function.

function with values according to table (6.3). The weak aberrations observed in section (6.5.1) is reflected in the energy correlation where the decay is slow along the propagation distance, Fig. (6.17). It should be expected, at least theoretically in highly aberrated materials, that the energy correlation decays and gets narrow as it propagates. It can be said that the acoustic field is interacting with grains. Otherwise, the propagation will imitate propagation in homogeneous materials.

The parameter l characterises material microstructure but the metallographic study of the sample tested did not clearly reveal the grain boundaries so the values in table (6.3) could not be satisfactorily validated using standard techniques. This

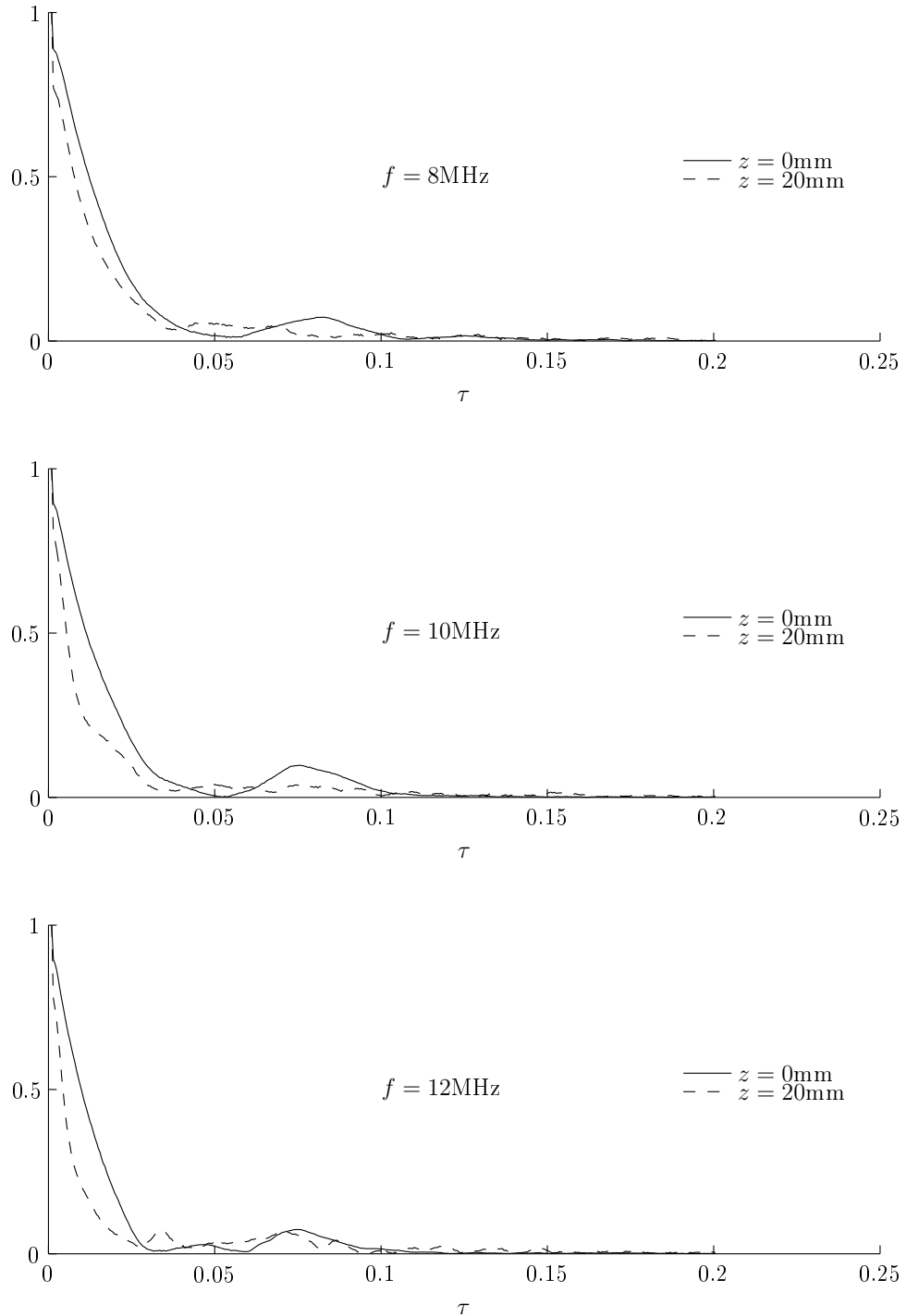


Figure 6.17: Correlation function measured from the acoustical ensemble in titanium showing the decay at different frequencies and distances. The dashed lines correspond to Γ_e whereas the continuous ones correspond to Γ_u at different distances.

compares to the results for aluminium where the parameters are in satisfactory agreement with the actual measured microstructure.

6.8 Analysis of the best fitting procedure

The values for σ and l were obtained numerically by minimising χ^2 in Eq. (6.4). This section discusses the range over which values obtained can be considered to be the best. The analysis has been done for the results shown in Fig. (6.16) for aluminium, in particular for the sample *C*. This sample was chosen arbitrarily as the others show similar behaviour.

Let us define the following function

$$r(\sigma, l) = \sqrt{1 - \frac{\chi^2}{s^2}} \quad (6.5)$$

where $s^2 = \sum_{x,z} f_{xz}^2$, $f_{xz} = u_{xz}^C$ and u_{xz}^C is the field shown in Fig. (6.12). The function r depends on σ and l . Let us also denote the best values for the standard deviation and correlation length by σ_b and l_b , respectively. These values will correspond to the values used in graph Fig. (6.16). The correlation r is calculated when a pair of values σ, l best fit and $r(\sigma_b, l_b)$ is expected to be very close to 1. The plot on the right in Fig. (6.18) shows that for values smaller and larger than σ_b the function r is far less than 1. A similar situation is shown on the left plot in the same figure. The function r is smaller than 1 for values smaller and larger than the best. In summary, the best values that minimise χ^2 can be found within 20% of the best values σ_b and l_b used in Fig. (6.16) for comparison.

The estimation of the parameters is affected by the noise generated by the system and is reflected in the correlation function. The additive noise goes away when the correlation function is estimated but the noise remains affecting mainly the width of the correlation function which is proportional to the mean grain size.

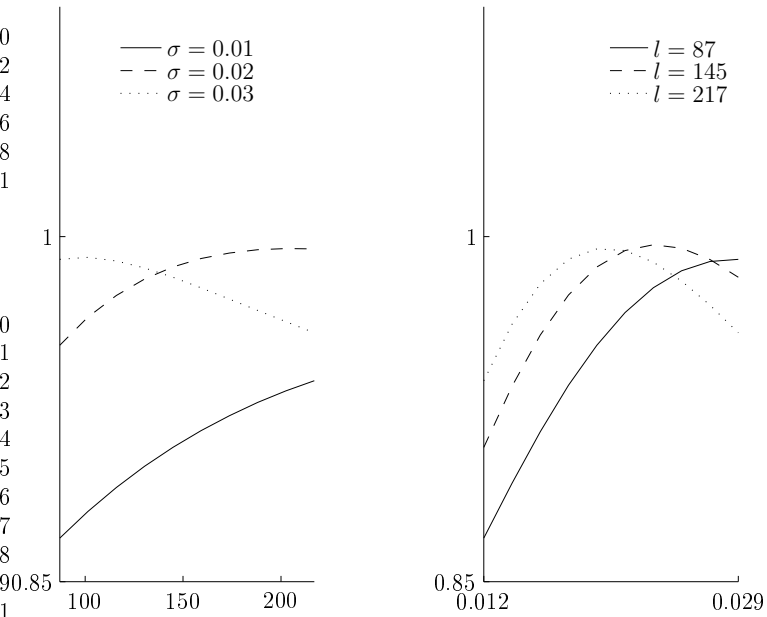


Figure 6.18: Plot of the function r as a function of σ , l . On the right side is r as a function of l for three different values of σ whereas on the left r is plotted as function σ at different values of l .

6.8.1 Noise in measurements

One of the difficulties with this technique is that the sample surface has to be polished to a mirror-like finish so “valleys” and “hills” on the sample surface are minimised with respect to the laser probe. Otherwise high levels of optical noise will arise. This in most cases can be accomplished if the right polishing technique is applied. Assessing the quality of the surface is achieved with an optical image of the surface by c-scanning the surface in the absence of ultrasound. Most surface features can be seen, e.g. scratches, by looking at the optical field. Another source of noise comes from the electronics in the detection system. This noise can vary from system to system so special filters have to be designed accordingly.

Accumulated noise at the central peak of the energy function gives a very sharp peak affecting the overall decay of the function, and therefore the estimated values of σ , l . The data was filtered assuming a linear model [100] of the form $y_1 = y_2 + e$ where e is white noise statistically uncorrelated to y_1 , and y_2 is data free of noise. When filtered with an optimum filter the residual is delta correlated, which corresponds to

noise. This can be removed by a filter based on wavelets with the retention of the desired signal. This very simple model considerably reduces the central peak due to noise.

The following table summarises the values obtained by minimising χ^2 using raw data without a filter. From table (6.4), it can be concluded that the most affected is

	M_A	M_B	M_C
σ	0.011 ± 0.002	0.021 ± 0.004	0.029 ± 0.006
l	404 ± 81	176 ± 35	112 ± 22

Table 6.4: Parameter estimated by minimising χ^2 without filtering the data

the correlation length for block B as the standard deviation remains constant within certain limits, compared the values for σ and l in table (6.2). Thus, in order to estimate parameters with acceptable accuracy it is necessary to gather data almost free of noise or apply a filter where possible.

6.9 Comparison of simulated microstructure

In sections (6.7.1), (6.7.2) a link was made between a theoretical and measured correlation function obtained from an ensemble of acoustic fields measured on real polycrystalline materials. The analysis showed that it is possible to relate this function to the actual properties of the polycrystal investigated.

In order to corroborate the analysis of this measured data, the phase screen approximation model described in section (4.1) was used to simulate a set of ultrasonic fields propagating through a simulated aberrating medium of known statistical properties. Each of these fields propagated through different simulated grain structures, and their corresponding propagating correlation functions were combined into an ensemble average as described by the average Eq. (6.3).

The symbols l_s , σ_s stand for correlation length and standard deviation used in the simulations, respectively. Whereas l_b , σ_b will stand for the best values obtained by minimising χ^2 , Eq. (6.4) for each simulation.

6.9.1 Simulated degree of inhomogeneity σ

The statistical analysis described in section (6.6.1) was performed and the results for standard deviation (σ) and mean grain size (l) were compared to the values used to generate the ultrasonic fields. The simulations were repeated for different values of standard deviation and mean grain size, and the results are illustrated in Fig. (6.19). In Fig. (6.19) σ_s denotes the standard deviation fed into the simulation

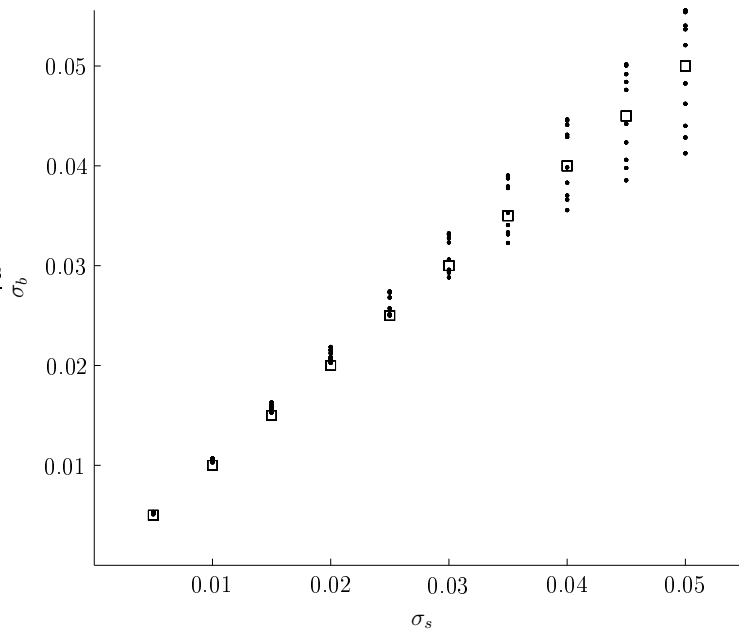


Figure 6.19: Comparison of the best value σ_b (dots on the graph) on simulated microstructure. The symbol σ_s stands for the standard deviation used to simulate the medium. The plot is a comparison between the standard deviation estimated by solving the minimisation problem Eq. (6.4), for the simulated acoustic fields in a simulated media with standard deviation σ_s , represented by a small square.

to generate different velocity variations on different simulated microstructures. The σ_b is obtained by minimising χ^2 in Eq. (6.4) with the simulated acoustic field. The small squares in the graph correspond to σ_s whereas the points correspond to the best fit.

In Fig. (6.19), σ_s is used for the abscissa as well as the ordinate, that is (σ_s, σ_s) . In the same graph, σ_s is plotted against σ_b so the plot should be a straight line coinciding with the line composed by squares, if they were equal. One can see that there are certain discrepancies for high values of deviation.

6.9.2 The correlation length l

Fig. (6.20) shows the result for the correlation length of the medium. The parameter σ_b and l_b were obtained by solving simultaneously the minimisation of χ^2 but shown on different graphs.

The agreement between the values used to simulate the random microstructure and the values obtained from statistical analysis of the ensemble autocorrelation functions is very good.

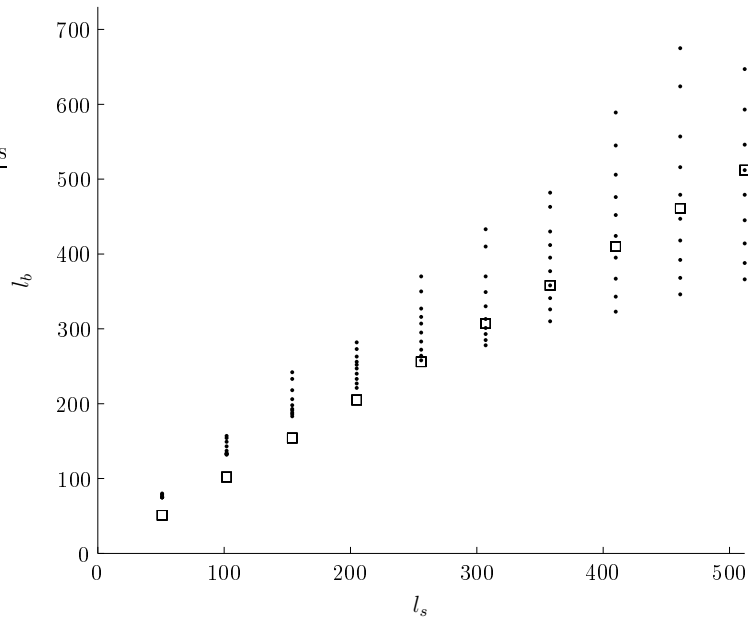


Figure 6.20: Comparison of the best value l_b (dots on the graph) on simulated microstructure. The symbol l_s stands for the mean grain size used to simulate the medium. The plot is a comparison between the correlation length l_b estimated by solving the minimisation problem Eq. (6.4), for the simulated acoustic fields in a simulated media with average grain size l_s , represented by small squares.

Acoustic field simulations

One hundred different media were simulated by feeding the algorithm with ten values for σ_s and ten for l_s , varying σ_s from 0.01 to 0.1, and l_s from 51 to 512. For each pair (σ_s, l_s) , one hundred fields were generated in order to give a good estimation of the average, Eq. (6.2). The agreement between the values used to simulate the random microstructure, and the values obtained from statistical analysis of the

ensemble autocorrelation functions is good, particularly for the standard deviation. The spread on the estimated grain size according to Eq. (6.4) is probably due to the fact that the mean grain sizes are reaching the size of the SLM, and the function Eq. (5.23) becomes complicated in that region. Thus, the spread will be reduced by choosing a wider aperture for the initial field.

Remarks on simulation

The microstructure was simulated using a different method from that of Voronoi cells. The Voronoi analysis for microstructure simulation was not available at the time of writing the paper [101], which was part of the results, so it was decided to use the algorithm already developed by the first author in [14]. Besides, the grain growth model used is equivalent to Voronoi tessellation for many pixels and is much faster.

The method used for simulating microstructure has no effect on the final result. The correlation function of the field coincides by using different methods as long as the simulated microstructure contains convex regions. All simulated methods lead to an exponential function which is the requirement of the analysis presented in chapter (4).

The above statement is equivalent to saying that as long as the simulated medium can be characterised by an exponential correlation function it will then approximate the case of Voronoi cells.

One of the reasons for the simulation not being repeated using Voronoi cells can be inferred from section (3.3.4), chapter (4) and chapter (5) as follows: The results showed in Fig. (6.19), Fig. (6.20) that by comparing an estimated to a theoretical correlation function, Eq. (6.3) and Eq. (5.23) respectively, then the input values σ_s and l_s correspond to those obtained by minimisation of χ^2 Eq. (6.4). Now, it is known from section (3.3.4) that the mean grain size actually corresponds to the correlation length of an exponential correlation function. It is also known that by using this correlation it is possible to generate realisations of the field, as it has been done in chapter (4) by using Eq. (4.17), based on Voronoi cells. By generating as many fields

as necessary a simulated ensemble can be generated, and also an estimated correlation function in a simulated medium. However, since the mean cross-correlation of the field in chapter (5) uses Eq. (4.17) to obtain the theoretical correlation field used for comparison in both experiments and simulations, the simulation of the field would be unnecessary.

6.10 Conclusions

In this chapter the experimental work carried out on two different polycrystalline materials, aluminium and titanium has been presented. Four specimens were prepared, three blocks of aluminium with different grain sizes and one piece of titanium. The aluminium samples were specially built to have mainly convex grains with random spatial distributions and to enable testing of the theoretical development as well as to give a better experimental understanding of aberrations in relation to microstructure. The titanium sample on the other hand was provided by industrial staff, so it was only necessary to polish it for ultrasonic testing. The etching of all specimens was performed by using standard techniques for both aluminium and titanium. In the case of aluminium, the procedure showed the required characteristics so the characterisation was performed as presented in section (6.3) by obtaining the mean grain size for all specimens. The etching of titanium proved to be more difficult than expected, thus characterisation of this specimen was not possible.

In order to measure the aberrations in all the specimens SAWs at frequencies of 82MHz were propagated in all the aluminium specimens. The acoustic field in each case was obtained by performing a c-scan to obtain a two dimensional image to show the deviations of the wavefront. The results were presented as a series of images in section (6.5). The aberrations are clearly seen in aluminium, especially in sample M_A , for which the acoustic field was taken at high resolution. The ultrasonic testing of titanium at 82MHz using SAW waves was not possible so it was necessary to change the method for SAW generation. It proved difficult to generate SAW in titanium using laser ultrasonics. A standard 10MHz transducer was used

instead. By applying the same procedure as with the aluminium samples the acoustic field was obtained. The aberrations in this particular sample were weak and later corroborated by looking at the correlation function of the field.

The aberrations of the acoustic field were statistically analysed so it was necessary to perform multiple measurements at different locations in the specimen. The aim was to measure a correlation function of the field. This correlation function needs a set of independent measures in the specimen with same statistical characteristics for microstructure. This was performed by scanning at different areas over the surface of each sample, thus building up an ensemble of acoustic fields. The procedure was repeated for each specimen under investigation thus obtaining a mean correlation function for each sample.

The importance of measuring a correlation function can be seen in the comparison of the theoretical against the experimental correlation function, which has been made in section (6.7) for the aluminium and titanium samples. From this comparison, it was possible to obtain two parameters that determine the behaviour of the correlation function. Theoretically, as shown in chapter (3) and (5) these parameters are the correlation length l , which is directly related to mean grain size of the polycrystal under investigation, and the degree of inhomogeneity σ . The estimation of the parameters from the measured correlation proved to be accurate only for samples M_B and M_C but not for M_A since the value of mean grain size obtained from the fitting did not agree with the value estimated from the characterisation of the sample. This does not conclusively mean that the theory is wrong since there were other factors involved in obtaining those results, such as the mean grain size of the specimen. The other reason was that, due to system limitations, it was not possible to measure completely the acoustic field along the axis of propagation.

As regards to the titanium sample, the values obtained for the degree of anisotropy and mean grain size unfortunately could not be corroborated since the photomicrograph does not show the grains as in aluminium samples; it was thus impossible to conclude anything about the microstructure of the sample.

In order to assess the technique even further a set of polycrystalline environments

were simulated to show how SAWs propagate in a polycrystalline material. From the simulated aberrations the mean correlation function was obtained showing encouraging results despite the spread in agreement for values close to 0.05 and 500 μm for the standard deviation and correlation length, respectively.

The overall procedure for obtaining the mean grain size from a measured correlation function can conclusively be used for polycrystalline material with relatively simple microstructures. It is believed that the technique could be a valuable tool in material characterisation.

Chapter 7

Discussions and further work

Introduction

The theoretical model and experimental work presented in this thesis covered in great detail the statistics of acoustic aberrations in polycrystalline materials. However, there is still research to do, specially in the theoretical part.

The combination of NDE methods such as the OSAM system together with the statistical technique developed in chapter (6) could well be serve as a tool in materials characterisation. The statistical analysis of aberrations could also aid in the ongoing research of correcting aberrations which is part of the continuous development of the OSAM system. There are several problems to be addressed concerning the work presented in this thesis along with some conclusions which will be discussed in the rest of the chapter.

7.1 The scalar model

Many aspects of the presented theoretical model are based on the elasticity of polycrystals modelled within the framework of stochastic processes. This theory makes use of the full vectorial equations for polycrystalline materials. It was shown in chapter (3), than in the very particular case of SAW propagation in polycrystalline material the full vectorial theory, governed by the elasticity Eq. (3.10), can be re-

duced to a scalar approximation to simplify the description of wave propagation in polycrystals. The elasticity theory in polycrystalline materials helped to establish many of the important characteristics of the materials, such as the anisotropy of the grains discussed in section (3.2.3).

The scalar model was shown to accurately describe acoustic aberrations of SAWs in polycrystals. The quantification of the aberrations was made through the two-parameter estimation in section (6.9), by comparison to the measured correlation function in chapter (6.6). These parameters relate to the statistics of the actual microstructure of polycrystals through the correlation of the acoustic field, developed in detail in chapter (5). The model gives an explicit expression for the correlation function, Eq. (5.23), being able to estimate standard deviation and correlation length.

The standard deviation was shown to be accurate when compared to values reported in the literature [23]. The model of the medium in section (3.3.3) also showed that, even under very restrictive circumstances, the correlation length obtained by comparison in (6.7) can realistically represent the mean grain size for polycrystals with mainly convex regions.

The scalar theory in chapter (3) was based on existing models already in use in other areas such as turbulence theory and underwater acoustics. Most of the approximations and mathematical methods were imported into this field and adjusted so they could be used to explain aberrations. The mathematical development was limited then to approximations already in use, although an attempt was made to improve them. For instance, in the chapter (5) the calculations for the correlation function were made without assuming that Γ_{μ} is delta correlated in the direction of propagation.

As far as the model presented in chapter (3) for SAW in polycrystalline materials is concerned, it only takes into account homogeneous isotropic solids. This way, it was possible to express the acoustic field in an isotropic medium as a plane wave expansion in chapter (4), which was later used in section (4.1.2) to approximate the acoustic field in a random medium. In order to extend the development in

chapter (4) to materials of general anisotropy, it is necessary to calculate the Green's function of the normal displacement for materials of general anisotropy. The Green's function for solids of general anisotropy has been reported in [21]. This, added to the development in chapter (4), would improve the theoretical description of the acoustic field in random media. A major improvement to the present research would be to describe SAWs in polycrystalline materials by removing the hypothesis of local isotropy, Eq. (3.7), on the elastic moduli, which means a complete description of a SAW based entirely on the elasticity Eq. (3.10) for polycrystals, without relying on a scalar description.

7.1.1 Modelling the medium

The most limited assumption was in modelling the medium. It has been assumed in section (3.3.1) that μ follows Gaussian statistics and is transversally isotropic. Without this assumption, the theoretical correlation of the field in chapter (5) could have been more difficult to calculate. This model works well with grains that behave on average as if they were spheres. However, as seen in the experimental work in Fig. (6.16), the assumption could lead to problems as was the case for the aluminium sample for which Fig. (6.2) in section (6.3.1) presented complicated geometrical features, as showed in the photomicrograph. A more realistic model would be to consider a more general expression for Γ_μ , in the sense that it would depend on two correlation lengths, i.e. in x and z directions so to model elongated grains. The anisotropy would also have to be taken into account, that is, Γ_μ would also depend on direction. This implies that the whole theoretical development would have to be reformulated to include this type of microstructure.

The scalar wave approach in section (3.3.3) will have to be modified so as to include a more general process to model the medium rather than simply assuming a process with a Gaussian correlation function. In addition, modelling microstructure within the approximations in section (3.3.4), where grains of similar size cluster together in certain areas in the sample, not to mention elongated and non-elongated grains within the cluster, would be prohibited. This behaviour did occur near the

walls of the container when preparing the aluminium samples, see section (6.2.1). The grains of different sizes were cut off by slicing the edges of the sample as they were of no interest for the current research.

Thus, future work in relation to microstructure and anisotropy within the framework of scalar approximation will be to find a more suitable process for describing microstructure. This means finding a random process to describe general anisotropy within grains as well as more complicated grain shape rather than mainly convex regions.

7.2 The phase screen model

The phase screen model, alongside the stochastic wave equation in chapter (3) and (4), has been developed to simulate ultrasound propagation through random media. This model has been used to corroborate the technique of statistical analysis of the propagating energy correlation function, and provides a useful test bed for developing the theory, alongside the experimental work.

One of the problems with the phase screen approximation is that it can only handle the forward field, although the same model could be used to forward and backward propagate the field to accommodate backscatter. This was not attempted since the primary interest was to assess the transverse correlation of the field, which resulted in the expression Eq. (5.23). The other problem is the mathematical justification to represent a “good” approximation to the paraxial approximation of the Helmholtz equation. This can only be done using continual integrals [60] that in practice are extremely difficult to evaluate. Nevertheless, the model was shown to be useful in obtaining an approximated expression for the correlation function with similar results if Γ_{μ} is assumed to be delta correlated along the propagation direction.

The phase screen model makes use of the angular spectral representation of the field, see section (4.1.3). In the actual calculation of the correlation of the field, a parabolic approximation was used by approximating the radical appearing in the

function propagator of the expansion. That is the function $h = \exp[iz\sqrt{1-p^2}]$ was approximated by $h \approx \exp[iz - \frac{1}{2}izp^2]$, making possible the calculation of integrals in chapter (5). This was one of the key points in making use of the approximation. The numerical simulation showed that under the conditions used in this work the original or the approximated expansion does not make a significant difference to the final result. The other interesting feature of this model is that it is possible to efficiently build realisations of the acoustic ensemble using the FFT algorithm, so it is possible to compare them to the measured aberrations in real samples. Looking into the future, it would be desirable to remove the dependence on the number of screens in Eq. (4.17) by replacing the multiple integrals by a continual integral so as to include propagation paths other than straight lines.

7.3 Experimental work

Two different materials or polycrystals were ultrasonically analysed using different ultrasonic sources, aluminium and titanium. In the aluminium sample the OSAM system was used whereas in the titanium sample a contact transducer technique was used as the ultrasonic source. The idea with the transducer was to test the model at different frequencies limited to the narrow frequency bandwidth of the transducer. Unfortunately, the titanium sample proved to be a difficult sample in the sense that the microstructure was unexpectedly complicated. So the mean grain size was not estimated. As a consequence, the correlation length obtained in (6.3) could not be demonstrated to correspond to the mean grain size of the material.

The technique for aluminium samples, on the other hand, both for preparation and characterisation of the samples generally fulfilled expectations.

The objective of the experimental work was to measure the deviations of the acoustic field caused by the grains within the material by looking at the forward propagating field. However, it appears that SAW reflection at grain boundaries can also be a source of deviations in the acoustic field, see section (3.2.2). Thus, from the experimental point of view it would be interesting as a part of further

research to measure the reflected field at grain boundaries. These reflections possibly would involve mode conversion complicating even further a theoretical description of acoustic propagation. It would be useful to modify the OSAM system so that it could look at backscatter to examine the reflected field at grain boundaries using the OSAM system.

The procedure used in this work to obtain parameters characterising materials by minimising Eq. (6.4) needs to be reviewed if the technique is to be used routinely for materials characterisation. That is, it will be necessary to design a better filter to process the data so that reliable and accurate estimation of parameters will be possible. It is a very important point to establish to what extent the level of noise affects the estimation of the parameters and how to remove it. The filter applied for the comparison in Fig. (6.16), did work well in general terms.

7.4 Final comments

The theoretical development of SAWs in polycrystalline materials presented in chapter (3) and (4), which culminates with the calculation of the correlation function of the acoustic field in chapter (5), proved to work very well in aluminium samples with mainly convex regions. This was demonstrated by comparing the measured correlation function to the theoretical one in chapter (6), with good agreement. Even when the value of the correlation length obtained by performing the inverse problem for sample M_A did not match the mean grain size in Fig. (6.2), it is believed that the technique as a whole can be a valuable tool for material characterisation, provided the conditions discussed in the thesis are met.

In summary, this work has contributed to the establishment of a wave correlation function that quantitatively describes the local anisotropy and mean grain size of polycrystalline materials with certain characteristics.

The statistical properties of SAWs in polycrystalline materials were defined by second order moments of the acoustic fields and these relate to material grain size and anisotropy via the theoretical correlation function developed in chapter (5).

Originality of the work

Part of the work done in this thesis has been presented in a series of conferences and has been published articles on acoustic aberrations [101, 102, 103, 104, 105].

Appendix A

Appendix

A.1 Multivariate propagation function

In this appendix a certain type of multiple integrals that arise in propagation of correlation function will be discussed. It will be shown that for very special cases those integrals can be evaluated for arbitrary function by making a simple change of variable.

Let $\mathbf{x} = (x_0, \dots, x_n)$, $\mathbf{z} = (z_0, \dots, z_n)$ be and denote the vector coordinate difference by $\mathbf{x}^- = (x_1 - x_0, \dots, x_n - x_{n-1})$ and $\mathbf{z}^- = (z_1 - z_0, \dots)$, respectively. The multidimensional Green's function is defined as

$$G(\mathbf{x}^-, \mathbf{z}^-) = \prod_{j=1}^n G(x_j^-, z_j^-) \quad (\text{A.1})$$

where $G(x - x', z - z') = (1 + i) \sqrt{\frac{k}{4\pi(z - z')}} e^{ikz} e^{ik \frac{(x - x')^2}{2(z - z'')}}$ is the Green function of the Helmholtz's equation in two dimensions. Some definitions are introduced in order to avoid lengthy equations, so let us say $C_n = (1 + i)^n (\frac{k}{4\pi})^{n/2}$, $\Lambda_s^- = \frac{2(z_{s-1} - z_s)}{k}$ and $r_s = (x_s - x_{s-1})^2 - (y_s - y_{s-1})^2$ with obvious definition for vectorial form.

Consider the following integral

$$I = \left(-\frac{1}{\pi}\right)^n \int \cdots \int f(\mathbf{x}, \mathbf{y}, \mathbf{z}) \prod_{s=1}^n \left\{ \frac{\exp[-i \frac{r_s}{\Lambda_s^-}]}{\Lambda_s^-} \right\} d\mathbf{x} d\mathbf{y} d\mathbf{z} \quad (\text{A.2})$$

where $d\mathbf{x}$ indicates that integration has to be performed on variables x_0, \dots, x_{n-1} and f is an arbitrary function.

If f is a function of $\mathbf{x} - \mathbf{y}$, \mathbf{z}^- only then I can be expressed in the following form

$$I = (-1)^n \int f(x_n - y_n, \dots, x_n - y_n, \mathbf{z}) dz_{0,n-1} \quad (\text{A.3})$$

where $d_{0,n-1} = dz_0 \cdots dz_{n-1}$

Let us make the following change of variable $\mathbf{p} = \mathbf{x} - \mathbf{y}$, $\mathbf{q} = \mathbf{x} + \mathbf{y}$ so $\mathbf{p} + \mathbf{q} = 2\mathbf{x}$ and $\mathbf{q} - \mathbf{p} = 2\mathbf{y}$ therefore their quadratic differences can be expressed as follow

$$(x_s - x_{s-1})^2 - (y_s - y_{s-1})^2 = (p_s - p_{s-1})(q_s - q_{s-1}). \quad (\text{A.4})$$

Also note that $dx_s dy_s = \frac{1}{2} dq_s dp_s$ then $dx_{0,n-1} dy_{0,n-1} = dx_0 \cdots dx_{n-1} dy_0 \cdots dy_{n-1} = \frac{1}{2^n} d\mathbf{q} d\mathbf{p}$.

Substitution of Eq. (A.4) into Eq. (A.2) after using the assumption on f gives

$$\begin{aligned} I &= \left(-\frac{1}{\pi}\right)^n \int f(\mathbf{p}, \mathbf{z}) \prod_{s=1}^n \left\{ \frac{\exp[-i \frac{p_s^- q_s^-}{\Lambda_s^-}]}{\Lambda_s^-} \right\} d\mathbf{p} d\mathbf{q} d\mathbf{z} \\ &= \left(-\frac{1}{\pi}\right)^n \int f(\mathbf{p}, \mathbf{z}) \exp \left[-i \sum \frac{p_s^- q_s^-}{\Lambda_s^-} \right] \prod_{s=1}^n \frac{1}{\Lambda_s^-} d\mathbf{p} d\mathbf{q} d\mathbf{z} \end{aligned} \quad (\text{A.5})$$

Since f is independent of \mathbf{q} the integral with respect a \mathbf{q} follows by expressing the argument in such way that it is possible to integrate with respect to the variable \mathbf{q} , hence

$$i \sum_{s=2}^n \frac{p_s^- q_s^-}{\Lambda_s^-} = i \sum_{s=1}^n \left[\frac{1}{\Lambda_s^-} p_s^- - \frac{1}{\Lambda_{s+1}^-} p_{s+1}^- \right] q_s \quad (\text{A.6})$$

with $p_1^- = p_{n+1}^- = 0$; section (A.1.1) shows how to obtain Eq. (A.6). Then integral Eq. (A.4) after inserting Eq. (A.6) and performing integration with respect to $dq_{1,n-1}$,

we have

$$I = b \int f(\mathbf{p}, \mathbf{z}) \prod_{s=1}^n \Lambda_s^- \delta(p_s^- - \frac{\Lambda_s^-}{\Lambda_{s+1}^-} p_{s+1}^-) \prod_{s=2}^n \frac{1}{\Lambda_s^-} dp_{0,n-1} dz_{0,n-1} \quad (\text{A.7})$$

where $b = (-\frac{1}{\pi}) \frac{(2\pi)^{n-1}}{2^{n-1}}$.

It is not difficult to realise that

$$f(p_n, \dots, p_n, \mathbf{z}) \prod_{s=2}^n \Lambda_s^- = \int f(\mathbf{p}, \mathbf{z}) \prod_{s=1}^n \Lambda_s^- \delta(p_s^- - \frac{\Lambda_s^-}{\Lambda_{s+1}^-} p_{s+1}^-) dp_{0,n-1} \quad (\text{A.8})$$

Therefore the integral reduces to

$$I = (-1)^n \int f(p_n, \dots, p_n, \mathbf{z}) dz_{0,n-1} \quad (\text{A.9})$$

A.1.1 Remarks

Equation Eq. (A.6) is revisited step by step to show how it was obtained by rearranging the sums. Thus,

$$\begin{aligned}
i \sum_{s=2}^n \frac{p_s^- q_s^-}{\Lambda_s^-} &= i \sum \frac{1}{\Lambda_s} (p_s - p_{s-1})(q_s - q_{s-1}) \\
&= -i \left[\sum_{s=2}^n \frac{1}{\Lambda_s} (p_s - p_{s-1})q_{s-1} + \sum_{s=2}^n \frac{1}{\Lambda_s} (p_{s-1} - p_s)q_s \right] \\
&= -i \left[\sum_{m=1}^{n-1} \frac{1}{\Lambda_{m+1}} (p_{m+1} - p_m)q_m + \sum_{s=2}^n \frac{1}{\Lambda_s} (p_{s-1} - p_s)q_s \right] \\
&= -i \left[(p_2 - p_1)q_1 \frac{1}{\Lambda_2} + \sum_{s=2}^{n-1} \frac{1}{\Lambda_{s+1}} (p_{s+1} - p_s)q_s + \right. \\
&\quad \left. + \sum_{s=2}^n \frac{1}{\Lambda_s} (p_{s-1} - p_s)q_s + \frac{1}{\Lambda_n} (p_{n-1} - p_n)q_n \right] \\
&= -i \left[\frac{1}{\Lambda_2} p_2^- q_1 + \sum_{s=2}^{n-1} \left(\frac{1}{\Lambda_{s+1}} p_{s+1} - p_s \left(\frac{1}{\Lambda_{s+1}} + \frac{1}{\Lambda_s} \right) + \right. \right. \\
&\quad \left. \left. + \frac{1}{\Lambda_s} p_{s-1} \right) q_s - \frac{1}{\Lambda_n} p_n^- q_n \right] \\
&= i \sum_{s=1}^n \left[\frac{1}{\Lambda_s^-} p_s^- - \frac{1}{\Lambda_{s+1}^-} p_{s+1}^- \right] q_s \tag{A.10}
\end{aligned}$$

where $p_1^- = p_{n+1}^- = 0$ has been made to complete the sum from $s = 1$ to n .

A.1.2 The mean for multiple phase screens

Let us denote the phase differences by $w_{ij} = \phi(x_i) - \phi(x_j)$ and the variance of their difference by $c = \{c_{ij}\} = \{\langle w_{ij}^2 \rangle\}$, which is the matrix of covariances

$$w = \{w_{jj}\}^t = \begin{bmatrix} w_{11} \\ \vdots \\ w_{nn} \end{bmatrix} = \begin{pmatrix} \phi(x_1) - \phi(y_1) \\ \vdots \\ \phi(x_n) - \phi(y_n) \end{pmatrix} \tag{A.11}$$

and

$$\xi = \begin{bmatrix} \xi_1 \\ \vdots \\ \xi_n \end{bmatrix}$$

an arbitrary vector variable. The mean Eq. (5.13) considered in chapter (5) follows by using the cumulative generating function for multivariable Gaussian variables [64], thus the ensemble average Eq. (4.14) can be expressed as,

$$\begin{aligned} \langle s(\mathbf{x})s^*(\mathbf{y}) \rangle &= \left\langle e^{i\sum_1^n \phi(x_j) - \phi(y_j)} \right\rangle \\ &= \left\langle e^{i\sum_1^n w_{jj}} \right\rangle \\ &= C(1, \dots, 1) \\ &= \left\langle e^{i\sum \xi_j w_{jj}} \right\rangle_{\xi=1} \\ &= \left\langle e^{i\sum \xi^t w} \right\rangle_{\xi=1} \end{aligned} \tag{A.12}$$

$$= e^{i\xi^t \langle w \rangle} e^{-\frac{1}{2}\xi^t c \xi} \Big|_{\xi=1} \tag{A.13}$$

$$= e^{-\frac{1}{2}\xi^t \langle w^2 \rangle \xi} \Big|_{\xi=1}$$

$$= e^{-\frac{1}{2}\sum_j \langle w_{jj}^2 \rangle}$$

$$= e^{-\sum \Gamma_\phi(0) - \Gamma_\phi(x_j - y_j)}$$

$$= e^{-\sum_j^n D_\phi(x_j - y_j)} \tag{A.14}$$

where $D_\phi(x_j - y_j) = \Gamma_\phi(0) - \Gamma_\phi(x_j - y_j)$. The equivalence between Eq. (A.12) and Eq. (A.13) follows from the well known result for Gaussian variables; the ensemble average of an exponential random variable is the ensemble average of its argument. After some algebra Eq. (A.14) follows, which is the desired equivalent form for $\langle s(\mathbf{x})s^*(\mathbf{y}) \rangle$. Thus, the mean $\langle s(\mathbf{x})s^*(\mathbf{y}) \rangle$ is an exponential sum of structure functions. Each structure function $D_\phi(x_j - y_j)$, corresponds to the structure function of the phase screen at position j . It has to be said that the above result is only valid for Gaussian variables.

A.2 The angular representation in inhomogeneous medium

The long expression obtained in section (4.1.3) is developed in this appendix step by step. The development of the expression is based on the angular representation of the field and the linearity of convolution and Fourier transform.

Let us first introduced the definition of convolution of two functions. It is customary to use t as the independent variable, thus the convolution of two functions f and g is defined as

$$f(t) \otimes g(t) = \int f(\tau)g(t - \tau)d\tau \quad (\text{A.15})$$

The starting point for writing the field representation in random media will be the recursive relationship Eq. (4.16) between the values of the field in each screen.

For instance, using the recursive relation Eq. (4.16) and Eq. (A.15) the field value at layer $n = 0, n = 1, n = 2, \dots$ are given by

$$n = 0 \quad u_1 = h_{p_1} \int \hat{u}_0 h_{p_0} \hat{s}_0(p_1 - p_0) dp_0 \quad (\text{A.16})$$

$$n = 1 \quad u_2 = h_{p_2} \int \hat{u}_1 h_{p_1} \hat{s}_1(p_2 - p_1) dp_1 \quad (\text{A.17})$$

$$n = 2 \quad u_3 = h_{p_3} \int \hat{u}_2 h_{p_2} \hat{s}_2(p_3 - p_2) dp_2 \quad (\text{A.18})$$

⋮

$$u_n = h_{p_n} \int \hat{u}_{n-1} h_{p_{n-1}} \hat{s}_{n-1}(p_n - p_{n-1}) dp_{n-1} \quad (\text{A.19})$$

The field u_2 depends on the values of the Fourier transform of u_1 from the previous layer, which in turn depends on the Fourier transform of u_0 . The process is continued until one reaches u_n then back substitution is performed to be able to express u_n as a function of u_0 which is the incident field v as an special case in this notation. In the recursive relation above there is the Fourier transform involved both for u_n and the screens s . To make things easy in writing successively u_n let us recall

that $k\hat{u}_n(k_0p_n) = a_n(p_n)$ for all n , where a_n is the angular representation of u_n within layer n . Moreover, it is understood that whenever \hat{s}_n appears in the following expressions what it really means is $\hat{s}_n(p_{n+1} - p_n)$.

Thus, using Eq. (A.16) to Eq. (A.19) by starting with u_n and substitution of the integral representation for a_{n-1} and a_{n-2} one has

$$\hat{u}_n = h_{p_n} \int a_{n-1} h_{p_{n-1}} \hat{s}_{n-1} dp_{n-1} \quad (\text{A.20})$$

$$= h_{p_n} \int \left(h_{p_{n-1}} \int a_{n-2} h_{p_{n-2}} \hat{s}_{n-2} dp_{n-2} \right) h_{p_{n-1}} \hat{s}_{n-1} dp_{n-1} \quad (\text{A.21})$$

$$= h_{p_n} \iint a_{n-2} h_{p_{n-2}} h_{p_{n-1}}^2 \hat{s}_{n-2} \hat{s}_n dp_{n-1} dp_{n-2} \quad (\text{A.22})$$

$$= h_{p_n} \iint \left(h_{p_{n-2}} \int a_{n-3} h_{p_{n-3}} \hat{s}_{n-3} dp_{n-3} \right) \quad (\text{A.23})$$

$$\times h_{p_{n-2}} h_{p_{n-1}}^2 \hat{s}_{n-2} \hat{s}_{n-1} dp_{n-1} dp_{n-2} \quad (\text{A.24})$$

$$= h_{p_n} \iiint a_{n-3} h_{p_{n-3}} h_{p_{n-2}}^2 h_{p_{n-1}}^2 \hat{s}_{n-3} \hat{s}_{n-2} \hat{s}_{n-1} dp_{n-3} dp_{n-2} dp_{n-1} \quad (\text{A.25})$$

Now it is clear from the above relationship that every time one substitutes a_n for its integral representation, the Fourier transform of each screen forms a multiplicative series. The same happens with the functions h_{p_n} inside the integral. Successive integration is possible because h_{p_n} and \hat{s}_n are independent for every n . The field u_n is now expressed as a function of a_{n-3} in Eq. (A.25). To end this, is necessary to substitute the representation for a_0, \dots, a_{n-3} as it has been done in Eq. (A.21), Eq. (A.24) for a_{n-1} and a_{n-2} , respectively. Allowing j to run from 0 to n the product series in Eq. (A.25) can be rewritten using a short notation, hence

$$\prod_{j=0}^{n-1} h_{p_j}^2 \hat{s}_j = h_{p_0} \cdots h_{p_{n-3}} h_{p_{n-2}}^2 h_{p_{n-1}}^2 \hat{s}_0 \cdots \hat{s}_{n-3} \hat{s}_{n-2} \hat{s}_{n-1} \quad (\text{A.26})$$

Using Eq. (A.26) the field u_n can be expressed as

$$\hat{u}_n = h_{p_n} \int \cdots \int a_0(p_0) \prod_{j=0}^{n-1} h_{p_j}^2 \hat{s}_j(p_{j+1} - p_j) dp_j \quad (\text{A.27})$$

which Eq. (4.17) written in the spatial frequency.

A.3 The Green's function for the correlation equation

A.3.1 Helmholtz's equation

This appendix is dedicated to the calculation of the Green function for the operators

1. $L = 2ik\frac{\partial}{\partial z} + \lambda$
2. $D = 2ik\frac{\partial}{\partial z} + \Delta_1 - \Delta_2$ where $\Delta_s = \frac{\partial^2}{\partial x_s^2}$

Case 1.

The Green's function for operator L is a function G which satisfy the following differential equation

$$2ik\frac{\partial}{\partial z}G + \lambda G = -\delta(z - \xi) \quad (\text{A.28})$$

where δ is the delta of Dirac and λ an arbitrary parameter.

There is a straightforward method of finding G by using Fourier's transform. Thus, in taking Fourier transform on both sides of Eq. (A.28) one gets

$$\begin{aligned} -2\omega k\hat{G} + \lambda\hat{G} &= \frac{1}{\sqrt{2\pi}}e^{-i\omega\xi} \\ \hat{G} &= \frac{e^{-i\omega\xi}}{\sqrt{2\pi}(-2k\omega + \lambda)} \end{aligned} \quad (\text{A.29})$$

Taking the inverse Fourier transform of the above relation gives

$$\begin{aligned} \frac{1}{\sqrt{2\pi}} \int G e^{i\omega z} d\omega &= \frac{1}{\sqrt{2\pi}} \int \frac{e^{i\omega(z-\xi)} d\omega}{\sqrt{2\pi}(-2k\omega + \lambda)} \\ G &= -\frac{1}{2\sqrt{2\pi}ki} \int \frac{ie^{-i\omega(z-\xi)} d\omega}{\sqrt{2\pi}(\omega + \frac{\lambda}{2k})}. \end{aligned} \quad (\text{A.30})$$

Using one of the integrals from table in appendix (A.7) G takes the form

$$G = -\frac{1}{2\sqrt{2\pi}ik} H(z - \xi) e^{i\frac{\lambda}{2k}(z-\xi)} \quad (\text{A.31})$$

H the Heaviside function.

The following function is also solution

$$G = H(z - \xi)e^{i\frac{\lambda}{2k}(z-\xi)} \quad (\text{A.32})$$

Case 2.

Once again in order to find the Green's function for D or a solution to the following differential equation

$$DG = -\delta(x_1 - a)\delta(x_2 - b)\delta(z - c) \quad (\text{A.33})$$

the Fourier transform technique is applied. The above problem is reduced to first case by taking

Fourier transform with respect to x_1, x_2 , in doing so, equation Eq. (A.33) on the frequency domain takes the form

$$2ik\hat{G}_z + [\omega_2^2 - \omega_1^2]\hat{G} = -\frac{1}{2\pi}e^{-i\omega_1 a - i\omega_2 b}\delta(z - c) \quad (\text{A.34})$$

Obviously, the above differential equation falls in the first case. In using this result a solution can be obtained for \hat{G} ,

$$\hat{G}(\omega_1, \omega_2, z) = -\frac{1}{2\pi}e^{-i\omega_1 a - i\omega_2 b}H(z - c)e^{i\frac{\omega_2^2 - \omega_1^2}{2k}(z-c)} \quad (\text{A.35})$$

The result follows after taking the inverse Fourier transform and using, once again one of the integrals in appendix (A.7), therefore by taking the inverse Fourier trans-

form of Eq. (A.35) we have

$$G = -\frac{1}{4\pi^2} \int \int e^{i\frac{\omega_2^2 - \omega_1^2}{2k}(z-c)} \times e^{i\omega_1(x_1-a) + i\omega_2(x_2-b)} d\omega_1 d\omega_2 \quad (\text{A.36})$$

$$G = -\frac{1}{4\pi^2} \int \int e^{-\beta_1\omega_1^2 - \beta_2\omega_2^2} \times e^{i\omega_1(x_1-a) + i\omega_2(x_2-b)} d\omega_1 d\omega_2 \quad (\text{A.37})$$

$$\begin{aligned} &= -\frac{1}{4\pi^2} \frac{\pi}{\beta_1\beta_2} e^{-(x_1-a)^2/4\beta_1^2} e^{-(x_2-b)^2/4\beta_2^2} \\ &= -\frac{1}{4\pi^2} \frac{2\pi k}{(z-c)} e^{ik\frac{(x_1-a)^2}{2(z-c)} - ik\frac{(x_2-b)^2}{2(z-c)}} \\ G &= -\frac{k}{2\pi(z-c)} e^{ik\frac{(x_1-a)^2}{2(z-c)} - ik\frac{(x_2-b)^2}{2(z-c)}} \end{aligned} \quad (\text{A.38})$$

where $\beta_1 = \frac{1}{2}\sqrt{\frac{z-c}{k}}(1+i)$, $\beta_2 = \frac{1}{2}\sqrt{\frac{z-c}{k}}(1-i)$

A.4 Colouring Voronoi cells

The algorithm for colouring Voronoi cell is based on expressing the function $\mathbf{1}_{B_n}$ into the complex version. The vertices that define each region B_n are irregular polygons and its vertices can be expressed in complex numbers denoted by w_1, \dots, w_n , $w_k \in \mathbb{C}$. Also points belonging to B are written in its complex version. In complex variable the wind number is defined as

$$n(w; \gamma) = \frac{1}{2\pi i} \int_{\gamma} \frac{d\xi}{\xi - w}. \quad (\text{A.39})$$

The function $n(w; \gamma)$ has the wonderful property that $n(w; \gamma) = 1$ if z belongs to the interior of γ and zero otherwise.

The path γ defining entirely a region B_n is defined piecewise by the vertices as

$$\gamma = \gamma_1 + \dots + \gamma_n \quad (\text{A.40})$$

where $\gamma_k = w_k + t(w_k - w_{k-1})$, $t \in [0, 1]$. The function $n(w; \gamma)$ counts how many times γ wraps around a point $w \in B$. It takes the value 1 because γ is a close

polygon that winds up only once around z .

The integral Eq. (A.39) is a line integral and since $\frac{d\gamma}{dt} = z_k - z_{k-1}$, Eq. (A.39) is equivalent to

$$\begin{aligned}
 n(w, \gamma) &= \frac{1}{2i\pi} \sum_i \int_{\gamma_i} \frac{d\xi}{\xi - w} \\
 &= \frac{1}{2i\pi} \sum_i \int_0^1 \frac{(w_i - w_{i-1})dt}{w_{i-1} - w + t(w_i - w_{i-1})} \\
 &= \frac{1}{2i\pi} \sum_i z_i \int_0^1 \frac{dt}{w_{i-1} - w + t(w_i - w_{i-1})} \\
 &= \frac{1}{2i\pi} \sum_i \ln \left[\frac{w_i - w}{w_{i-1} - w} \right] \tag{A.41}
 \end{aligned}$$

So the wind number is the logarithm evaluated at the vertices forming a region. In order to define $k(\mathbf{r})$ is to enough to determine the second term in Eq. (3.22). Let us denote $\gamma_s = \gamma_{s1} + \dots + \gamma_{sl}$ be the close curve each Voronoi cell B_s has for boundaries, $s = 1, \dots, N(B)$ and l is determine by the Voronoi construction then

$$\mu(\mathbf{r}) = \sum_s c_s n(w; \gamma_s) \tag{A.42}$$

This a Gaussian process simulating the wave number that relates the wave velocity to the statistics of the microstructure.

A.5 Algorithm for wave propagation

This section presents the algorithm to numerically implement the long Eq. (4.17). An image showing the simulated field has been already shown in chapter (4), Fig. (4.7).

A.6 Principle of laser-generation

The simplest and most direct way of generating ultrasound using a laser is by directing the beam onto the surface of a specimen [88]. The absorbed light energy cause

Algorithm 1 Calculate $u(x, z)$ *Start with:* $N \leftarrow$ Number of screens $\lambda \leftarrow$ Wavelength $\phi_j \leftarrow$ Random processes, $j = 1, \dots, N$, $v \leftarrow$ Incident field**for** $j = 1$ to $j = N$ **do** $s \leftarrow e^{i\phi_j}$ $\hat{w} \leftarrow \int (vs)e^{-ixq} dx$ Propagate \hat{w} to a distance δz :

$$\hat{u} \leftarrow [\hat{w}h(q, \frac{\delta z}{2}) \otimes \hat{s}]h(q, \frac{\delta z}{2})$$

 $u \leftarrow \int \hat{u}e^{-ixq} dq$ Back to spatial domainStore u and make it the new incident field v $v \leftarrow u$ **end for**

strain to the material thus generating ultrasound. The physics and the mathematics behind this process is carefully considered in [106], for instance. The author gives a relation between the rise in temperature due to a pulsed laser hitting the surface and Rayleigh waves.

In this appendix the formulation of the thermal expansion boundary problem due to a laser is reproduced only for completeness. Nothing has been added to its solution nor its formulation.

The spatial and temporal temperature distribution is governed by the heat equation. If Q represents the total input heat due to a pulse laser, $w(\mathbf{r})$ the normalised spatial distribution of the laser onto the surface and $q(t)$ the temporal profile of the laser, the appropriate boundary problem heating a free surface of sample is given by, [17, 106]

$$\begin{aligned} \Delta T + \chi \frac{\partial T}{\partial t} &= Qw(\mathbf{r})q(t) \\ T = \frac{\partial T}{\partial t} &= 0 \quad t \leq 0 \end{aligned} \quad (\text{A.43})$$

where χ is the temperature conductivity.

As the temperature rises (above ambient temperature) at (\mathbf{r}, t) the absorbed light

produces stress-free strain. The author in [17], considers the additional boundary condition

$$\mathbf{n} \cdot \nabla T(\mathbf{r}, t) = 0, \quad \mathbf{r} \in S, \quad t > 0. \quad (\text{A.44})$$

This condition establishes that no heat is lost by conduction or radiation as pointed out by the author. Since strain is related to the temperature by the following relation

$$\epsilon_{kl}(\mathbf{r}, t) = \alpha \delta_{kl} T(\mathbf{r}, t) \quad (\text{A.45})$$

Here α represents the thermal conductivity and δ_{kl} the Kronecker delta. One of the remarks in [17] is that the displacement can be directly related to displacement generated by thermal expansion as

$$u(\mathbf{r}, t) = Aq(t) \otimes g(\mathbf{r}, 0, t) \quad (\text{A.46})$$

where A is a constant that depends on material characteristics and g is the Green's function that gives the normal displacement due to a point source. The displacement represented as a convolution of the Green's function and the laser pulse is very convenient for extended sources. The constant A is important for theoretical and practical purposes but in this work is less important since we are mostly considering normalised quantities.

For the sake of completeness the definition of the constant A is given, that is

$$A = -\frac{1}{8} \frac{\kappa}{\pi \mu c_T^2} \frac{E \alpha k Q}{(1 - 2\nu) K} S \quad (\text{A.47})$$

where

E, μ = Young and shear modulus, respectively

c_L, c_T = Longitudinal and transverse wave speeds, respectively

ν = Poisson ratio

k, K = The thermal diffusivity and conductivity, respectively

α =linear coefficient of thermal expansion

$$\kappa = \frac{c_T^2}{c_L^2}.$$

The whole article [17] is dedicated to the calculation of g for different source locations including the case when the source lies on the surface. This representation for g is the one that is used in this thesis to theoretically represent SAW in homogeneous materials. The function q depends on the laser used. In the experimental work an Nd:YAG laser was used that has $q = \frac{t}{\tau^2}e^{-t/\tau}$ as temporal profile. Here, τ is the pulse duration which is approximately 12ns for Nd:YAG Laser.

A.6.1 Displacement from an array of lines

The pattern delivered onto the surface by the SLM is a series of straight lines, Fig. (A.1). The displacement for an array of N straight lines evenly distributed is easily extended using the development in section (4.1.1) in chapter (4). Thus, once again if u_y is the displacement for a single line, the displacement of a source composed of N lines is given by

$$u = \sum_{n=1}^N u_y(t - n\Delta t) \quad (\text{A.48})$$

The differential time is $\Delta t = \frac{\lambda_R}{c_R}$ where λ_R is the wavelength of the Rayleigh wave. The reason for appearance of the ultrasonic wavelength in the separation of the lines is because this the only way to generate SAW using this type of sources. Thus previous knowledge of the wave velocity in the material to investigate is required or at least a good guess in order to generate SAW with the OSAM system. A typical value for λ_R in aluminium would be 35.5 μm approximately for ultrasound generation at the frequency of 82MHz. The size of the SLM is fixed, so is a with an approximated value of 2mm. The value b is a function of λ_R and the number of lines.

The sum above is easier to look in the ω -domain; thus, performing Fourier trans-

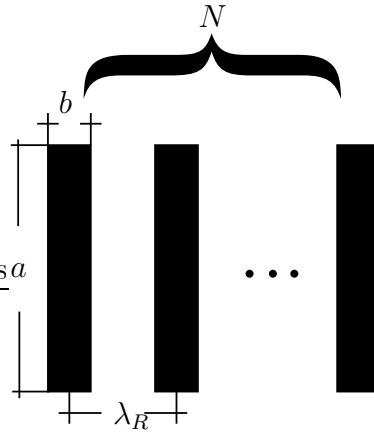


Figure A.1: Array of N illuminated lines by a laser. a , b are the width and length, respectively of the lines and λ_R is the Rayleigh wavelength which is the distance of separation between adjacent lines.

form gives

$$\begin{aligned}\hat{u}(\mathbf{r}, \omega) &= \hat{u}_y(\mathbf{r}, \omega) \sum e^{2\pi i \omega n \Delta t} \\ &= e^{\pi i \omega (N+1) \Delta t} \frac{\sin(\pi \omega N \Delta t)}{\sin(\pi \omega \Delta t)} \hat{u}_y(\mathbf{r}, \omega)\end{aligned}\quad (\text{A.49})$$

where \hat{u}_y is the Fourier transform of u_y . Here, ω is the angular frequency $\omega = 2\pi f$, f the normal frequency. Looking at the Eq. (5.13), one can observe that the amplitude of displacement due to a line source is being modulated by $\frac{\sin(\pi \omega N \Delta t)}{\sin(\pi \omega \Delta t)}$ and the phase by an amount of $\pi \omega (N+1) \Delta t$ for each frequency component. For a more detailed analysis of sources of the this type [107] is suggested.

A.7 Useful integrals

Useful integral used within the text

$\int e^{-\beta^2 t^2 - iqt} dt = \frac{\sqrt{\pi}}{\beta} e^{-q^2/4\beta^2}$	$\Re \beta > 0$	[70]
$\int e^{-i\omega t} dt = 2\pi \delta(\omega)$		
$\frac{i}{\sqrt{2\pi}} \int \frac{e^{-i\omega t} d\omega}{(\omega + \xi + ic)}$		[78]

Table A.1: Useful integrals

Bibliography

- [1] M. C. Roggemann, B. M. Welsh, and R. Q. Fugate. Improving the resolution of ground-based telescopes. *Review of Modern Physics*, 69(2):437–505, 1997.
- [2] C. R. Hill. Ultrasound for cancer investigation: An anecdotal history. *Ultrasound*, 14(2):79–86(9), 2006.
- [3] M. Kumar, T. Sarmah, and B. Kumar. Case report: Prenatal ultrasound diagnosis of fetal diastematomyelia. *Ultrasound*, 14(2):124–125(2), 2006.
- [4] P. Vankayalapati and B. Hollis. Role of ultrasound in obstetrics. *Current Obstetrics and Gynaecology*, 14:92–98, 2004.
- [5] M. Hoheisel. Review of medical imaging emphasis on X-ray detectors. *Nuclear Instruments and Methods in Physics Research A*, 563:215–224, 2006.
- [6] K. R. Leonard and M. K. Hinders. Lamb wave tomography of pipe-like structures. *Ultrasound*, 43:574–583, 2005.
- [7] M. H. S. Siqueira, C. E. N. Gatts, R. R. da Silva, and J. M. A. Rebello. The use of ultrasonic guided waves and wavelets analysis in pipe inspection. *Ultrasonics*, 41:785–797, 2004.
- [8] Z. Su, L. Ye, and Y. Lu. Guided Lamb waves for identification of damage in composite structures: A review. *Journal of Sound and Vibration*, 295:753–780, 2006.
- [9] G. Zumpano and M. Meo. A new damage technique based on wave propagation for rails. *International Journal of Solids and Structures*, 43:1023–1046, 2006.

- [10] M. J. Vellekoop. Acoustic wave sensors and their technology. *Ultrasonics*, 36:7–14, 1998.
- [11] T. Adachi, Y. Kondo, A. Yamaji, S. Ho Yang, and In-Y. Yang. Nondestructive evaluation of micro-cracks in a ceramic ferrule by resonant ultrasound spectroscopy. *NDT and E International*, 38:548–553, 2005.
- [12] H. Proudhon, J. Y Buffiere, and S. Fouvry. Characterisation of fretting fatigue damage using synchrotron X-ray micro-tomography. *Tribology International*, 39:1106–1113, 2006.
- [13] H. H. Barret and K. J. Myers. *Foundations of Image Science*. John Wiley and Sons, Inc., Hoboken, New Jersey, 2004.
- [14] M. Clark, S. D. Sharples, and M. G. Somekh. Optimisation using measured Green’s function for improving spatial coherence in acoustic measurements. *Ultrasonics*, 42:205–212, 2004.
- [15] G. Alers, M. Tennison, R. B. Thompson, and B. R. Tittmann. Visualisation of surface elastic waves on structural materials. *Ultrasonics*, 11(4):174–177, 1973.
- [16] L. Noui and R. J. Dewhurst. A laser beam deflection technique for the quantitative detection of ultrasonic Lamb waves. *Ultrasonics*, 31(6):425–432, 1993.
- [17] L. R. F. Rose. Point-source representation for laser-generated ultrasound. *J. Acoust. Soc. Am.*, 75(3):723–732, 1984.
- [18] S. D. Sharples, M. Clark, and M. G. Somekh. Dynamic higher-order correction of acoustic aberration due to material microstructure. *Applied Physics Letters*, 81(2):2288–2290, 2002.
- [19] S. D. Sharples. *All-optical Scanning Acoustic Microscope*. PhD thesis, University of Nottingham, 2003.

- [20] E. Kröner. *Statistical Modelling*, In: J. Gittus and J. Zarka, Editors, *Modelling Small Deformations in polycrystals*, pages 229–291. Elsevier Applied Science, London, 1986.
- [21] T. C. T. Ting and Ven-Gen Lee. The three-dimensional elastostatic Green's function for general anisotropic linear elastic solids. *Q. JI Mech. Appl. Math.*, 50(3):407–426, 1997.
- [22] C. Y. Wang. Elastic field produced by a point source in solids of general anisotropy. *Journal of Engineering Mathematics*, 32:41–52, 1997.
- [23] R. Ranganathan and S. Dattagupta. Theory of ultrasonic scattering by grains in polycrystals. *Phys. Stat. Sol.*, (a) 54:537, 1979.
- [24] F. E. Stanke and G. S. Kino. A unified theory for elastic wave propagation in polycrystalline material. *J. Acoust. Soc. Am.*, 75(3), 1984.
- [25] S. Hirsekorn. The scattering of ultrasonics waves by polycrystals. *J. Acoust. Soc. Am.*, 72(3):1021–1163, 1982.
- [26] K. Sobczyk. *Stochastic Modelling of Microstructures*. Birkhäuser, 2001.
- [27] R. D. Doherty, D. A. Hughes, F. J. Humphreys, J. J. Jonas, D. J. Jensen, M. E. Kassner, W. E. King, T. R. McNelley, H. J. McQueen, and A. D. Rollet. Current issues in recrystallisation: a review. *Materials Science and Engineering*, A238:219–274, 1997.
- [28] O. Rezvanian, M. A. Zikry, and A. M. Rajendran. Microstructural modelling of grain subdivision and large strain inhomogeneous deformation modes in F. C. C. crystalline materials. *Mechanics of Materials*, 38:1159–1169, 2006.
- [29] E. P. Papadakis. *Physical Acoustics. Ultrasonic Attenuation Caused by Scattering in Polycrystalline Materials*, volume IV, Part B. Academic Press, 1968.
- [30] Jr. F. C. Karal and J. B. Keller. Elastic, electromagnetic, and other waves in a random medium. *J. Math. Phys.*, 5(4):537–547, 1964.

- [31] V. H. Lopez, S. Truelove, and A. R. Kennedy. Fabrication of al-tic master composites and their dispersion in al, cu and mg melts. *Materials Science and Technology*, 19:925–930, 2003.
- [32] Y. Han, D. Shu, J. Wang, and B. Sun. Microstructure and grain refining performance of Al-5Ti-1B master alloy prepared under high-intensity ultrasound. *Materials Science and Engineering A*, 430:326–331, 2006.
- [33] A. Brahme, M. H. Alve, D. Saylor, J. Fridy, and A. D. Roller. 3d reconstruction of microstructure in a commercial purity of aluminium. *Scripta Mathematica*, 55:75–80, 2006.
- [34] J. Ohser and F. Mücklich. *Statistical Analysis of Microstructure in Materials Science*. John Wiley and Sons, Ltd, New York, 2000.
- [35] S. H. Tang, S. Wu, S. T. Tu, and M. Kobayashi. Characterising texture in polycrystalline materials by ultrasonic waves. *Theoretical and Applied Fracture Mechanics*, 45:128–138, 2006.
- [36] D. Royer and E. Dieulesaint. *Elastic Waves in Solids II*. Springer Verlag, Berlin, 1999.
- [37] E. Papadakis. Influence of preferred orientation on ultrasonic grain scattering. *J. Appl. Phys.*, 36(5):1738–1740, 1964.
- [38] W. Voigt. *Lehrbuch der Kristallphysik*. B. G. Teubner, Leipzig, Berlin, 1910.
- [39] M. Grigoriu. *Stochastic calculus*. Birkhäuser, Boston, MA, 2002.
- [40] J. J. McCoy. A parabolic theory for stress wave propagation through inhomogeneous linearly elastic solids. *J. Applied. Mech.*, 44:462–468, 1977.
- [41] Z. Sun and G. Wickman. The inversion of transient reflection data to determine solid grain structure. *Wave Motion*, 18:143–162, 1993.
- [42] G. Nakamura and G. Uhlmann. Inverse problems at the boundary for an elastic medium. *SIAM. J. Math. Anal.*, 27(2):263–279, 1995.

- [43] V. A. Buryachenko, N. J. Pagano, R. Y. Kim, and J. E. Spowart. Quantitative description and numerical simulation of random microstructures of composites and their effective elastic moduli. *International Journal of Solids and Structures*, 40:47–22, 2003.
- [44] R. L. Mullen, R. Ballarini, Y. Yin, and H. Heuer. Monte carlo simulation of effective elastic constants of polycrystalline thin films. *Acta Materialia*, 45(6):2247–2255, 1997.
- [45] M. Ostoja-Starzewski. On geometric acoustics in random, locally anisotropic media. *Continuum Mechanics Thermodynamics.*, 13:131–134, 2001.
- [46] K. Sobczyk. *Stochastic Wave Propagation*. PWN-Polish Scientific Publishers, Krakowskie Przedmiescie 7,00-068, Warszawa, Poland, 1984.
- [47] A. Ishimaru. *Wave Propagation and Scattering in Random Media*. Academic Press, Inc, New York, 1970.
- [48] J. A. Turner. Elastic wave propagation and scattering in heterogeneous anisotropic media: Textured polycrystalline materials. *J. Acoust. Soc. Am.*, 106(2):541–551, 1999.
- [49] J. A. Hudson. A parabolic approximation for elastic waves. *Wave Motion*, 2:207–214, 1980.
- [50] V. I. Tatarskii. The effects of the turbulent atmosphere on wave propagation. *Israel Program for Scientific Translation*, 1971.
- [51] P. G. Richards. Weakly coupled potential for high-frequency elastic waves in continuously stratified media. *Bulletin of the Seismological Society of America*, 64(5):1575–1588, 1974.
- [52] O. A. Grigorev and T. D. Shermergor. The scattering of ultrasonic waves in polycrystals. *Phys. Stat. Sol.*, (a) 64:385–394, 1981.

- [53] S. T. McDaniel. Application of the parabolic approximation to predict acoustical propagation in the ocean. *Am. J. Phys.*, 41(1):63–68, 1978.
- [54] E. R. Floyd. Using rigorous ray tracing to incorporate reflection into the parabolic approximation. <http://arxiv.org/pdf/physics/9909001>, 1999.
- [55] F. D. Tappert. *The parabolic approximation method*, In: J. B. Keller and J. S. Papadakis, Editors, *Wave Propagation and Underwater Acoustics*. Springer-Verlag, Berlin, 1977.
- [56] D. Lee, A. D. Pierce, and Er-C. Shang. Parabolic equation development in the twentieth century. *Journal of Computational Acoustics*, 8(4):527–637, 2000.
- [57] D. J. Thomson. A wide-angle split-step algorithm for the parabolic equation. *J. Acoust. Soc. Am.*, 74(6):1848–1854, 1983.
- [58] G. D. Manolis and C. Z. Karakostas. Derivation of mutual coherence function of the pressure field envelope using the parabolic equation method. <http://sbcx.mit.edu/pmd/tatarskii.pdf>, 2000.
- [59] J. W. Goodman. *Statistical Optics*. John Wiley and Sons, Inc., New York, 2000.
- [60] V. U. Zavorotnyi, V. I. Klyatskin, and V. I. Tatarskii. Strong fluctuations of the intensity of electromagnetic waves in randomly inhomogeneous media. *Sov. Phys. JETP*, 46(2):252, 1977.
- [61] R. L. Fante. Imaging of an object behind a random phase screen using light of arbitrary coherence. *J. Opt. Soc. Am.*, 2(12):2318–2328, 1985.
- [62] I. G. Yakushkin and V. U. Zavorotny. Statistics evolution of wavefields in random media. *Waves in random media*, 2:165–172, 1992.
- [63] J. P. Fouquet, G. Papanicolaou, and Y. Samuelides. Forward and markov approximations: the strong-intensity-fluctuations regime revisited. *Waves in Random Media*, 8:303–314, 1988.

- [64] L. Mandel and E. Wolf. *Optical Coherence and Quantum Optics*. Cambridge University Press, Cambridge, 1995.
- [65] J. J. McCoy. On the correction of field quantities in a random linearly elastic solid. *J. Math. Phys.*, 13:1804–1814, 1972.
- [66] B. J. Uscinski. Intensity fluctuations in a multiple scattering medium. solution of the fourth moment equation. *Proc. R. Soc. Lond.*, A380:137–169, 1982.
- [67] B. J. Uscinski. Analytical solution of the fourth-moment equation and interpretation as a set of phase screens. *J. Opt. Soc. Am. A*, 2(12):2077–2091, 1985.
- [68] K. Sobczyk. Scattering of Rayleigh waves at random boundary of an elastic body. *Proceedings of vibration problems*, 4(7):363–374, 1966.
- [69] L. C. Le. Wave propagation in a random medium: A complete set of the moments equations with different wavenumbers. *J. Math. Phys.*, 15(9):1431–1435, 1974.
- [70] D. A. de Wolf. Backscatter corrections to the parabolic wave equations. *J. Opt. Soc. Am.*, 6(2):174–179, 1989.
- [71] J. Oz and E. Heyman. A Green’s function method to SH-wave motion in a random continuum. *Engineering Analysis with Boundary Elements*, 27:93–100, 2003.
- [72] V. G. Gavrilenko and S. S. Petrov. Transport of radiation incident obliquely on the boundary of an absorbing randomly inhomogeneous medium. *Radio-physics. Quantum Electron*, 28:983–986, 1985.
- [73] P. D. Bons, M. W. Jessel, L. Evans, T. Barr, and K. Stüwe. Modelling of anisotropic grain growth in minerals In: H. A. Koyi and N. S. Mancktelow, Editors, Tectonic modelling: A volume in honour of Hans Ramberg. *Geological Society of America*, 193:45–49, 2000.

- [74] S. Ghosh, Z. Nowak, and K. Lee. Quantitative characterisation and modelling of composites microstructures by Voronoi cells. *Acta Materialia*, 45(6):2215–2234, 1997.
- [75] S. Sathish and R. W. Martin. Quantitative imaging of Rayleigh wave velocity with a scanning acoustic microscope. *IEEE Transactions on ultrasonics, Ferroelectrics, and Frequency control*, 49(5):550–557, 2002.
- [76] I. A. Viktorov. *Rayleigh and Lamb Waves*. Plenum Press, Acoustic Institute, Academy of Science of the USSR, Moscow, USSR, 1967.
- [77] J. D. Achenbach. *Wave Propagation in Elastic Waves*. Elsevier Science Publishers B. V., The Netherlands, 1999.
- [78] K. F. Graff. *Wave Motion in Elastic Solids*. Oxford University Press, Ely House, London W. I, 1975.
- [79] C. Y Wang and J. D. Achenbach. Lamb’s problem for solids of general anisotropy. *Wave Motion*, 24:227–242, 1996.
- [80] K. Walker. Fourier integral representation of the Green’s function for an anisotropic elastic half-space. *Proc. R. Soc. Lond. A*, 443:367–3898, 1993.
- [81] N. R. Ogg. A huygen’s principle for anisotropic media. *J. Phys. A: Gen. Phys.*, 4:382–388, 1971.
- [82] R. M. White. Generation of elastic waves by transient surface heating. *J. Appl. Phys.*, 34(12):3559–3567, 1963.
- [83] P. A. Doyle. On epicentral waveforms for laser-generated ultrasound. *J. Phys. D: Aplp. Phys.*, 19:1613–1623, 1986.
- [84] P. A. Doyle. Calculations of ultrasonic surface waves from an extended thermoelastic laser source. *Journal of Nondestructive Evaluation*, 8(3):147–164, 1989.

- [85] C. M. Scala and P. A. Doyle. Time-and frequency-domain characteristics of laser-generated ultrasonics surface waves. *J. Acoust. Soc. Am.*, 85(4):1569–1576, 1989.
- [86] D. Royer and C. Chenu. Experimental and theoretical waveforms of Rayleigh waves generated by a thermoelastic laser line source. *ultrasonics*, 38:891–895, 2000.
- [87] S. Kenderian and B. B. Djordjevic. Narrow band laser-generated surface acoustic waves using a formed source in the ablative regime. *J. Acoust. Soc. Am.*, 113(1):261–266, 2003.
- [88] C. B. Scruby and L. E. Drain. *Optical Detection of Ultrasound*, In: A. E. de Barr, Editors, *Laser Ultrasonics: Techniques and Applications*. Adam Hilger, IOP Publishing Ltd, Bristol, England, 1990.
- [89] S. D. Sharples, M. Clark, and M. G. Somekh. All-optical adaptive scanning acoustic microscope. *Ultrasonics*, 41:295–299, 2003.
- [90] A. Papoulis. *Probability, Random Variables, and Stochastic Processes*. McGraw-Hill, 1221 Avenue of the Americas, New York, NY 10020, 2002.
- [91] D. R. Atthey. The propagation of elastic waves through a textured granular material. *Int. J. Eng. Sci.*, 23(9):937–951, 1985.
- [92] M. J. Beran and J. Molyneaux. Use of classical variational principle to determine bounds for the effective bulk modulus in heterogenous media. *Q. Appl. Math.*, 24(2), 1966.
- [93] M. J. Beran and J. J. McCoy. Mean field variations in a statistical sample of heterogeneous linearly elastic solid. *International Journal of Solids and Structures*, 6:1035–1054, 1970.
- [94] ASTM International. Standard test methods for determining average grain size. *ASTM International*, pages 267–291, 2000.

- [95] J. A. Neubert. Asymptotic solution of the stochastic Helmholtz equation for turbulent water. *J. Acoust. Soc. Am.*, 48(5):1203–1211, 1970.
- [96] P. Byron and R. B. Thompson. A paraxial theory for the propagation of ultrasonic beams in anisotropic solids. *J. Acoust. Soc. Am.*, 85(6):2290–2300, 1989.
- [97] C. L. Rino. On propagation in continuous random media. *Waves in random media*, 2:59–72, 1991.
- [98] V. E. Ostashev and V. I. Tatarskii. Representation of the Helmholtz equation solution in the form of a series based on backscattering multiplicity. *Waves in Random Media*, 5:125–135, 1995.
- [99] L. G. Parratt. *Probability and Experimental Errors in Science*. Dover Publications, Inc, New York, N. Y., 1961.
- [100] S. G. Mallat. *A Wavelet Tour of Signal Processing*. Academic Press, San, Diego, 1999.
- [101] J. A. Hernández, M. Clark, , S. D. Sharples M. Somekh, and V. H. Lopez. Aberrations in materials with random inhomogeneities. *J. Acoust. Soc. Am.*, 127(3):1396–1405, 2007.
- [102] T. Stratoudaki, J. A. Hernández, M. Clark, and M. Somekh. Cheap optical transducers (CHOTs) for narrowband ultrasonic applications. *Measurement Science and Technology, Institute of Physics Publishing*, 18:843–851, 2007.
- [103] J. A. Hernández, M. Clark, S. D. Sharples, and M. Somekh. Aberrations in polycrystalline materials. *Review of Quantitative Nondestructive Evaluation*, 24B(760):1316–1322, 2005.
- [104] J. A. Hernández, M. Clark, M. Somekh, and S. D. Sharples. Statistical characterisation of metals from ultrasonic aberrations. *Ultrasonic Symposium, IEEE*, 2(18-21):1139–1142, 2005.

- [105] M. Clark, J. A. Hernández, S. D. Sharples, and M. G. Somekh. An adaptive technique using measured Green's functions for extending spatial coherence in aberrating materials. *Ultrasonic Symposium, IEEE*, 1(5–8):262–265, 2003.
- [106] A. A. Karabutov. Laser excitation of surface acoustic waves: a new direction in opto-acoustic spectroscopy of a solid. *Sov. Phys. Usp.*, 28(11):1042–1051, 1995.
- [107] J. Huang, S. Krishnaswamy, and J. D. Achenbach. Laser generation of narrow-band surface waves. *J. Acoust. Soc. Am.*, 92(5):2527–2531, 1992.